ΕΞΕΤΑΣΗ ΜΗΧΑΝΙΣΜΩΝ ΚΑΤΑ ΤΗΝ UV ΦΩΤΟΑΠΟΔΟΜΗΣΗ ΠΟΛΥΜΕΡΩΝ

Διδακτορική Διατριβή

Γιάννης Μπούνος

Πανεπιστήμιο Κρήτης
Τμήμα Φυσικής
&
Ίδρυμα Τεχνολογίας και Έρευνας
Ινστιτούτο Ηλεκτρονικής Δομής και Λέιζερ

Ηράκλειο
Απρίλιος 2007

EXAMINATION OF THE MECHANISMS OF UV LASER ABLATION OF POLYMERS

Ph.D. Dissertation

Giannis Bounos

UNIVERSITY OF CRETE
Department of Physics

&
IESL-FORTH

Heraklion, Crete, Greece
April 2007

Dedicated to my parents

Κωνσταντίνο Μπούνο
Ζωή Μπούνου

Ευχαριστίες:

Οι ευχαριστίες στα πλαίσια μίας διδακτορικής διατριβής δεν είναι αποτέλεσμα της συναισθηματικής φόρτισης που νιώθουμε στην ολοκλήρωση μιας τέτοιας εργασίας. Η ύπαρξή τους προϋπήρχε όλα αυτά τα χρόνια καθημερινά.

Εκφράζω τη βαθύτατη ευγνωμοσύνη και το μεγαλύτερο μέρος των ευχαριστιών μου στον υπεύθυνο της παρούσας διατριβής Δρ. Σ. Γεωργίου, Ερευνητή Α, για την καθοδήγησή και την άμεση υποστήριξή του. Η συμβολή του υπήρξε καθοριστική και πολύτιμη στην ολοκλήρωση της Διατριβής και την ανάπτυξη της επιστημονικής μου προσωπικότητας.

Ευχαριστώ το Διευθυντή του Ινστιτούτου Ηλεκτρονικής Δομής και Λέιζερ και καθηγητή του τμήματος Φυσικής κ. Κ. Φωτάκη, που μου έδωσε την ευκαιρία να πραγματοποιήσω αυτή τη διατριβή στο χώρο του Ινστιτούτου. Θα ήθελα επίσης να ευχαριστήσω το Ινστιτούτο Ηλεκτρονικής Δομής και Λέιζερ για την υλικοτεχνική του υποδομή και την οικονομική υποστήριξη που μου παρείχε κατά τη διάρκεια των σπουδών μου.

Σημαντική στην ολοκλήρωση αυτής της διατριβής υπήρξε η συνεργασία με την Δρ. M. Castijello, όπως και τη Δρ. E. Rebollar από το Ινστιτούτο “Rocasolano” στη Μαδρίτη και το Δρ. N. Bityurin από την Ακαδημία Επιστημών στη Ρωσία.

Ιδιαίτερα ευχαριστώ άμεσους συνεργάτες και φίλους, την Ο. Κοκκινάκη και τον Α. Σελίμη, για την άψογη συνεργασία στο χώρο του εργαστηρίου. Επίσης ένα μεγάλο ευχαριστώ στον Δρ. Άγγλο, Ερευνητή Β, για τις χρήσιμες συζητήσεις και τις επιστημονικές συμβουλές.

Ευχαριστώ την επταμελή που δέχτηκε να κρίνει αυτή τη διατριβή. Επιπλέον ένα μεγάλο ευχαριστώ στους καθηγητές μου στο Μεταπτυχιακό Πρόγραμμα Μικροηλεκτρονικής-Οπτοηλεκτρονικής.

Τέλος θα ήθελα να ευχαριστήσω το τεχνικό προσωπικό του Ινστιτούτου Ηλεκτρονικής Δομής και Λέιζερ για την υποστήριξη των πειραμάτων μου.

Οι περισσότερες ευχαριστίες μου είναι για αυτούς που δεν κατάλαβαν και πολλά, αλλά προσέφεραν σχεδόν τα πάντα. Και δεν είναι άλλοι από την οικογένειά μου, Κωνσταντίνο Μπούνο, Ζωή Μπούνου, Νίκο Μπούνο που σε όλα αυτά τα χρόνια των σπουδών μου έδειξαν αμέριστη κατανόηση και υπομονή.

SUMMARY

Laser ablation of polymers constitutes the basis for a wide range of applications ranging of restoration of artworks to medical applications. There are several reasons for the difficulties in establishing the mechanism(s), but the most important one appears to be the limitations in the systematic examination of the influence of material parameters. To overcome this problem, we turn to the examination of polymer molecular weight (Mw) on laser induced processes and in ablation. In the comparison of polymers of different Mws, the chemical and optical properties are nearly identical, and the systems differ only in the number of bonds. Thus, the relevance of the various mechanisms that have been suggested for UV ablation of polymers can be directly tested.

The study concentrates on Poly(methylmethacrylate) (PMMA) and on Polystyrene (PS) which examined as model systems of varnishes in the painted artworks at three excimer wavelengths (193 nm, 248 nm and 308 nm). At weakly absorbed wavelengths, the ablation thresholds increase with increasing Mw, whereas at strongly absorbed wavelengths, the ablation thresholds are nearly the same. Different trends in the morphological changes are observed. For a more detailed assessment of the mechanism, a methodology for assessing the temperature evolution and polymer viscosity changes was developed by relying on monitoring the kinetics of products formation by photolysis of photosensitive compounds (probes) dispersed within the examined polymers. For both PMMA and PS, at all wavelengths, high temperatures well above the 'ceiling' decomposition temperatures are attained. At weakly absorbed wavelengths higher temperatures are attained with increasing Mw whereas at strongly absorbed wavelengths, the temperatures are about the same independently of polymer Mw. In addition, for all Mws, melting is demonstrated. These results unequivocally demonstrate that UV laser ablation is a thermal process; yet, significant deviations between the experimental temperatures and theoretically predicted ones on the basis of the bulk photothermal model (relying on conventional decomposition of polymer to monomers/oligomers) are noted. To eludicdate the reason for this discrepancy, the nature of the ejected material has been characterized by SEM and AFM examination of the material deposited on a surface (under vacuum). For low Mw, decomposition to monomers and oligomers is extensive; whereas for high Mw the process is uncompleted. In parallel, the photoscattering experiments show that at weakly absorbed wavelengths, the translational distributions of

the ejecta from low Mw are very broad and slow, whereas the ones from the high Mw systems are very sharp and peak at high velocities, indicating that ejection from the high Mw systems is much more 'impulsive'. At strongly absorbed wavelengths the distributions are high, nearly the same for both high and low Mw. The indications by the examination of translational distributions have been confirmed by piezoelectric measurements of the pressure developed in the substrates. We argue that the observed features are similar to the characteristics of explosive boiling observed in the fast superheating of simple compounds (liquids). A model for the explosive boiling of polymers is developed and shown that it can consistently account for all observations, as well as for most inconsistencies noted in previous studies on laser ablation of polymers.

Besides the mechanistic implications, the results are also of direct relevance to the optimization of laser processing schemes, since in a number of applications (e.g. pulsed laser deposition of polymeric films, laser restoration of artworks, medical applications) the molecular weight may vary a lot from case to case. Most surprisingly the influence of Mw has not taken into account on the optimization of laser processing schemes. Especially in the restoration of artworks, even on the same artwork, the upper layers appear a higher degree of polymerization (because of UV exposure and humidity)

In the last part of thesis, we present a preliminary study on the chemical modifications effected to PMMA doped with iodonaphthalene or iodophenanthrene upon femtosecond UV (500 fs, λ=248 nm) irradiation. The most important observation is that product formation is quite limited and selective upon irradiation at high fluences close to the ablation thresholds. A plausible explanation based on formation at weak plasma within the substrate is advanced. At any rate, the results indicate that in the fs processing of biopolymers, besides the well known excellent etching morphology, an additional factor for the success relates to the high selectivity of the induced chemical modifications.

This thesis constitutes the basis for 9 publications in international high quality peer reviewed scientific journals (e.g. Journal of Physical Chemistry B, Journal of Applied Physics), one chapter in a scientific book related to ablation of molecular substrates and numerous presentations in national and international scientific conferences. Four more articles are in the processes of preparation and will be submitted to scientific journal shortly.

ΠΕΡΙΛΗΨΗ

Η φωτοαποδόμηση των πολυμερών αποτελεί τη βάση ενός μεγάλου αριθμού εφαρμογών όπως της αποκατάστασης ζωγραφικών έργων τέχνης. Το κυριότερο προβλημα για την διασαφήνηση των μηχανισμών είναι η δυσκολία για την συστηματική εξέταση της επίδρασης των παραμέτρων του πολυμερούς. Σε αυτήν την διατριβή εξετάσθηκε η επίδραση του Μοριακού Βάρους (ΜΒ) του πολυμερούς. Με την αλλαγή του ΜΒ οι υπεύθυνοι μηχανισμοί του φαινομένου μπορούν να εξετασθούν άμεσα και συστηματικά.

Η παρούσα μελέτη εστιάζεται στην εξέταση της επίδρασης του ΜΒ στην φωτοαποδόμηση του Poly(methylmethacrylate) (PMMA) και Polystyrene (PS) σε τρία υπεριώδη μήκη κύματος (193 nm, 248 nm και 308 nm) που αποτελούν απλά μοντέλα των βερνικιών που χρησιμοποιούνται στην επικάλυξη ζωγραφικών έργων τέχνης. Σε ασθενώς απορροφούμενα μήκη κύματος, τα κατώφλια της φωτοαποδόμησης βρέθηκαν να αυξάνονται με την αύξηση του ΜΒ, ενώ στα ισχυρά απορροφούμενα μήκη κύματος ίδια κατώφλια παρατηρήθηκαν με την αλλαγή του ΜΒ. Επίσης παρατηρήθηκαν αλλαγές και στην μορφολογία. Για την λεπτομερή εξέταση των μηχανισμών, αναπτύχθηκε μια μεθοδολογία εκτίμησης των αναπτυσσόμενων θερμοκρασιών και των αλλαγών του ιξώδους, η οποία στηρίζεται στην παρακολούθηση των προϊόντων που σχηματίζονται κατά την υπεριώδη ακτινοβόληση εμπλουτισμένων πολυμερών με φωτοευαίσθητες ενώσεις. Σε όλα τα ΜΒ των δύο πολυμερών, κατά την ακτινοβόληση στα τρία υπεριώδη μήκη κύματος, αναπτύσσονται πολύ υψηλές θερμοκρασίες. Στα μήκη κύματος που απορροφούνται ασθενώς, οι θερμοκρασίες αυξάνονται με την αύξηση του ΜΒ. Επιπρόσθετα, σε όλα τα ΜΒ παρατηρήθηκε τήξη. Η εξέταση της φύσης του εκτινασσόμενου υλικού έδειξε ότι για τα πολυμερή των μικρών ΜΒ, παρατηρήθηκε έντονη θερμική αποσύνθεση σε μονομερή ή ολιγομερή. Αντίθετα, στα πολυμερή μεγάλων ΜΒ παρατηρήθηκε εκτίναξη ενός μεγάλου ποσοστού συσσωματωμάτων. Παράλληλα, πειράματα σκέδασης έδειξαν ότι οι κινητικές κατανομές των εκτινασσόμενων σωματιδίων που προέρχονται από τα πολυμερή των υψηλών ΜΒ είναι πολύ μεγαλύτερες από τις αντίστοιχες που προέρχονται από τα πολυμερή μικρών ΜΒ. Το γεγονός αυτό δείχνει ότι σε αυτά τα μήκη κύματος η εκτίναξη είναι πόλυ πιο ‘εκρηκτική’ στα πολυμερή των υψηλότερων ΜΒ. Στα μήκη κύματος που απορροφούνται ισχυρά από τα πολυμερή, παρατηρήθηκε ότι οι ταχύτητες είναι υψηλές και ανεξάρτητες του ΜΒ. Οι παραπάνω ενδείξεις επιβεβαιώθηκαν απο πιεζοηλεκτρικές μετρήσεις των πίεσεων που αναπτύσσονται στα υποστρώματα των πολυμερών. Τα χαρακτηριστικά εκτίναξης στα πολυμερή των υψηλών ΜΒ είναι παρόμοια με τα χαρακτηριστικά του ‘εκρηκτικού βρασμού’ σε γρήγορα υπερθερμενόμενα απλά συστήματα. που μπορεί να

εξηγήσει όλες τις πειραματικές παρατηρήσεις και επιπλέον τις ασυμβατότητες που παρατηρήθηκαν σε προηγούμενες μελέτες.

Εκτός από την μηχανιστική τους σημασία, τα αποτελέσματα έχουν άμεσες συνέπειες στις εφαρμογές. Στα ζωγραφικά έργα τέχνης, ο βαθμός πολυμερισμού των βερνικιών διαφέρει σημαντικά από έργο σε έργο ανάλογα με το βαθμό (έκταση) γήρανσης. Ακόμη πιο σημαντικό, ακόμη και σε ένα συγκεκριμένο έργο, ο βαθμός πολυμερισμού συνήθως αλλάζει από την επιφάνεια προς το εσωτερικό, ως αποτέλεσμα της διαφορετικής έκθεσης των διαφόρων στρωμάτων σε περιβαλλοντικούς παράγοντες (π.χ. έκθεση στο UV, υγρασία κλπ). Μέχρις στιγμής, η μεθοδολογία που έχει καθιερωθεί παγκοσμίως για την αποκατάσταση των έργων τέχνης με λέιζερ είχε πλήρως αγνοήσει την πιθανή επίδραση του MB. Η παρούσα εργασία αποδεικνύει ότι ο βαθμός πολυμερισμού του βερνικιού είναι καθοριστικός για την επιτυχία της τεχνικής της αποκατάστασης με λέιζερ (ειδικά σε μήκη κύματος όπως το 248 nm όπου παρατηρούνται σημαντικές διαφορές μεταξύ των συντελεστών απορρόφησης διαφόρων βερνικιών όπως π.χ. μεταξύ δάμαρης και μαστίχας). Επιπλέον, καθώς ο βαθμός πολυμερισμού συνήθως μειώνεται με αυξανόμενο βάθος από την επιφάνεια, είναι σημαντικό όπως αντίστοιχα διαφοροποιείται η ενέργεια του παλμού λέιζερ να εξασφαλίζεται η ελάχιστη δυνατή συσσώρευση επιβλαβών προϊόντων.

Στο τελευταίο μέρος αυτής της διατριβής παρουσιάζεται μία προκαταρκτική μελέτη πάνω στις χημικές αλλαγές που επάγονται στα εμπλουτισμένα συστήματα του PMMA κατά την UV femtosecond (fs) ακτινοβόληση. Η πιο σημαντική παρατήρηση είναι ότι ο σχηματισμός των προϊόντων είναι περιορισμένος κι επιλεκτικός κατά την ακτινοβόληση στις υψηλές πυκνότητες ενέργειας κοντά στα κατώφλια της φωτοαποδόμησης. Είναι φανερό ότι η τεχνολογία των fs λέιζερ παρέχει νέες δυνατότητες (εφαρμογές) κατεργασίας φωτοευαίσθητων υποστρωμάτων, όπως στην ιατρική και στην αποκατάσταση των έργων τέχνης. Ειδικότερα για τα ζωγραφικά έργα τέχνης, η τεχνολογία των fs λέιζερ εμφανίζει την δυνατότητα αποκατάστασης ακόμη και σε περίπτωση έλλειψης ή εξαιρετικά λεπτού υμενίου βερνικίου. Αυτή η δυνατότητα μπορεί να αποτελέσει ένα καθοριστικό πλεονέκτημα της αποκατάστασης έργων τέχνης με λέιζερ σε σχέση με την χρήση συμβατικών τεχνικών.

Η παρούσα διατριβή έχει αποτελέσει την βάση 9 δημοσιεύσεων σε διεθνή επιστημονικά περιοδικά υψηλού κύρους (π.χ. Journal of Physical Chemistry B, Journal of Applied Physics), ενός κεφαλαίου σε επιστημονικό βιβλίο και διαφόρων παρουσιάσεων σε διεθνή και εθνικά συνέδρια. 4 επιπλέον άρθρα προετοιμάζονται προς υποβολή σε διεθνή επιστημονικά περιοδικά.

TABLE OF CONTENTS:

Chapter 1 INTRODUCTION 1

1.1 UV LASER POLYMER ABLATION AND APPLICATIONS 1

1.2 PHENOMELOGICAL DESCRIPTION AND MODELS 4

1.3 LIMITATIONS AND CAVEATS 6

1.4 MECHANISMS OF UV LASER POLYMER ABLATION 8

1.4.1 The photothermal mechanism 9

1.4.2 Explosive boiling 12

1.4.3 The photomechanical mechanism 15

1.4.4 The photochemical mechanism 18

1.5 MOLECULAR DYNAMICS SIMULATIONS 19

1.6 PREVIOUS WORK ON THE INFLUENCE OF POLYMER MOLECULAR WEIGHT 20

1.7 SCOPE OF THIS WORK 21

1.7.1 Experimental methodology for temperature and viscosity estimation 21

1.7.2 Examination of the influence of polymer Mw 23

1.8 REFERENCES 24

Chapter 2 EXPERIMENTAL TECHNIQUES 27

2.1 SAMPLE PREPARATION 27

2.2 TIME RESOLVED LASER INDUCED FLUORESCENCE (LIF) 28

2.3 PULSED LASER DEPOSITION 31

2.4 PIEZOELECTRIC MEASUREMENTS 32

2.5 PROBE BEAM SCATTERING 33

2.6 REFERENCES 35

Chapter 3 EXAMINATION OF UV ABLATION OF PMMA VIA THE USE OF PHOTOACTIVE DOPANTS 37

3.1 INTRODUCTION 37

3.2 PRODUCT CHARACTERIZATION 38

3.3 F_{LASER}-DEPENDENCE OF PRODUCT FORMATION 39

3.4.1 Absorption process 44

3.4.2 Excitation processes 45

3.4.3 ArH Formation modelling/Temperature estimation 46

3.5 KINETICS OF PRODUCT FORMATION 51

3.6 DISCUSSION 56

3.7 REFERENCES 56

Chapter 4 INFLUENCE OF POLYMER MOLECULAR WEIGHT 59

4.1 INTRODUCTION 59

4.2 ABLATION THRESHOLDS AND MORPHOLOGICAL CHANGES 60

4.2.1 Substrate transmission 64

4.2.2 Discussion of morphological changes 66

4.3 ArH AND Ar_2 FORMATION 68

4.3.1 Modelling of ArH formation; estimation of attained temperatures *72*
4.3.2 Modelling of Nap_2 formation; estimation of viscosity changes *74*

4.4 EXAMINATION OF PMMA AT 193 nm 77

4.5 EXAMINATION OF POLYSTYRENE at 308 nm 78

4.6 CONCLUSIONS 79

4.7 REFERENCES 80

Chapter 5 EXAMINATION OF EJECTION PROCESS AND OF EJECTA UPON LASER ABLATION 83

5.1 INTRODUCTION 83

5.2 CHARACTERIZATION OF DEPOSITED EJECTA 83

5.3 EJECTA TRANSLATIONAL DISTRIBUTIONS 87

5.4 PIEZOELECTRIC MEASUREMENTS 93

5.4 SUMMARY AND CONCLUSIONS 94

5.5 REFERENCES 95

Chapter 6 MODELLING OF THE INFLUENCE OF POLYMER MOLECULAR WEIGHT 97

6.1 INTRODUCTION 97

6.2 MODELLING BY THE BULK PHOTOTHERMAL MODEL 97
6.2.1 Qualitative description *97*
6.2.2 Mathematical modelling *99*

6.3 A NEW MODEL OF ABLATION OF POLYMERS BY EXTENDING THE CONCEPT OF EXPLOSIVE BOILING 103
6.3.1 The factors suggesting the need of such a model *103*
6.3.2 Semiquantitative modelling of explosive boiling of polymers *106*
6.3.3 Application to the UV ablation of polymers *110*

6.4 CONCLUSIONS AND IMPLICATIONS 114

6.5 REFERENCES 115

Chapter 7 FEMTOSECOND POLYMER ABLATION 117

7.1 INTRODUCTION 117

7.2 ETCHING RATES AND MORPHOLOGICAL CHARACTERISTICS 118

7.3 EXAMINATION OF CHEMICAL EFFECTS IN ArI DOPED POLYMERS 121

7.4 TIME RESOLVED OPTICAL MONITORING OF EJECTION PROCESS 123

7.5 PLAUSIBLE EXPLANATION/MECHANISMS 126

7.6 CONCLUSIONS 132

7.7 REFERENCES 132

APPENDIX: FORTRAN program for ArH and Ar_2 calculation i

LIST OF FIGURES:

Figure 1.1: *a) Example of ink jet nozzle array fabricated by excimer laser ablation. b) Microlenses arrays designed on DPT-doped PMMA using excimer irradiation at 308 nm. c) Section of electrode structure for Flat Panel Displays by polyimide treatment on Copper substrate using the third harmonics of Nd:YAG.* 2
Figure 1.2: *a) A periodic structure of transferred HRP protein and b) HRP film.* 3
Figure 1.3: *LASIK technique on cornea using 193 nm.* 3
Figure 1.4: *a) Thickness of ablated material per single laser pulse as a function of laser fluence for irradiation of polyimide with ArF, KrF, XeCl, and XeF excimer lasers. b) The same experimental points are presented in "Arrhenius" format (i.e., ln(h) vs 1/F_{LASER})* 4
Figure 1.5: *a) Temperature profile in doped polymer as a function of depth at different times after the laser pulse. b) Temperature profile at the surface of doped PMMA.* 10
Figure 1.6: *Typical (P, T) thermodynamic phase diagram. Illustration of explosive boiling concept.* 14
Figure 1.7: *Schematic illustrating the photomechanical mechanism..* 16
Figure 1.8: *Thermoelastic stress wave signal recorded using a PVDF film transducer for PMMA irradiated with the 308 nm XeCl laser.* 16
Figure 1.9: *Peak pressure generated in polyimide for excimer irradiation at the indicated wavelengths.* 18
Figure 1.10: *Normalized intensity of emitted particles versus mass for (a) photochemical processes and (b) photothermal processes..* 20
Figure 2.1: *Chemical structure of examined polymers and dopants.* 28
Figure 2.2: *Time resolved Laser induced fluorescence setup.* 30
Figure 2.3: *a) Vacuum chamber used for PLD. b) Substrate holder.* 32
Figure 2.4: *Experimental setup for stress transient measurements and the characteristics of PVDF acoustic sensor.* 32
Figure 2.5: *Probe beam scattering setup.* 34
Figure 3.1: *a) Probe product LIF spectra following irradiation with one 248 nm laser pulse of PhenI/PMMA (0.5% wt). b) Probe product LIF spectra recorded from 1.2% wt NapI/PMMA following irradiation at 308 nm, 248 nm and 193 nm d.* 38
Figure 3.2: F_{LASER}*-dependence of the PhenH product in the irradiation of PhenI/PMMA (0.5% wt) at (a) 308 nm, 248 nm. (b) The corresponding* F_{LASER}*-dependence at 193 nm.* 40
Figure 3.3: F_{LASER}*-dependence of PhenH product formed in the 248 nm irradiation of PMMA doped with 0.5%, 1% and 2% wt PhenI.* 42
Figure 3.4: *Intensities of* Nap_2 *as a function of* F_{LASER} *in the irradiation of 1.2%wt NapI/PMMA at 248 nm and 308 nm..* 43
Figure 3.5: *a) PhenH product estimated to form as a function of laser fluence in the irradiation of 0.5 % wt PhenI/PMMA at 308 nm, 248 nm and 193 nm b) Estimated* F_{LASER}*-dependence of* Nap_2 *formation for irradiation of 1.2% NapI/PMMA at 308 nm and 248 nm.* 47
Figure 3.6: *PhenH product intensity for PhenI/PMMA films (0.5 wt%) recorded as a function of the pump-probe delay time for irradiation at (a) 248 nm (b) 193 nm..* 52
Figure 3.7: *PhenH product estimated to form as a function of time in the irradiation of 0.5 % wt PhenI/PMMA upon irradiation at the indicated fluences a (a) 248 nm and (b) 193 nm.. The details of the simulation are described in the text.* 53
Figure 3.8: *α)* Nap_2 *formation kinetics in the irradiation of 1.2 wt% NapI/PMMA at 248 nm at the indicated fluences. (b) The solid lines represent the simulated kinetics of* Nap_2 *formation..* 54
Figure 4.1: *Optical micrographs (magnification 50 x) of films areas irradiated with a single laser pulse at the indicated fluences.* 61
Figure 4.2: *Bubble average diameter dependence as a function of fluence for samples of 1.2% NapI/PMMA, Mw 2.5, 120 and 996 kDa irradiated at 248 nm.* 62
Figure 4.3: *ESEM micrographs of 0.5% PhenI/PS, irradiated with a single pulse at 248 nm. The fluence in both cases was 650 mJ/cm^2.* 62
Figure 4.4:*Time resolved relative transmission of a CW HeNe laser by 1.2% PhenI PMMA films irradiated at 248 nm with polymer 2.5 kDa (thick line) and 996 kDa (thin line)* 64
Figure 4.5: *Fluence dependence of the minimum relative transmission of irradiated films (248 nm) of 1.2% NapI/PMMA of Mw 2.5 kDa (open circles) and 996 kDa (full circles).* 65
Figure 4.6: F_{LASER}*-dependence of the PhenH product formed upon a single pulse at 248 nm on virgin doped samples (0.5% wt) for the indicated PMMA Mws.* 69

Figure 4.7: *(a) Kinetics of PhenH formation for PhenI-doped PMMA of the indicated molecular weights (b) Kinetics of PhenH formation as predicted by the simulation.* 70
Figure 4.8: *F_{LASER}-dependence of Nap_2 formed upon a single pulse at 248 nm on virgin NapI-doped samples (1.2% wt) for different Mw PMMAs.* 71
Figure 4.9: *(a) Kinetics of Nap_2 formation in the irradiation of the PMMA samples doped with 1.2% wt NapI. (b) Simulated kinetics of Nap_2 formation.* 71
Figure 4.10: *Estimation of viscosity evolution for 2.5kDa and 120 kDa PMMA deriving from Nap_2 kinetics formation as described in the text.* 76
Figure 4.11: *a) F_{LASER}-dependence of PheH formed upon a single pulse at 193 nm on PhenI-doped PMMA (0.5% wt) for two differerent Mw. b) The corresponding kinetics of PhenH formation.* 77
Figure 4.12: *F_{LASER}-dependence of PheH formed upon a single pulse at 308 nm on virgin PhenI-doped PS samples (0.5% wt) for different Mw PSs..* 79
Figure 5.1: *Scanning electron microscopy images SEM (with resolution 100 μm at the left and 1μm at the right) of deposits from 1.2 wt NapI/PMMA target at 248 nm.* 84
Figure 5.2: *Size distrtribution of clusters in the deposits from 1.2 % wt NapI/PMMA target at 248 nm as determined by software analysis of the SEM images Fig.5.1.* 84
Figure 5.3: *Atomic force microscopy (AFM) images of deposits of doped polystyrene films at 248 nm. The irradiation conditions shown on the graph.* 85
Figure 5.4: *Scattering signal (inverted) upon irradiation of the a) 2.4 kDa and b) 996 kDa 0.5% wt PhenI /PMMA with 248 nm at several fluences.* 88
Figure 5.5: *a) Attenuation signals (inverted) for 0.5% PhenI/PMMA after irradiation at 248 nm (F_{LASER} =2,2 J/cm²).b) The corresponding velocity distributions.* 89
Figure 5.6: *Velocity curves for the two "peaks" observed for 2.5 kDa PMMA.* 90
Figure 5.7: *Integrated attenuation curves for several molecular weights and pump fluences.* 91
Figure 5.8: *Velocity distributions for a) 0.5% wt PhenI/PMMA and b)2.0% wt PhenI/PMMA.* 92
Figure 5.9: *Sample traces of stress transients as measured by stress transducer.* 93
Figure 6.1: *Parameter ε versus reduced temperature and reciprocal heating rate* 109
Figure 6.2: *Critical point for explosive boiling for a polymer+monomer system.* 110
Figure7.1: *Etching rate curves for the systems: a) 0.5%PhenI PMMA and b) 1.2%wt NapI PMMA upon the irradiation with 500 fs at 248 nm.* 119
Figure 7.2: *Wavy- like structure formation on PS upon irradiation with 500 fs pulses at 248 nm.* 119
Figure 7.3: *LIF spectra of 4.0 % wt NapI/PMMA upon the irradiation with 500 fs at 248 nm. a) F_{LASER}=10mJ/cm^2 and b) F_{LASER}=300mJ/cm^2..* 121
Figure 7.4: *a) F_{LASER}-dependence of the PhenH product in the irradiation (λ=248 nm, τ_{pulse}=500 fs) of PhenI/PMMA. b) For comparison purposes the corresponding nanosecond F_{LASER}-dependence for the same system is presented..* 122
Figure 7.5: *Shawdographic examination of the material ejection process for the system 0.5%wt PhenI PMMA upon the irradiation with one pulse at 248 nm with pulse duration 500 fs. Mw_{PMMA}=996 kDa for above and Mw_{PMMA} =2.5 kDa for below series.* 124
Figure 7.6: *a)Ultrafast photografic examination in the bulk of neat PMMA upon the irradiation with one 248 nm pulse 500 fs. b) The corresponding reduction of transmittance.* 125
Figure 7.7: *Interplay of multiphoton and avalanche ionization in the process of plasma formation.* 127

LIST OF TABLES:

Table1: *Linear absorption coefficients, effective absorption coefficients, the corresponding swelling and ablation thresholds at 3 excimer wavelengths for different doped PMMA systems* 41
Table 2: *Swelling onset and ablation and substrate transmission transient thresholds (in mJ/cm^2), optical penetration depth as estimated from the small-signal values ($1/\alpha$) at 248 nm of doped polymer films and average maximum bubble diameter after a single pulse. Errors are estimated in 10-20% for determination of thresholds and about 10% for determination of bubble size.* 63
Table 3: *Glass transition temperature T_g of PMMA and PS of different molecular weights calculated according to the Flory-Fox equation.* 67
Table 4: *Theoretical temperatures as predicted by bulk photothermal model and experimental temperatures at the corresponding ablation thresholds at 248 nm and 193 nm.* 102
Table 5: *Dependence of estimated free electrons density on the absorption cross-section* 130

Chapter 1 INTRODUCTION

1.1 UV LASER POLYMER ABLATION AND APPLICATIONS

Irradiation of molecular solids with highly intense laser pulses, results in the removal of a material amount and the formation of a crater (depth from nm to μm). This phenomenon has been named (pulsed laser) Ablation deriving from the latin term "ablatio".

UV laser ablation constitutes the basis for a broad range of applications entailing material removal, surface modification and film deposition. Thus, UV laser ablation has found many important applications in a wide spectrum of fields ranging from microelectronics, microstucturing, laser cleaning, chemical analysis (Matrix Assisted Laser Desorption of Biomolecules-MALDI) in biology and in medicine (photorefractive keratectomy). The main characteristic/feature exploited is the minimal extent of thermal damage to the remaining substrate, coupled with the convenience of processing in an air or inert gas environment. Thus, UV ablation offers for machining polymers with sub-micron spatial and depth resolution [1, 2]. Most known application of laser ablation of polymers was considered as an alternative to the conventional photoresist technology. Some specific application examples from many that have been developed include:

- Via drilling in polyimide layers and multilevel polymer circuit boards. Pioneered by IBM and Siemens in the 1980's [3, 4], this continues to be a major use for excimer laser micromachining. An account highlighting the main developments in this field at IBM up to 1997 can be found in Brannon and Wassick's paper [5].
- Drilling ink-jet nozzles in polymeric substrates for which precise geometrical configurations can be realised (Fig.1.1a).
- Writing sub-micron period relief gratings on polymer surfaces. This is of practical importance for optoelectronic device applications and also provides a gauge of the potential resolution that might be attainable via ablation machining. Phillips et al., for example, have demonstrated sub-100-nm structures in polyimide with the KrF laser using a form of Talbot interferometer [6].

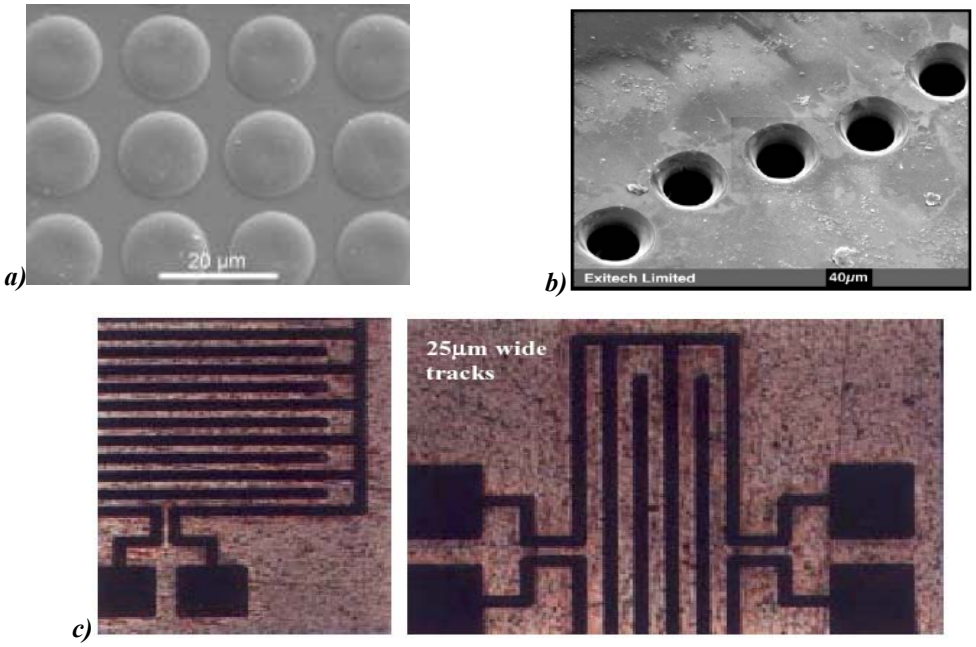

Figure 1.1: *a) Example of ink jet nozzle array fabricated by excimer laser ablation. b) Microlenses arrays designed on DPT-doped PMMA using excimer irradiation at 308 nm. c) Section of electrode structure for Flat Panel Displays by polyimide treatment on Copper substrate using the third harmonics of Nd:YAG.*

- Fabricating microchannels in polymers for 'lab-on-chip'components [7] (Fig. 1.1c).
- Forming complex 3-D surface relief structures using programmed mask scanning or diffractive optics techniques [8] (Fig.1.1b). Applications for this include micro-optical components such as diffractive lenses [8].
- Stripping polymer insulation from fine wires [9] and the acrylic jacket from optical fibres [10], for which noncontact processing is advantageous.
- Laser restoration of painted artworks, as described in detail in several publications from FORTH-IESL and subsequently by several other groups.
- New applications for ablation are foreseen with the growth of interest in organic materials for photonic devices, e.g. OLEDs (Organic Light Emitting Diodes). Excimer laser ablation may be exploited as a means of pattering organic films for display use and also offers the possibility of growing novel organic layers by ablation deposition [11].
- Other concepts such as laser induced material forward transfer (LIFT) are still under development. In LIFT the ablated material is coated onto a transparent substrate. The material, which should be transferred to a receiving layer, is coated on top of the propellant. The laser irradiates the propellant through the substrate and the released

gaseous products and shockwave which transfer the material from the substrate to the receiving layer. The transferred material can be deposited on top of the receiving layer or can be implanted below the surface of the receiving layer. It should be noted that for this method also other organic and inorganic materials can be used as propellant.

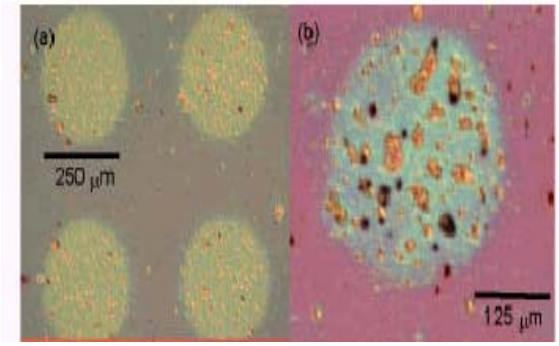

Figure 1.2: *a) A periodic structure of transferred HRP protein and b) HRP film with thickness ~10 nm (in DAB solution).*

From biological aspects, there is a lot interest on the formation of periodic structure of proteins Fig.1.2 (for easier genetic characterization study) using LIFT technique without any damage on their chemical structure.

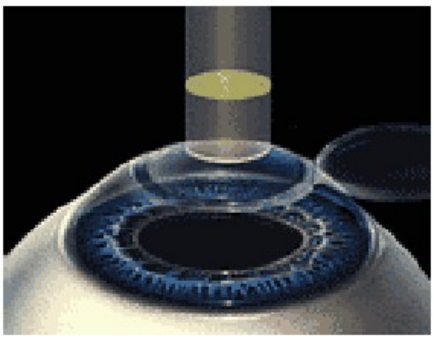

Figure 1.3: *LASIK technique on cornea using 193 nm.*

Another known application of UV laser ablation of biopolymers includes the photorefractive keratectomy. LASIK stands for Laser-Assisted in Situ Keratomileusis and is a procedure that permanently changes the shape of the cornea, the clear covering of the front of the eye, using an excimer laser (Fig.1.3). A knife, called a microkeratome, is used to cut a flap in the cornea. A hinge is left at one end of this flap. The flap is folded back revealing the stoma, the middlesection of the cornea. Pulses from a computer-controlled laser vaporize a portion of the stroma and the flap is replaced. With

this way, different focusing problems e.g. myopia or hyperopia are successfully encountered.

1.2 PHENOMELOGICAL DESCRIPTION AND MODELS

For the last 20 years, numerous papers describing this phenomenon were published. Despite the high research activity, the nature of UV laser ablation of polymers is still far from being fully understood, e.g., one can find contradictory interpretations of the same results in different papers. At least from the practical standpoint, the first aspect to consider concerns the efficiency and accuracy of material removal that can be attained with laser irradiation. This question is directly addressed by the examination of the etching curves (Fig.1.4)

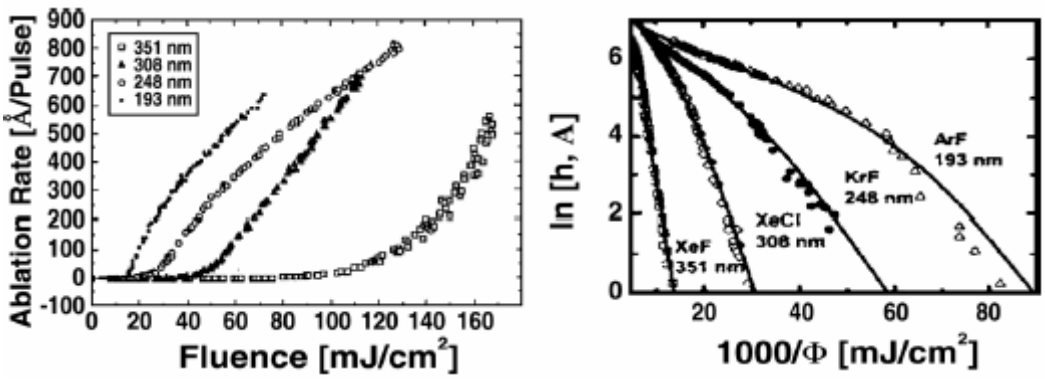

Figure 1.4: *a) On the left, thickness of ablated material per single laser pulse as a function of laser fluence for irradiation of polyimide with ArF, KrF, XeCl, and XeF excimer lasers. b) On the right, the same experimental points are presented in "Arrhenius" format (i.e., ln(h) vs $1/F_{LASER}$). The solid lines represent the best approximation to the experimental data clearly different sections can be delineated with different slopes[21].*

The term ablation/etching rate is often used to denote the material thickness removed per laser pulse. Various simple phenomenological models have been developed for describing the features of the etching curves. (i.e. for describing the amount of material removed as a function of the fluence). Two models have found most use in the literature, namely the so-called "steady-state" and "blow-off" models [12-20].

If it can be assumed that material removal occurs for fixed absorbed energy density (per unit mass), once a threshold fluence value (F_{thr}) is exceeded. This assumption results in the steady-state (or stationary) model [14-20]. In this case, the etching depth δ scales linearly with F_{LASER} :

$$\delta = \frac{F_{LASER} - F_{thr}}{\rho E_{cr}} \qquad \text{for } F_{LASER} \geq F_{thr} \tag{1.1}$$

where E_{cr} represents the critical energy per unit mass (sometimes denoted as ablation enthalpy [20]) and ρ is the density. The formula presumes that the rate of energy deposition is balanced by the rate of energy removal due to material ejection (which accounts for the "steady-state" nature of the model). For this balance to be attained, material ejection must start early on during the pulse. Thus, strictly speaking, this model is applicable for microsecond or longer laser pulses.

On the other hand, for nanosecond pulses, the equilibrium implied by Eq. (1.1) cannot be attained. In this case, it can be argued that material ejection is determined largely by the spatial distribution of the absorbed energy. The basic premise here is that for incident fluence, all material within a depth "exposed" to a fluence above a threshold value (F_{thr}) is removed. This assumption [12] results in the so-called "blow-off model" for nanosecond laser pulses. Assuming Beer's law for the absorption process, the dependence of etching depth (δ) on incident fluence is now given by:

$$F_{thr} = F_{LASER} e^{-a_{eff}\delta} \Rightarrow \delta = \frac{1}{\alpha_{eff}} \ln\left(\frac{F_{LASER}}{F_{thr}}\right) \text{ for } F_{LASER} \geq F_{thr} \tag{1.2}$$

where F_{thr} is the fluence transmitted at depth δ and α_{eff} is the (effective) absorption coefficient. F_{LASER} represents the incident laser fluence on the substrate, assuming no reflection. Thus the ejected material thickness increases gradually with increasing F_{LASER} (Fig.1.4); for this reason, it is also referred to as the "layer-by-layer removal" model. According to this model, what matters is the fluence absorbed at depth δ whereas the energy absorbed in the ejected layers is essentially wasted (largely transformed into kinetic energy of the ejected material).

According to Eq.(1.2), for high α_{eff}, sufficient energy is absorbed within a shallow depth to achieve efficient material removal, while penetration of light further into the bulk is much reduced, with a consequent limitation of any thermal and chemical

effects there. As a result, material is removed with minimal morphological change or other side-effects and a highly smooth surface may be obtained. This is usually described as *clean etching*.

According to either Eq.(1.1) or Eq.(1.2), the basic parameter characterizing laser removal processes is the *ablation threshold.* The ablation threshold corresponds to the minimum fluence required to achieve non-selective ejection of a volume of material. Generally, the ablation threshold F_{thr} scales as E_{cr} / a_{eff} (the proportionality constant depending on the units employed for E_{cr}. Thus, it depends strongly on the substrate absorptivity, while E_{cr} reflects the dependence on other substrate properties such as cohesive energy.

1.3 LIMITATIONS AND CAVEATS

Though convenient, the above functional dependences are largely idealizations based on specific assumptions and simplifications. Various processes contribute to the material ejection process and the exact shape of the etching curves may differ according to material and laser parameters [15]. Thus, it is understandable that Eq. (1.1) or Eq. (1.2) may not have a general applicability or may fail to describe the complete etching curve. For instance, closer examination reveals that sections of the etching curves (Fig.1.4) have different dependences: below the threshold, an exponential dependence may be obeyed, whereas, close to the ablation threshold, δ may scale linearly with $\left(F_{LASER} - F_{thr}\right)$ even for ns laser pulses (although the interpretation of this linear dependence may not be the one implied by Eq. (1.1)). In addition, other processes such as absorption of incident radiation by the ejected plume may affect the shape of the etching curves. In all, etching curves yield only limited insight into the underlying physical processes.

It is important to note that the parameter values in Eq.(1.1) and Eq.(1.2) are usually chosen empirically, since in most cases they cannot be directly related with

known material parameters. Thus, plots of δ vs. $\ln(F_{LASER})$ yield straight lines, as expected from Eq.(1.2), but in many cases, the slope deviates substantially from $1/\alpha_{eff}$.

Besides the above limitation, the measurement of the etching depth presents a number of subtleties. In particular, irradiation with successive laser pulses can result in different morphological changes and removal rates. UV irradiation can result in chemical modifications to the substrate, with a consequent change in the absorption coefficient and therefore reduction of the fluence necessary for material ejection. Thus, for F_{LASER} somewhat below the single-pulse ablation threshold, ablation may be induced after a certain number of pulses ("incubation effect")[12-15]. Likewise, for ablation at fluences slightly above F_{thr}, the thickness removed per pulse may vary with successive laser pulses, until a constant etching depth per pulse is attained. Thus, in determining the ablation threshold, it is crucial to specify the number of pulses used; unfortunately in practice, this dependence is often disregarded.

Furthermore, different techniques yield different values for etching depth. Profilometry is very easy to use, but the method is prone to errors because the irradiated surface may be highly irregular (in fact, for weakly absorbing systems exhibiting swelling at moderate fluences, it may be very difficult to determine the fluence at which etching actually occurs). If the etching depth is very small, the application of the technique may require a multipulse protocol, in which case, the measurement may suffer from the limitations discussed in the previous paragraph. On the other hand, measurements of mass loss by quartz microbalance have been shown to be sensitive even to mass loss due to fragment desorption; but this does not necessarily correspond to ablation [14,21].

Furthermore, many commercially available polymers absorb the laser light only in the far UV, where appropriate lasers are not intense enough or their operation is quite extensive. This drawback could be overcome by blending, doping or crosslinking the polymers with chromospheres which include absorption at longer irradiation wavelengths. This doping reduces the ablation thresholds at the longer irradiation wavelengths but the obtained structures revealed normally poor quality. An

understanding of the ablation process will help to improve the polymers designed for laser ablation.

1.4 MECHANISMS OF UV LASER POLYMER ABLATION

Originally, UV laser ablation of polymers was believed to be a pure photochemical effect, resulting from the direct bond breaking by UV photons [12, 13]. Gradually, investigators obtained evidence that laser heating of materials is significant and a pure thermal nature of laser ablation was considered [21].Polymers are complex materials; therefore, laser ablation of polymers is also a complicated phenomenon. In this section, we will focus on the models of laser ablation. In addition, we inevitably have to answer the question of what are the specific features of laser ablation of polymers that distinguish them from the laser ablation of other materials (metals, semiconductors, inorganic dielectrics, molecular solids).

It has been proposed that either thermal, photothermal, photochemical, or a combination of these mechanisms may be dominating the ablation process. The first step of the laser ablation process will in all cases be the absorption of the photons and the creation of excited states. A clear differentiation of the following pathways is very difficult as the results obtained by different measurement techniques are often quite different. For instance, measurements detecting the ablation depth with a stylus detected a sharp threshold of ablation, while measurements with quartz crystal microbalances (QCM) reveal an exponential increase which is also called Arrhenius tail.

An alternative method to distinguish the different models describing the laser ablation process is to divide them into surface and volume models [21]. The surface models describe the ablation only with processes occurring within several monolayers, while the volume models describe the mechanism with processes within the bulk of the material. The different models have thereby the following properties:

• Photochemical surface model: these are only valid for higher irradiation fluences and longer pulse lengths.

• Thermal surface models: these models can describe the Arrhenius tail but can not describe the sharp ablation thresholds.

• Photochemical volume models: predicts a sharp ablation threshold and linear dependence of ablation rate with the logarithm of the laser fluence. This model does not explain the Arrhenius tail observed in measurements with the QCM.

The ablation process follows an Arrhenius-like thermal decomposition of the polymer and assumes that a certain number of bonds have to be broken before ablation is observed. This model predicts an Arrhenius tail and a sharp ablation threshold. This model has only been applied to polyimide and some of the applied parameters were calculated with temperature coefficients which were obtained for slow heating rates (several K s^{-1}). It is still unclear whether this model is also valid for other polymers and if the temperature coefficients are the same for the heating rates occurring during ablation. None of the above described models can describe all observed effects during ablation process for the different polymers and it is difficult to attribute the ablation process to a single model by only measuring the ablation rates.

1.4.1 The photothermal mechanism

Following absorption, a good part of the absorbed energy – at least for irradiation with typical nanosecond pulses – will be converted into heat. The extent of the subsequent heat diffusion is described in terms of *thermal diffusion length,* $l_{th} = 2(D_{th}t)^{1/2}$ or in terms of *thermal diffusion time*

$$t_{th} = \frac{1}{D_{th} \cdot \alpha_{eff}^2} \tag{1.3}$$

Here, D_{th} is the thermal diffusivity and α_{eff} is the effective absorption coefficient. Consider now that the material at the attained temperatures thermally decomposes [22-27]. Thermal decomposition (typically a unimolecular reaction) usually follows an Arrhenius equation with a rate constant, $k(T) = Ae^{-Eact/R_G T}$, where A is the pre-exponential factor, E_{act} is the activation energy and R_G is the universal gas constant. For organic material, typically, $A \sim 10^7$-10^{10} sec^{-1}, $E_{act} \sim$ 50-200 kJ/mole. For a specific thermal transient, the number of bonds thermally decomposed up to time t can be

expressed as $N_D(t) = \int_0^t A \exp\left(-\frac{E_{act}}{R_G T(t')}\right) dt'$. If the decomposition results in small enough fragments or oligomers, that have a small binding energy to the matrix, these can desorbs in the gas phase. By doing so, they remove energy, thereby lowering the substrate temperature.

Fig.1.5b shows the temperature evolution with depth in a polymeric substrate following irradiation at three different fluences. For nanosecond or shorter laser pulses at high enough fluences, decomposition and material removal occurs fast enough that heat diffusion to the substrate is minimal. On the other hand, for microsecond laser pulses, heat diffusion and the consequent thermal degradation in the substrate is extensive enough. This can be more precisely expressed in terms of

$$t_{th} = \frac{1}{D_{th} \cdot \alpha_{eff}^2} >> \tau_{pulse} \qquad \textit{(thermal confinement)}$$

Thus, for the *photothermal mechanism* of ablation, ablation is exclusively due to the thermal decomposition and desorption of material.

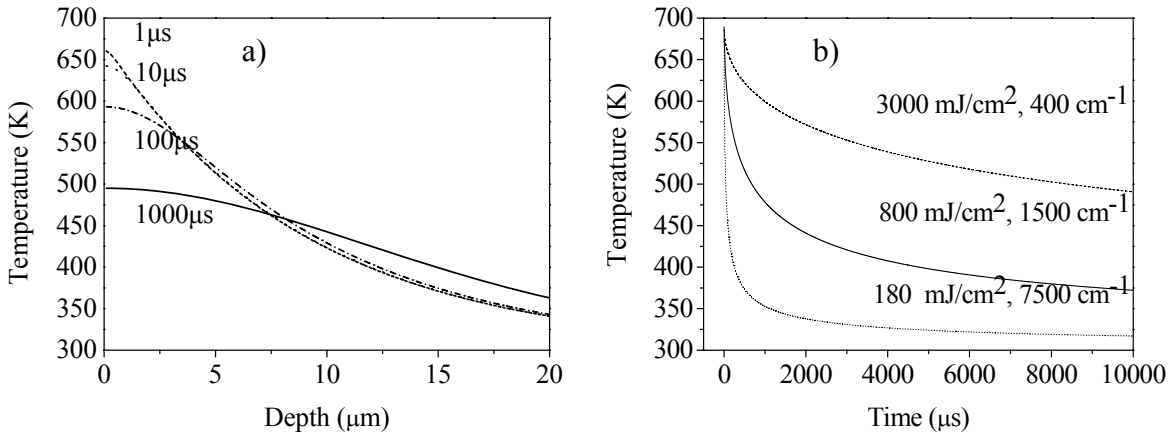

Figure 1.5: *a) Temperature profile in doped polymer as a function of depth at different times after the laser pulse. The absorption coefficient is assumed to be* α *=1100cm*$^{-1}$*.*F_{LASER}*=0.5J/cm*^{2}*. b) Temperature profile at the surface of doped PMMA for different combinations of fluence and absorption coefficients.*

In this case, the minimum energy (per unit mass) or per unit volume required for material ejection is given by $E = c_P \Delta T + \Delta H_{transf} + \Delta H_{diff}$ where the first term represents the energy required for heating a mass to its decomposition temperature T,

ΔH_{transf} represents the energy required for polymer decomposition and desorption of products to the gas phase and ΔH_{diff} is the energy lost by heat diffusion to the sub-layers. Accordingly, $F_{thr} = \frac{E_{cr}}{a_{eff}} \Rightarrow F_{thr} = \frac{C_p \Delta T + \Delta H_{transf} + \Delta H_{diff}}{a_{eff}}$. Thus a high thermal diffusivity, D_{th}, results in high heat losses to the sublayers with a consequent increase in the ablation threshold. More detailed analytical description [14, 21, 28] can be obtained by considering the heat diffusion equation. In this case $\frac{dT}{dt} = V\frac{dT}{dz} + \frac{K}{\rho C_p}\frac{d^2T}{dz^2} + \frac{\alpha_{eff}\mathrm{I}}{\rho C_p}$ where V is the rate of material removal, K is the heat conductivity, ρ is density, C_p is heat capacity, I the laser intensity and z the depth (distance) from moving interface (with z=0 corresponding to the surface). The first boundary conditions is $\mathrm{K}\frac{dT}{dz}\Big|_{z=0} = \rho V \Delta \mathrm{H}_s$ which describes the change of the temperature at the surface due to the energy removed by the desorbing material (ΔH_s is the enthalpy for polymer to gas transformation). The second boundary condition is that T at $z \to \infty$ and T at t=0 are both equal to the initial room temperature). The rate of material removal is assumed to be $V=V_0\exp(-E_\alpha/k_B T_s)$. The enthalpy form of the heat equation is usually employed because of its convenience in dealing with phase changes including melting. Written in the frame of reference of the receding surface (assumed to be along the z-direction), this becomes:

$$\frac{\partial H}{\partial t} - \upsilon_{\mathrm{int}}\frac{\partial H}{\partial z} = \frac{\partial}{\partial z}\left(\xi\frac{\partial T}{\partial z}\right) - \frac{\partial(Ie^{-\alpha_{\mathrm{eff}}z})}{\partial z}, \text{ where } H(T) = \rho\int_{T0}^{T} C(T')dT \qquad (1.4)$$

Where ξ is the thermal conductivity, υ_{int} the interface velocity and the boundaries conditions concerning e.g. the energy loss at the surface due to material removal. Satisfactory solution has been obtained only for ablation with long pulses, in which case a steady-state condition is attained as in Eq.(1.1) where the rate of material removal during the laser pulse is constant. However, this condition is hardly reached in the irradiation with ns pulses. The approximations necessary for solving the equation for the non-stationary case have been discussed amply in the literature [21]. In this case the rate at which material is removed is

specified either by the temperature attained at the surface or by the condition that the surface concentration of broken bonds reaches a specific level. The former condition leads to the so-called "surface" photothermal model, whereas the latter one leads to the "volumetric" photothermal model. The applicability of each particular model depends on the substrate absorptivity, with the surface model being more appropriate for substrates of a very high absoprtivity (e.g., metals), whereas the volume model for substrates of somewhat lower α . Despite any approximations and shortcomings, this "volume" photothermal model has been most successful in explaining various experimental aspects of polymer ablation. For further information on these formulations, the reader is referred to [21].

1.4.2 Explosive boiling

For metals, semiconductors and same simple molecular solids, a mechanism that has become quite favourable is that so-called *explosive boiling*. For a simple compound, the processes can be understood in terms of the usual (P, T) thermodynamic diagrams. For a slow heating process, the system follows the binodal and the liquid-gas transition can be described as vaporization. The transition is well described by the Clausius-Clapeyron equation $P \approx P_0 \exp\left[-\frac{\Delta H_{vap}}{R_G}\left(\frac{1}{T}-\frac{1}{T_0}\right)\right]$, where P represents the pressure at temperature T and P_0 the reference pressure at reference temperature T_0, (usually T_0 the boiling point at P_0 = 1 atm).

According to Gibbs thermodynamic theory there are two limits to the existence of the condensed phase; the binodal line, the equilibrium curve (P, T) for the liquid and vapour, and the spinodal line, the boundary of thermodynamic stability of the liquid phase. The spinodal line is defined by the condition $-(\frac{\partial P}{\partial V})_T = 0$, $(\frac{\partial T}{\partial S})_P = 0$ which is a physical impossibility. Between these boundaries there is a region of metastable (superheated) liquid. In crossing the spinodal line loss of stability of the liquid phase occurs, with the spontaneous disintegration of the system in to a two phase, consisting of individual gas molecules and liquid droplets (Fig.1.6).

Alternatively, the metastability can be understood in terms of the barrier to the formation of bubbles as necessary for boiling. The creation of homogeneous vapour nuclei in a defect-free volume of the superheated volume is accompanied by an increase in the Gibbs free energy. In the formation of a spherical critical nucleus this increase is $\Delta G_k = \frac{16\pi\sigma^3}{3g^2}$ the parameter g characterizes the depth of penetration into the region of metastable states. A given metastable state at the point (P_o, T) can be reached by raising the temperature from T_o to T at constant P_o (T_o is the boiling point at the pressure P_o). In that case, $\Delta G_k = \frac{16\pi\sigma^3}{3(\rho_o\lambda_o\beta)^2}$ where ρ_o is the density of saturated vapour, λo is the specific heat of vaporization at the point (P_o, T_o) and $\beta=(T-T_o)/T_o$ is the relative superheat. Under stationary conditions, the rate of nucleus formation of homogeneous nucleation at a temperature T is given by $J = B\exp(-\Delta G_k / k_B T)$ where B is a function which depends weakly on temperature and pressure in comparison with the exponential factor. The nucleation rate *J(t)* under nonstationary conditions is related to J by $J(t) = J \times \exp(-\frac{t}{\tau})$ where *t* is the time and τ is the time for establishment of stationary nucleation after instantaneous superheating of the system.

According to the previous, at low rates of heat deposition no significant superheating of the liquid is achieved, since practically all the heat goes into the growth of heterogeneous vapour nuclei (ordinary boiling) which arise in the liquid at pre-existing centers (impurity). At very high heating rate (as those that may be attained by laser heating) the time for vaporization and thus the mass of material which is vaporized within heterogeneous nuclei (suggested to be ≥ 1μs) will be insignificant; therefore, the achievement of high superheating close to the spinodal line may be possible. This possibility, in relation with laser damage of metals was first advanced by Martynyuk [43] but little attention was given to it. The last years [44, 45], through the parallel contribution of molecular dynamics simulations and thermodynamic considerations it has been suggested that the explosive boiling mechanism may be feasible in laser irradiation of molecular solids.

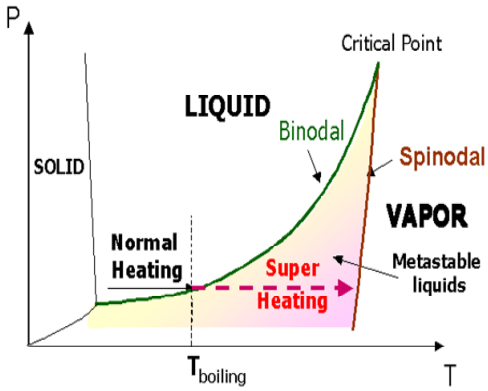

Figure 1.6: *Typical (P, T) thermodynamic phase diagram. Illustration of explosive boiling concept.*

However, the liquid-gas transformation requires the formation of gaseous bubbles. Their formation is energetically costly, as energy is required in order to form the necessary interface. The required energy is specified by the surface tension σ of the compound. The overall work (W) necessary for the formation of a bubble of radius r is $W = \frac{4\pi r^3}{3}(\mu_v - \mu_l) + 4\pi r^2 \sigma$, where the first term, expressed in terms of the chemical potentials of the compound in the gas and liquid phases, gives the "driving" energy, whereas the second term represents the required energy (work) for interface formation. The rate of bubble nucleation scales as $e^{-W/k_B T}$. The ratio of the two terms $\frac{\frac{4\pi r^3}{3}(\mu_v - \mu_l)}{4\pi r^2 \sigma}$ scales as $(1/r)$. So for very small r, the surface tension term is much larger than the driving force (with W having large positive value). As a result, formation of nuclei is a rather slow process (microseconds to milliseconds). The implication is that for ns laser pulses, the system can be heated to temperatures much higher than its boiling point, before bubble growth occurs. With increasing T, the driving force eventually becomes sufficiently high to overcome the surface tension limitation, i.e., the nuclei formation rate becomes competitive with the heating rate. These results in "abrupt" liquid-gas phase transformation and accounts for the explosive character of laser ablation. An example of the applicability of these concepts can be found in laser ablation of metals, semiconductors, organic liquids, steam laser cleaning etc [29-32].

However, the extension of the concept to more complex systems, such as polymers, is not yet well-defined. The reason for this is simple: with increasing molecular complexity/size, thermal decomposition sets in at lower temperatures than the temperature for liquid-gas phase equilibrium. Thus, strictly speaking, it is not possible to define the degree of "overheating" in relationship to a reference phase transformation temperature. Nevertheless, the term is sometimes indiscriminately used to describe the ablation of complex substrates. The reader is cautioned that this is not fully validated scientifically.

1.4.3 The photomechanical mechanism

Laser irradiation can result in the development within the sample of stress waves with amplitudes of several hundred bars [33-37]. These stress waves may be generated in different ways. Normally, these high temperatures due to rapid heating suggest thermal expansion of the substrate. But this may not be feasible at the very high heating rates involved with nanosecond or shorter laser pulses. Therefore heating may occur under nearly constant volume (isochoric) condition. This situation results in a pressure rise given by

$$\Delta P = \frac{\beta \alpha F_{LASER}}{\rho \kappa_T C_V} \left(\frac{1-e^{-\theta}}{\theta}\right) \tag{1.5}$$

where β is the thermal expansion coefficient, C_V is the heat capacity at constant volume, κ_T is the isothermal compressibility and $\vartheta = \tau_{pulse} / \tau_{ac}$, where $\tau_{ac} = 1/c_s \alpha$ (c_S is the speed of sound) is the time required for an acoustic wave to traverse the irradiated thickness. The factor in parenthesis corrects for the reduction in the stress amplitude due to wave propagating out of the irradiated volume during the laser pulse (assumed to have a rectangular time profile). This pressure rise results in three waves (appropriately, termed *thermoelastic*) propagating through the material: a radially propagating cylindrical wave, which can usually be neglected for beam diameters (mm to cm) substantially wider than the light penetration depth (typically few micrometers), and two plane waves counter-propagating along the beam axis (one towards the surface and

the other into the sample). The wave that travels towards the free surface (substrate/air interface) suffers a change of amplitude sign upon reflection from it, due to the higher acoustic impedance of the irradiated medium, ρc_S , than that of air. Physically, the thermal expansion directed into the medium generates compression stress whereas the outward expansion generates tensile stress (rarefaction wave) (Fig.1.7). Thus, the axial wave produced by this mechanism is bipolar as evidenced in measurements by piezoelectric transducers attached to the substrate (Fig.1.8).

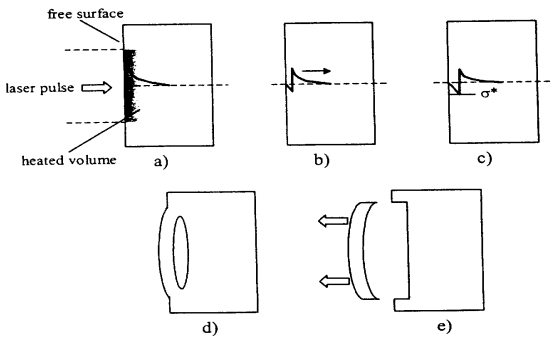

Figure 1.7: *Schematic illustrating the photomechanical mechanism. The stress wave signal of material removal developed by thermoelastic mechanism (a-c) at some depth the tensile strength σ* is exceeded and the material fractures, (d, e) detachment and ejection of material from the front surface [34].*

The faster the heating, the higher the magnitude of the generated thermoelastic stress in the medium, with the ultimate efficiency attained for heating time much faster than the time required for stress to propagate through the irradiated depth, i.e., for $\tau_{pulse} < 1/\alpha_{eff} c_s$ ("stress confinement regime").

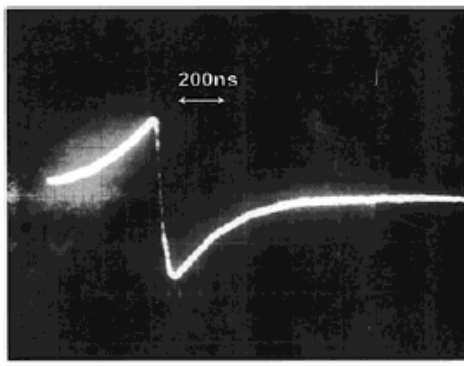

Figure 1.8: *Thermoelastic stress wave signal recorded using a PVDF film transducer for PMMA irradiated with the 308 nm XeCl laser. Laser pulse duration t_p=24 ns, fluence F= 10^3 J m^{-2}, PMMA absorption coefficient α=1500 m^{-1}.*

Another source of stress waves derives from expansion of any gases produced by thermal or photochemical decomposition within the substrate [34]. This factor, for instance, has been invoked to account for the transient stresses of about 0.1 MPa detected in the UV irradiation of polyimide below the ablation threshold [36]. In the case of doped- *PMMA* irradiation with 150 ps pulses at 1064 nm, the thermoelastic mechanism and the expansion of decomposition by-products contribute about equally to the generated pressure at the ablation threshold [35].

If the pressure wave amplitude exceeds the substrate tensile strength, (defined as the minimum tension pressure required for material fracture) then it can result in ejection of material essentially via fracture (Fig.1.7) ("photomechanical mechanism" of ablation). Since fracture can occur without the overheating of the material implied by the thermal mechanism, it offers the possibility for "cold" ablation. As a result, it has attracted much attention, in particular in medical applications. Indeed, the operation of a photomechanical-based ablation can be significant in the nanosecond laser irradiation of liquids, as well as in soft tissues (largely because of their low tensile strength). On the other hand, for (thick) polymeric substrates (i.e. in the absence of interfaces), for typical UV *nanosecond* pulses, the generated stress waves turn out to be rather weak for being exclusively responsible for material ejection.

For irradiation above the ablation threshold, a third source of stress wave relates to the back momentum exerted by the ejected material (independently of the mechanism responsible for its ejection). This results in a compressive wave propagating through the substrate. The peak stress amplitude (and its scaling with incident fluence) depends on the time scale of material removal, as well as on the nature of the process. At even higher fluences where plasma formation becomes significant, the pressure relates to the plasma expansion, in which case $P_{\max}$ scales as $F_{LASER}{}^{3/4}$.(Fig.1.9).

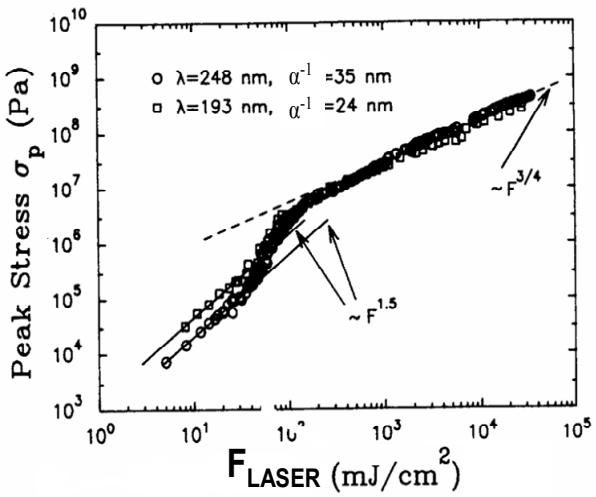

Figure 1.9: *Peak pressure generated in polyimide (measured via piezoelectric film coated on the substrate) vs. F_{LASER} for excimer irradiation at the indicated wavelengths. The abrupt change in slope is due to the onset of ablation* [36].

1.4.4 The photochemical mechanism

According to this mechanism, UV ablation of molecular solids is intricately related with the cleavage of chemical bonds and formation of new products. In its simplest version, the photochemical mechanism assumes that material ejection from molecular systems occurs when the number of broken bonds exceeds a critical value $N_D(z) = \eta \times \frac{\sigma N F_{LASER}(z)}{h\nu} \geq N^{cr}_D$ where η is the quantum yield and N the total number density of absorption centers (chromophores), i.e. if $N_D\ (z \leq \Delta z) \geq N^{cr}_D$. Then we obtain from Beer's law that $\Delta z = \frac{1}{\alpha} \times \ln(\frac{F}{F_{thr}})$ with $F_{thr} \propto \frac{h\nu}{\eta\alpha} N_D^{cr}$. Presumably the formation of a large number of photofragments with high translational energies results in material ejection. However, there is no criterion usually in specifying the critical number of bonds to be broken. A different scenario is that the fragments that are formed in the photolysis produce gases (e.g. CO_2, CH_4) by reactions with surrounding molecules. In that case, material ejection is due to the high pressures that are exerted by the expanding gases in the underlayers.

The photochemical mechanism was advanced in order to account for the clean etching observed with UV laser pulses as compared with IR pulses. According to this

model, because photon energy is largely "consumed" in bond dissociations, heat generation and diffusion is minimal. Because of its simplicity, this model became quite popular in the field and an overly used explanation, especially in applications. However, even for simple, well-defined molecular systems, it has turned out very difficult to assess the contribution of such a mechanism. In fact, the issue of photochemical vs. thermal mechanisms has been the most hotly debated one in the field of ablation.

More recent theoretical and experimental work, suggests that although the extreme view of the exclusive contribution of a photochemical mechanism is unlikely, still chemical processes like bond decompositions may result in the disruption of the substrate structure, thereby facilitating material ejection. Furthermore, besides the pressure exerted by any gaseous by-products, heat released by exothermic reactions effectively contributes to material ejection. Thus, the ablation threshold is estimated to be at lower fluence than it would be in the absence of such reactions. Given all these controversies even for relatively simple polymers, it is very difficult to be sure that a photochemical mechanism is applicable in the irradiation of the chemically complex materials.

1.5 MOLECULAR DYNAMICS SIMULATIONS

Recently B.J. Garrison have employed molecular dynamics simulations to examine the processes upon laser irradiation of PMMA [38,39]. This is not actually a new model (i.e., something new in addition to the previous models described in previous section); but rather the use of simulations for assessing the contribution of the various factors described/advanced by the analytical models.

The simulations are based essentially on a "breathing-sphere model" of the atoms, atoms/monomers are represented by spheres that have a single vibrational degree ("breathing") and are connected with each other with rigid bonds (or springs). To investigate the role of photochemical processes, the model is appropriately modified to

allow photon absorption to break a chemical bond in the molecule, breaking into radicals who can subsequently undergo abstraction and recombination reactions.

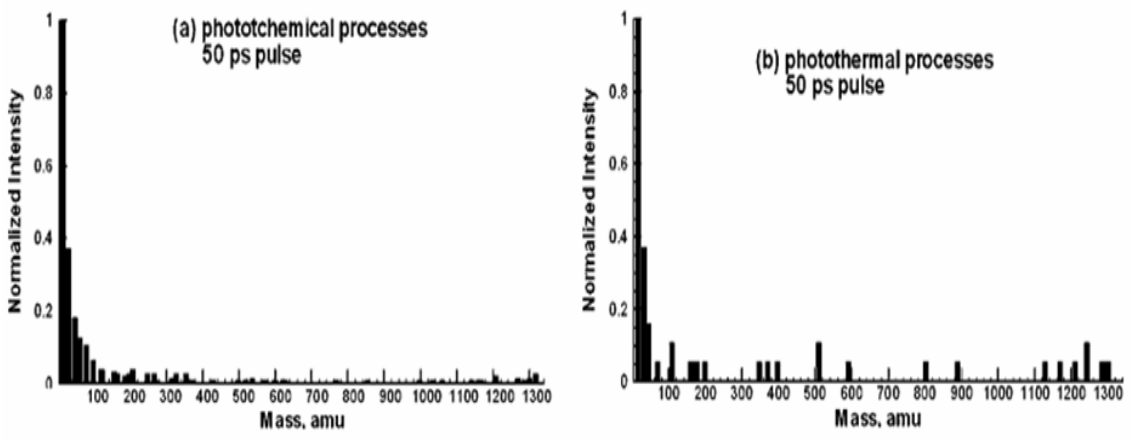

Figure 1.10: *Normalized intensity of emitted particles versus mass for (a) photochemical processes and (b) photothermal processes. One MMA group has a mass of 100 amu [39].*

On the basis of this approach, the team first estimated the enthalpies and the activation energies for various reactions that may take place upon UV laser photoexcitation. Subsequently, they examined how the results (e.g. ablation threshold, nature of ejecta, ejecta translational distributions) would be affected by contributions) would be affected by the contribution of thermal and of (photo)chemical processes [39]. A major result of their simulations is that exothermic reactions of the various radicals liberate energy that can be effective in promoting material ejection (i.e., this contribution result in a lowering of the ablation threshold). A particularly interesting result is the fact that for thermal mechanism, the plume includes particles of relatively high mass (even up to few 1000 Daltons), whereas ejection of large particles (Fig.1.10) is minimal for a “pure” photochemical mechanisms. Furthermore, they find that developed pressure in the substrate plays an important role in material ejection.

1.6 PREVIOUS WORK ON THE INFLUENCE OF POLYMER MOLECULAR WEIGHT

In the previous studies focused mainly on the examination of processes at low laser fluences. Masuhara, Fukumura and coworkers [40] have examined in detail the

dynamics of laser-induced expansion and contraction of different Mws poly(methyl methacrylate) (PMMA) and polystyrene via time-resolved interferometry. They found that the time-scale of these processes depend sensitively on polymer Mw. This dependence was ascribed to the different initial state of the examined polymers; the low Mw polymers being in rubbery state at room temperature, whereas the high Mw ones in glassy state. Thus, the polymers are characterized by different thermal expansion coefficients and also plausible differences in the entanglement state.

In the previous studies focused mainly on the examination of processes at low laser fluences. At higher fluences at which material removal, via desorption or ablation, becomes important, the polymer Mw can be expected to exert a more pronounced influence. In particular, Mw determines the number of bonds that must be broken and thus the value of the ablation threshold, as well as the rate of formation of monomer/oligomer that desorb and thus the rate of energy removal. Indeed, in an early study, Lemoine et al. [41] noted that in the 248 nm ablation of polystyrene films, the polymer Mw influences the "incubation behavior". More informative is the study by Lippert et al.[42], who found that for doped PMMAs at 308 nm, the etching rate of 500 kDa PMMA is ~10% higher than that a ≈97 kDa sample. We have observed a similar trend in a preliminary examination of ablation of doped PMMAs at 248.

1.7 SCOPE OF THIS WORK

1.7.1 Experimental methodology for temperature and viscosity estimation

In this work the thermal and structural changes effected to a wide range of Mw PMMAs upon ultraviolet irradiation; are assessed via the examination of the formation yields of the products formed by the photolysis of iodoaromatics (iodonaphthalene and iodophenanthrene -ArI-) dopants. It is also important to note that, the species remaining in the substrate following irradiation are monitored, so that the interpretation of the results is free from the complications plaguing gas-phase studies. Specifically, the aryl (Ar) radicals produced by ArI photolysis may abstract a hydrogen from the polymer to form ArH, i.e. via a (thermally) activated process. Therefore, the yield and the kinetics

of ArH product reflect the temperature evolution in the substrate following irradiation. In addition, at least for the NapI dopant, biaryl species (1,1-binaphthalene - Nap_2 – and perylene) are also detected. For the employed dopant concentrations, these species are formed via diffusion-limited reaction. Consequently, their formation affords a direct experimental probe of the extent of the substrate melting upon laser irradiation (in contrast to the usual approach, in which laser-induced melting is largely inferred by indirect morphological examination).

In the following, the presentation develops as follows: In chapter 3 we describe the application of the methodology in PMMA and PS at the 3 excimer wavelengths. This presentation, on one hand, illustrates the potential/methodology of using dopants for assessing the temperature and viscosity changes upon laser irradiation- on the other hand, it provides an overview of the processes for PMMA and PS. As it will be seen, initial studies on PMMA and PS at the 3 excimer wavelengths suggested a thermal mechanism to operate. However, there are a number of features that are not fully compatible with a simple thermal process. The main problem is that by changing wavelength, the optical parameters change significantly and thus comparison between experimental and theoretical results is not as strict/unique.

As described clear from the previous presentation, there are a number of different models/hypotheses that have been advanced to describe the mechanisms for material ejection induced upon UV laser irradiation. The main competing models are to distinguish between photothermal and photochemical ones. Because the experimental results are largely phenomelogical, e.g. etching rate measurements, simple morphological characterization of the irradiation spot, etc it is very difficult to decide between these models. Clearly, a major observable that is needed would be monitoring (assessment) of the temperatures developed in the substrate and in case of melting (as suggested by the thermal models) monitoring/ assessment of the viscosity changes.

The temperature may by monitored by using thermocouple attached to the substrate. This has been attempted in few studies, but various limitations of the technique became evident. One major problem is that necessarily there is some distance between the thermocouple and the optical penetrated depth (bulk), so that the temperature actually measured is due to heat diffusing to the attachment point; thus, an extrapolation has to be made to estimate the actual temperature within the irradiated

spot. As for the viscosity monitoring, there is no simple physical technique for its measurement with the temporal resolution (μs-ms) required for the laser-induced processes.

1.7.2 Examination of the influence of polymer Mw

For overcoming these limitations and attaining a more detailed examination of the process, we have turned to the study of the influence of polymer molecular weight on the laser irradiation-induced process. The reason for this is that in the comparison, the basic chemical composition of the polymer is the same, so that questions relating to the extent of chemical processes contributing to the laser ablation are simplified. Thus the major difference is the number of bonds between monomers; for a simple thermal process which proposes that material is removed by breaking the bonds between monomers, we conclude that with increasing molecular weight, the efficiency of material removal should decrease (since more bonds must be broken). On the other hand, for a photochemical mechanism, the nature of the fragmented side groups should not depend on Mw; however, even for a photochemical process may exhibit some dependence on Mw, because the Mw affects the cohesive energy of the system (that is the energy of interactions between the chains) so that larger chains may require higher pressures in order to be ejected in the gas phase.

Chapter 4 applies the previous methodology for examining the influence of Mw exerts a strong influence on the laser induced processes, but the extent of the influence depends also on the absorptivity.

For understanding further the above importance of absorptivity, in chapter 5, have used a number of techniques for examining the nature of the ejecta and the translational distributions of the ejected material. In particular, we find that the nature/size of the ejecta show unexpected and pronounced dependences on the molecular weight.

Chapter 6 provides the theoretical model for explaining for the influence of Mw on laser-induced processes. In particular, it leads to a new, more elaborate description of the laser ablation of polymers, namely to the introduction of the explosive boiling of polymers.

Finally, chapter 7 describes preliminary corresponding studies on the ablation of polymers with sub-picosecond (500 fs) UV laser pulses. It is shown that chemical processes differ distinctly from the ones in irradiation with nanosecond laser pulses. A preliminary model is presented.

1.8 REFERENCES

1. P.E. Dyer: Laser Ablation of Polymers, in *Photochemical Processing of Electronic Materials*, ed. by I.W. Boyd, R.B. Jackman (Academic, London 1992).
2. M.C. Gower: In *Laser Processing in Manufacturing*, ed. by R.C. Crafer, P.J. Oakley (Chapman and Hall, London 1993).
3. F. Bachmann: Chemtronics **4**, 149 (1989).
4. J.R. Lankard, G. Wolbold, Appl. Phys., **A54**, 355, (1992).
5. J.H. Brannon, T.A. Wassick: Proc. SPIE **2991**, 146, (1997).
6. H.M. Phillips, D.L. Callahan, R. Sauerbrey, G. Szabo, Z. Bor, Appl.Phys. A., **54**, 158, (1992).
7. D.L. Pugmire, E.A. Wadell, R. Haasch, M.J. Tarlov, E. Locascio, Anal.Chem. **74**, 871, (2002).
8. T. Lippert, C. David, M. Hauer, C. Phipps, A. Wokaun: Rev. Laser Eng. ,**29**, 734, (2001).
9. J.H. Brannon, A.C. Tam, R.H. Kurth, J. Appl. Phys., **70**, 3881, (1991).
10. F. Barnier, P.E. Dyer, P. Monk, H.V. Snelling, H. Rourke, J. Phys. D **33**, 1, (2000)
11. S.R. Farrar, A.E.A. Conteret, M. O'Neill, J.E. Nicholls, A.J. Eastwood, S.M. Kelly, Appl. Phys. Lett., **76**, 2553, (2000).
12. R .Srinivasan, and B. Braren, Chem Rev, **89**, 1303, (1989).
13. R.Snirivasan, Laser ablation principles and applications, in Miller , J.S., Springer Ser Muter, Springer-Verlag, Berlin, 1994.
14. D.Bauerle, *Laser Processing and Chemistry,* 3rd ed., Springer-Verlag, Berlin, 2000
15. P. Dyer, *Appl. Phys. A Mater.,* **77**,167, (2003).
16. S. Georgiou,and F. Hillenkamp, *Chem. Rev.,* **103**, 317 (2003).
17. T. Lippert and T.J Dickinson,. *Chem. Rev.,* **103**, 453, (2003).
18. K. Dreisewerd, *Chem. Rev.,* **103**, 395, (2003).
19. L.D. Laude, *Excimer Lasers,* Kluwer Academic, Dordrecht, (1994).
20. A.Vogel and V.Venugopalan, *Chem. Rev.,* **103**, 577 (2003).
21. N. Bityurin , et al., Models for laser ablation of polymers, *Chem. Rev.,* **103**, 519, (2003).
22. H Schmidt,J Ihlemann, and K.E.A Luther, *Appl. Surf. Sci.,***139**, 102, (1999).
23. H Schmidt, J Ihlemann, and B Wolff-Rottke, *J. Appl.Phys.,* **83**, 5458, (1998).
24. V. Venugopalan, N.S Nishioka, and B.B.Mikic, *Biophys. J.,* **69**,1259 (1995)
25. N.Bityurin, et al., *Appl. Surf. Sci.***127–129**, 164, (1998).
26. I.Y.S.Lee, et al., *J. Appl. Phys,* **72**, 2440, (1992).

27. S. Kuper, J. Brannon, and K.Brannon, *Appl.Phys. A.* **56**, 43, (1993).
28. J.H.Brannon, A.C.Tam, and R.H Kurth, *J. Appl. Phys.,* **70**, 3881, (1991).
29. K.Dongsik, H.K Park, and C.P.Grigoropoulos, *Int. J. Heat Mass Trans.* **44**, 3843, (2001).
30. O.J.Yavas, et al., *Phys. Rev. Lett.,* **72**, 2021, (1994).
31. Y.P.Lee, et al., *Jpn. J. Appl. Phys.* **37**, 2524, (1998).
32. A.C.Tam, H.K Park, and C.P Grigoropoulos, *Appl. Surf. Sci.,* **127/129**, 721, (1998).
33. V.E Gusev, and A.A.Karabutov, *Laser Optoacoustics,* American Institute of Physics, New York, (1993).
34. G. Paltauf, and P.E Dyer, *Chem Rev.,* **103**, 487, (2003).
35. E Hare, et al., *J. Appl. Phys,* **77**, 5950, (1995).
36. A.D Zweig, V.Venugopalan, and T.F Deutch, *J. Appl. Phys,* **74**, 4181, (1993).
37. S Siano, R.Pini, and R.Salimbeni, *Appl. Phys. Lett.* **74**, 1233, (1999).
38. P.F Comforti, B.J. Garrison,Chem Phys Lett., **406,** 294, (2005).
39. Y.G. Yigling, B.J. Garrison, J Phys Chem B., **109**, 16482, (2005).
40. T. Mascubusci, et.al., J Phys Chem B., **105**, 2518, (2001).
41. P.Lemoine, W.Blau, A.Drury, C.Keely, Polymer, **34**, 5023, (1993).
42. T.Lippert, et.al., Makromolek Chem. **213**, 127, (1999).
43. M.M.Martynyuk, Combust Explos. Shock waves **13,** 178, (1977).
44. A. Miotello, R.Kelly, *Appl. Phys. Lett.* ***67***, 3535, (1995).
45. A. Miotello, R.Kelly, *Appl. Phys.* ***A 69***, S67, (1999).

Chapter 2 EXPERIMENTAL TECHNIQUES

2.1 SAMPLE PREPARATION

A wide range of molecular weight is examined. In particular, we use PMMA molecular weights on average Mw ~80 kDa, 120 kDa, 212 kDa, 996 kDa from Aldrich and from Polymer Standard Service on average Mw ~2.5 kDa, 23.2 kDa. In the case of PS we use on average Mw ~532 kDa, 280 kDa, 15.2 kDa from Aldrich. The higher molecular weights were subjected to extensive purification for removing fluorescing impurities that are found to interfere with photoproduct emission measurements. Bromo- and iodonaphthalene (Aldrich) are purified by flash chromatography. 1.1-binaphthyl and perylene (Aldrich) are employed as received. Samples are prepared by casting on quartz plates solutions of the polymer and of the dopant in dichloromethane. The samples are dried initially in air and then in vacuum for 24 hr. For the low polymer Mw samples, we have observed cracking after few hours of drying due to the weak interface adhesion forces between polymer-substrate (due to low polymer viscosity). Cracking characteristics were more obvious using dichloromethane. To this end, we used toluene with slower rate of vaporization. The film thickness is typically in the 20-50 μm range, as measured by profilometry (Diftek).

For the employed concentrations/thickness, the substrates are “optically thin” at the probing wavelength; thus the fluorescence intensity is directly proportional to the product amount formed (i.e., minimal self-absorption effects). However, at higher fluences, the fluorescence quantification may be inadvertently affected by the morphological changes resulting in enhanced scattering of the probe beam. Time-resolved transmission/reflection examination shows that the morphological changes are completed faster than the chemical processes probed here, so their influence on the fluorescence measurements (at a single fluence) can be considered constant. On the other hand, the fluorescence measurements at different fluences may be affected to a different extent.

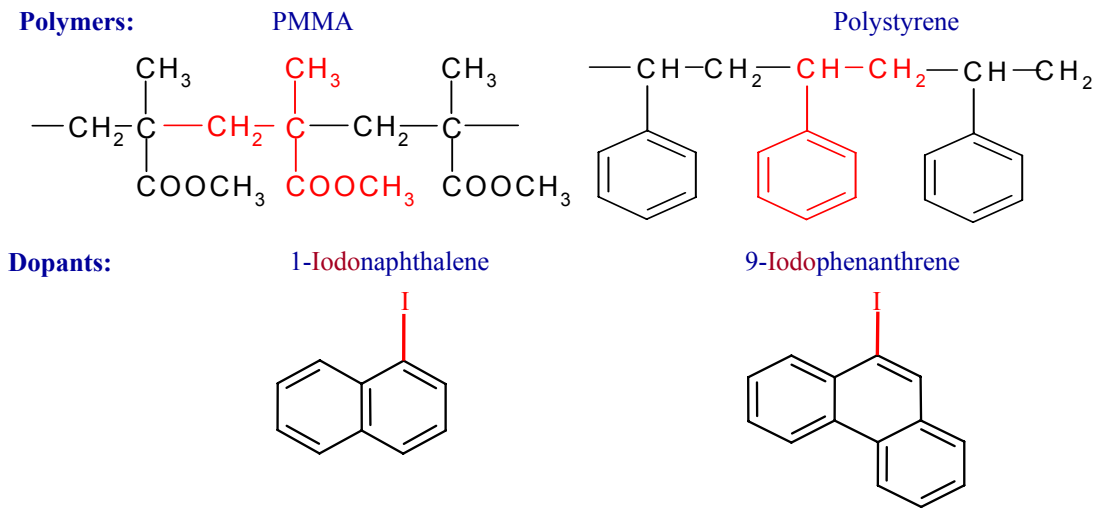

Figure 2.1: *Chemical structure of examined polymers and dopants.*

Surface morphology of the irradiated substrates is examined by profilometry. For the examined weakly absorbing systems, a fluence range can be delineated in which swelling of the polymer is affected. Swelling of weakly doped PMMA upon irradiation at 248 nm or PS at 308 nm at fluences below the ablation threshold has been well documented in the literature. Ablation, i.e. macroscopic removal of material, is effected at higher fluences. The thresholds for swelling and etching determined for the various systems are collected in Table 1 and Table 3.

2.2 TIME RESOLVED LASER INDUCED FLUORESCENCE (LIF)

Experimentally, the study takes advantage of the fact that the haloaromatics precursors (ArI) do not fluoresce, whereas the aryl-deriving photoproducts are relatively "good" emitters. Thus, photoproducts can be characterized and quantified via laser-induced fluorescence (LIF). LIF is employed for the detection of the aryl products that *remain in the substrate* following irradiation. (ArI do not fluoresce, whereas the aryl products fluoresce strongly). A "pump-probe" fluorescence scheme as indicated in Fig.2.2, is employed, in which irradiation/ablation is performed at 248 nm, 193 nm (Lambda-Physik LPX 210) with pulse duration τ =30 ns or 308 nm (LPX 315 nm) with pulse duration τ =25 ns, and a excitation beam operating always at 248 nm (Compex 110) with pulse duration τ =25 ns, at very low fluences ($F_{LASER} \approx 5$ mJcm^{-2}) induces

product fluorescence after variable time delay. This fluence is low enough to ensure that photolysis by the probe beam is negligible. In the case of femtosecond ablation, irradiation is performed at 248 nm with pulse duration t~500 fs. The femtosecond irradiation produced by KrF excimer pumped dye laser system based on the principle of a distributed feedback dye laser (DFDL). The energy output is 10-30 mJ/pulse while the average pulse-to-pulse fluctuation is 15%.

The pump and probe beams are focused perpendicularly and coaxially via a quartz spherical lens (f=+500 mm) onto the sample. For experiments entailing ablation at different wavelengths, the probing 248 nm beam is focused to a size somewhat smaller than the ablated/irradiated area (pump ≈6-10 mm^2, probe ≈4-8 mm^2 within the "pumped" area). In all cases, presented data represent results following a single laser pump pulse on virgin polymer. The emission induced by the probe beam is collected by an optical fibre oriented nearly perpendicularly to the sample ~1-2 cm away from its surface (i.e., front-face excitation mode is generally employed). Cut-off filters (< 290 nm) are employed to minimize detection of laser scattered light. The emission is spectrally analysed in a 0.20 m grating spectrograph equipped with a 300 grooves/mm grating. The emission spectrum is recorded on an optical multichannel analyser (OMA III system, EG&G PARC Model 1406) interfaced to a computer. A (Stanford) pulse generator is used to synchronize the probe laser and the OMA. For the further characterization of the photoproducts, temporally resolved fluorescence spectra are recorded for various detection gates of the OMA.

A digital pulse generator (Stanford) is employed for the delay of the lasers. The minimum delay is determined to ~ 0.5 μs by the typical jitter (10 ns) of the excimer lasers and the employed delay from the electronic connections with the use of typical photodiodes (response time 2 ns). The driving pulse (a typical TTL pulse 5 Volts in amplitude with 5 μs pulse duration) is given by the OMA to "pump" laser. Subsequently, the delay between "pump" and "probe" is induced by the first Stanford delay unit and then the second delay unit was triggered by the "probe" laser. The second delay unit determines the gate of detection. According to the previous, t=0 is the time which the "pump" arrives on the sample. A relatively long delay (of the order of tens seconds) between the pump and probe pulses is employed for ensuring nearly quantitative reaction of the aryl radicals and formation of stable products. The

photoproduct fluorescence intensity remains constant for longer delay times. The main source of error in the photoproduct fluorescence measurements derives from the thickness variation across a given sample or different samples (and thus differences in the amount of dopant present). Data presented herein derive from films with a thickness variation of less than 20%.

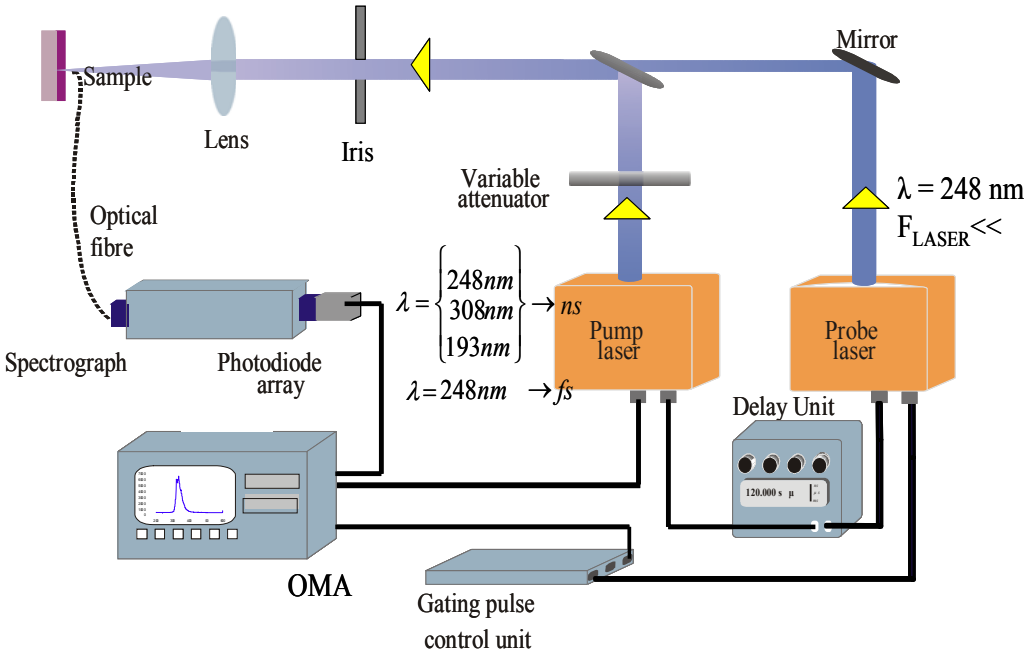

Figure 2.2: *Time resolved Laser induced fluorescence setup.*

Irradiation is performed in ambient atmosphere. The presence of ambient oxygen may affect the nature of the photoproducts formed. Photooxidation of ArH to endoperoxide species has been shown to occur in related polymer systems. Indeed, in the irradiation of neat ArH-doped PMMA, fluorescence of the dopant is found to decrease with successive laser pulses and/or with increasing fluence. However, the decrease in the present case is mainly ascribed to thermal desorption of the dopant, as indicated by Fukumura et al, since we have observed comparable signal decrease in the irradiation of the samples in vacuum. In the case of ArI-doped systems, there is no clear evidence that the presence of oxygen affects aryl photoproduct formation, at least for the ones observed following the first pulse on virgin surface (the main focus of this study). At the very least, it does not appear to be of direct consequence for the comparison of the products formed above vs. below the ablation threshold.

2.3 PULSED LASER DEPOSITION

Pulsed-laser deposition (PLD) has been an successful technique for depositing thin films of a large variety of inorganic materials. PLD has also been applied to the growth of thin polymeric and organic films, albeit with varying degrees of success. For example, when PLD is used to fabricate chemical sensors from polymer–carbon nanocomposites, both the molecular weight distribution and the chemical structure of the polymeric material are substantially altered, but the required functional groups for the sensor remain intact [1]. In other cases, the damage caused during UV ablation is limited to a reduction in the molecular weight with the chemical structure remaining intact [2]. It has been shown that certain polymers such as poly-methyl methacrylate (PMMA), poly-tetraflouroethylene (PTFE), and poly- amethyl styrene (PAMS), undergo rapid depolymerization during UV laser ablation, with the monomer of each strongly present in the ablation plume. For these polymers, the molecular weight distribution of the deposited thin-film material can be increased by simply raising the substrate temperature [3]. Therefore, even in the most successful cases of UV PLD of polymers there is an intense interaction between the target material and laser resulting in chemical modification of the polymer during ablation. If depolymerization is incomplete at the substrate, this can lead to both a reduction of molecular weight and a change in chemical structure.

In this work we used PLD technique for examining the size of the polymeric deposits varying the Mw of the target. PMMA and PS deposits were analysed by using Atomic Force Microscopy (AFM) and Scanning Electron Microscopy (SEM). The targets were placed inside a vacuum chamber at a distance of 20-40 mm from a quartz substrate (flat of 25 mm diameter). The chamber was evacuated down to a pressure of 5 10^{-5} mbar using a turbo-molecular pump. The beam was focused by a lens (f=30 cm) and incident at 45º to the target surface. The target was spun during the deposition process for uniform cratering of the target. The PLD chamber used in the experiment is shown in Fig.2.3.

Laser ablation of the targets was carried out with a KrF laser (Lambda-Physik, Compex 210i) operating at 248 nm (photon energy 4.99 eV) and with a pulse duration

of 20 ns. The fluences of irradiation were in the range 1.0-3.5 J/cm^2 and the spot size was ~1.5 mm^2. Pulse frequencies of 1 Hz and 10 Hz were used in the experiments.

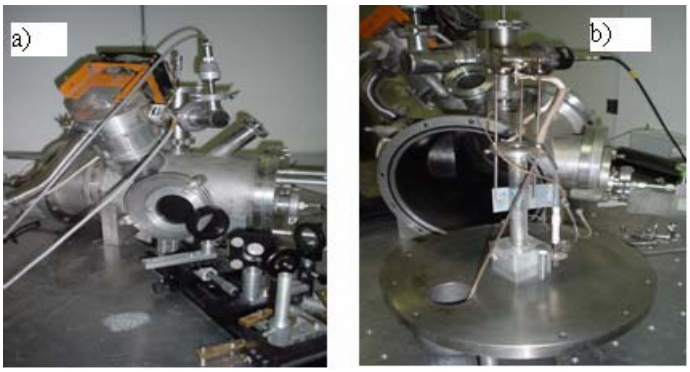

Figure 2.3: *a) Vacuum chamber used for PLD. b) Substrate holder.*

2.4 PIEZOELECTRIC MEASUREMENTS

For measuring the stress transient resulting from excimer irradiation of different Mws of PMMA and Polystyrene we use a wide bandwidth polyvinylidenefluoride (PVDF) piezoelectric transducer.

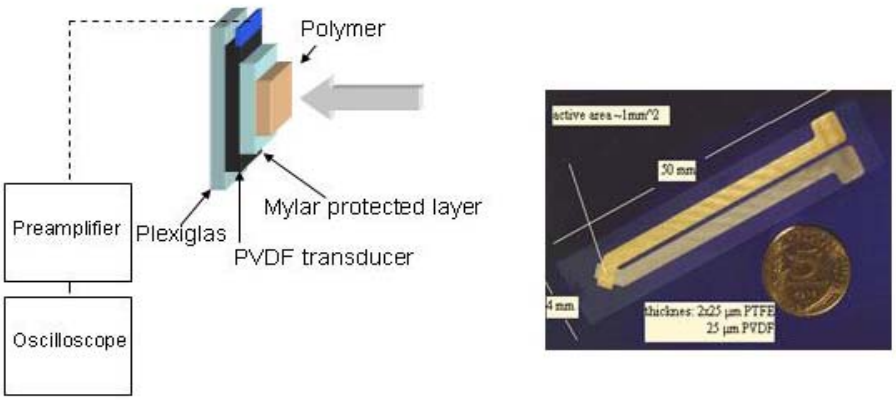

Figure 2.4: *Experimental setup for stress transient measurements and the characteristics of PVDF acoustic sensor.*

The transducer consisted of 4x50 mm^2, 24 µm PVDF piezoelectric film (PIEZOTECH) overlaid from both sides with 25 µm PTFE layer (Fig.2.4) covered with 0.5 µm metallic surface electrodes. Because of the low absorptivity of doped PMMA films, the transducer is covered with a Mylar protected layer ensuring the similar acoustic impendence with the examined polymers. The transducer was placed on a

plexiglass.The plexiglas backing disk acts as a acoustic impedance matching stab producing a response time limited by the acoustic transit time (<4 ns) in the PVDF film. In this geometry stress wave generated laser irradiated surface propagate trough the polymer and the Mylar to be detected as an electric output from piezoelectric transducer. When the signal is amplified using a ORTEG 474 timming filter amplifier the transducer output voltage (50Ω ,400MHz oscilloscope) gives a direct measurement of a time resolved normal force of transducer according to $F(t) = (C_D + C_L)V(t)/d_t$ Here C_D and C_L are the transducer and load capacitance respectively, d_t=22.5pC/N is the thickness mode strain constant for PVDF, and *V(t)* the time-dependent voltage. More details for the experimental method are included in the ref [4].

2.5 PROBE BEAM SCATTERING

For probe beam scattering (PBS) measurments a cw-laser-beam parallel to the polymer surface is used to monitor the ejected material. By monitoring the intensity of the cw-beam it is possible to detect the velocity distribution of the ejected species. As the attenuation of probe beam is directly proportional to the amount of material passing the beam at a time (assuming one species of scattering particles) the attenuation of the beam reflects the amount of material ejection; also from the distance it is relatively simple to transform that particle distribution into a velocity-distribution. The PBS experiments were performed in vacuum $1x10^{-5}$ mbar in a vacuum-chamber especially designed for that experiment. The vacuum was produced by a turbo-pump supported by a rotary-pump. The sample was mounted on a holder which could be moved perpendicular to the probe beam to enable a distance dependence measurement. The probe-beam was generated by a HeNe and its position over the sample could be adjusted by an adjustable mirror. The pump laser entered the chamber through a quartz window on the front. It was focused by a quartz lens (f=50mm) and its fluence could be adjusted by a variable attenuator. After the probe beam passed the chamber it was detected by a photomultiplier.

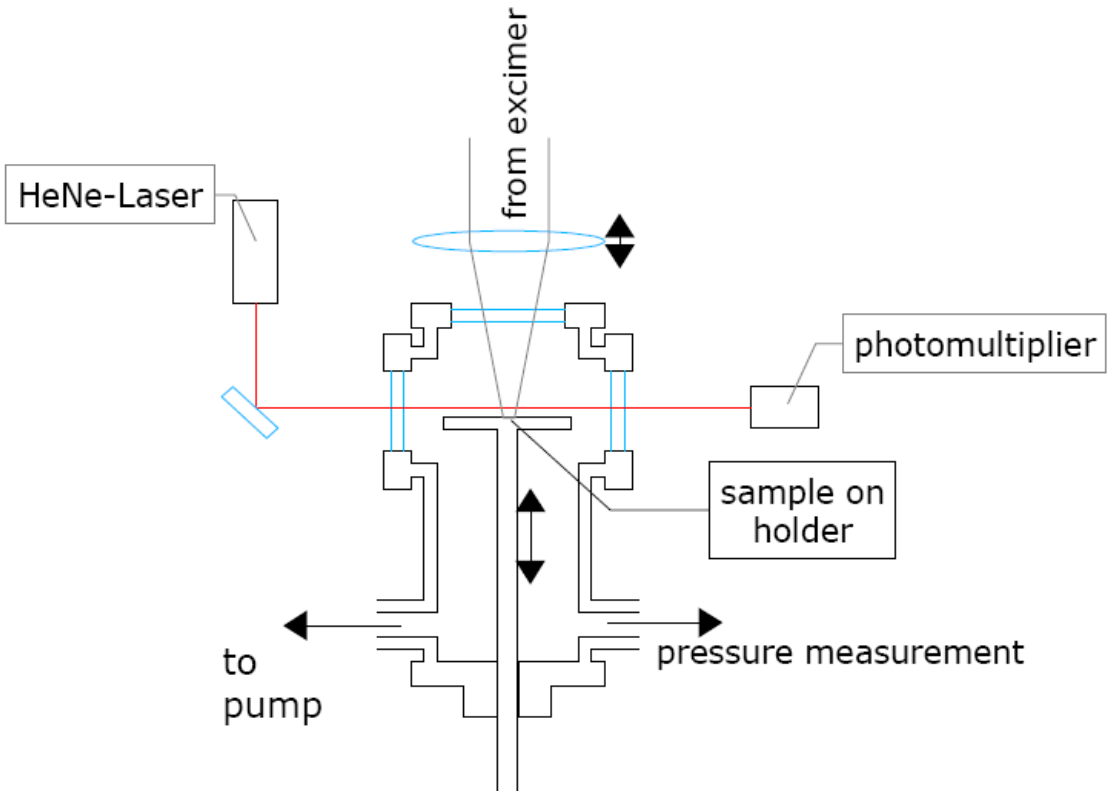

Figure 2.5: *Probe beam scattering setup.*

At first a simple photodiode was used but much better results could be archived using the photomultiplier due to its better resolution and amplification. The response time of the probe beam attenuation setup is determined by the response time of photodiode and photomultiplier and the associated electronics. This is estimated to be about 5 ns in the present case. To detect an attenuation of the probe beam a minimum number of particles is required in the probed volume. Thus, the delay times measured with this method contain not only the time needed for degradation of the polymer but also a mean of time of flight of the products to reach to probe beam. The time needed by the decomposition products to reach the detection beam can be estimated from the mean particle velocity and the beam diameter. It was ensured that only the attenuation of the probe beam caused by the ablation products was recorded and not the deflection due to acoustic waves or the diffusion of the heat in the atmosphere.

2.6 REFERENCES

1. D. M. Bubb, R. A. McGill, J. S. Horwitz, J. M. Fitz-Gerald, E. J. Houser ,R. M. Stroud, P. W. Wu, B. R. Ringeisen, A. Pique´ and D. B. Chrisey, J. Appl. Phys. **89**, 5739, (2001).

2. S. G. Hansen and T. E. Robitaille, J. Appl. Phys. **64**, 2122, (1988).

3. G. B. Blanchet, J. Appl. Phys. **80**, 4082, (1996).

4. A.D.Zweig, V.Venugopalan, and T.F Deutch, *J. Appl. Phys,* **74**, 4181, (1993).

Chapter 3 EXAMINATION OF UV ABLATION OF PMMA VIA THE USE OF PHOTOACTIVE DOPANTS

3.1 INTRODUCTION

In this chapter, we present the potential of using simple photosensitive organic compounds such as iodonaphthalene, iodophenanthrene (ArI), etc dispersed within polymers for studying aspects of UV ablation. The species remaining in the substrate following irradiation are monitored, so that the interpretation of the results is free from the complications plaguing gas-phase studies. Most importantly, the aryl product formation affords direct information about the processes induced in the substrate upon laser irradiation. Specifically, the aryl (Ar) radicals produced by ArI photolysis may abstract a hydrogen from the polymer to form ArH, i.e. via a (thermally) activated process. Therefore, the yield of ArH product reflects the temperature evolution in the substrate following irradiation. In addition, at least for the NapI dopant, biaryl species (1,1-binaphthalene - Nap_2 – and perylene) are also detected. For the employed dopant concentrations, these species are formed via diffusion-limited reaction. Consequently, their formation affords a direct experimental probe of the extent of the substrate melting upon laser irradiation (in contrast to the usual approach, in which laser-induced melting is largely inferred by indirect morphological examination).

Here, we employ approach for examining the processes induced upon irradiation of poly(methylmethacrylate) (PMMA) at the excimer laser wavelengths 193 nm, 248 nm and 308 nm. The UV ablation of PMMA has been examined extensively and a number of conflicting hypotheses, ranging from “pure” photothermal to photochemical and even combination of them, have been advanced (especially, for irradiation at 193 nm) [1-5], [12-23]. To this end, we examine the formation yields of ArH and biaryl species in the irradiation of PMMA doped with ArI. Their yield is examined as a function of laser fluence (F_{LASER}) (from ≈25 mJ/cm^2 to well over the ablation thresholds), thereby assessing the thermal and structural changes (melting) in the polymer with increasing laser fluence. In addition, we examine the kinetics of the dopant-deriving products upon irradiation at 248 nm and 193 nm. The study

demonstrates that the kinetics of ArH and Nap_2 formation constitutes a sensitive and direct probe, respectively, of the temporal evolution of the temperature and of the viscosity of the polymer matrix upon irradiation.

3.2 PRODUCT CHARACTERIZATION

The probe LIF spectra recorded following irradiation of lightly doped ArI/PMMA (≤ 0.8 % wt) at the three wavelengths, exhibit an emission band centered at ~ 330 nm in the case of NapI, or at ~370 nm in the case of PhenI (Fig. 3.1a).

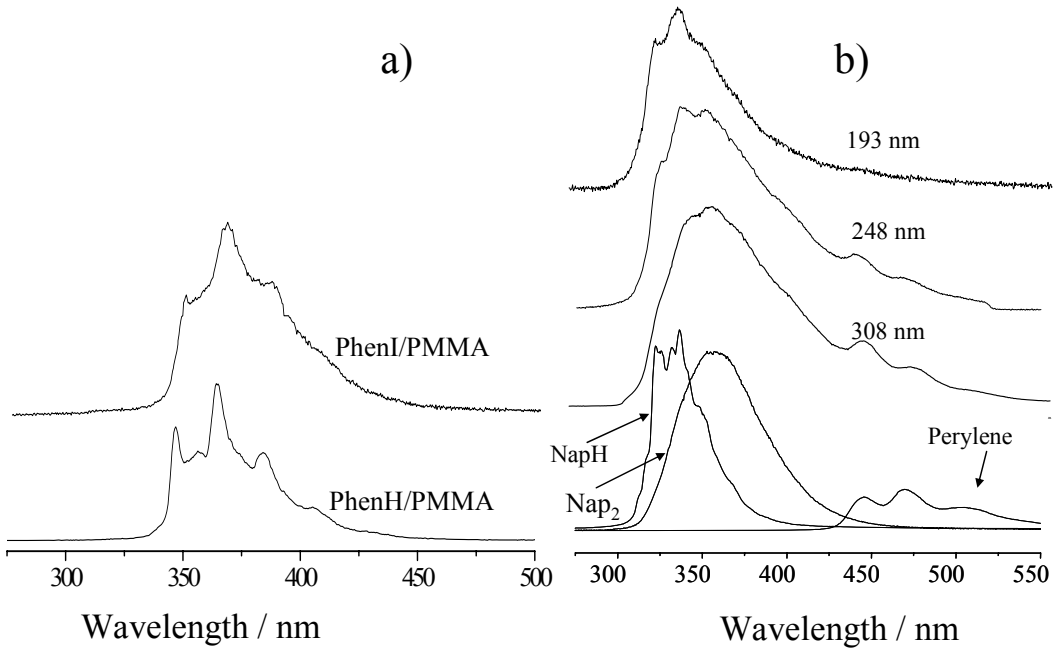

Figure 3.1: *a) Probe product LIF spectra following irradiation with one 248 nm laser pulse of PhenI/PMMA (0.5% wt). Spectrally identical product spectra are recorded following irradiation at any excimer wavelength. For comparison purposes, a spectrum recorded from PhenH/PMMA is also illustrated b) Probe product LIF spectra recorded from 1.2% wt NapI/PMMA following irradiation at 308 nm, 248 nm and 193 nm (in all cases probing effected at 248 nm) at fluences close to the corresponding ablation thresholds. For comparison purposes, the LIF spectra recorded from PMMA doped with the indicated compounds are also presented.*

By comparison with spectra recorded for NapH/PMMA (PhenH/PMMA) films, the band is ascribed [26,28] to the $^1B_{3u} \rightarrow {}^1A_{1g}$ transition characteristic of NapH (PhenH). In all cases, the decay lifetime of the emission (100 ± 25 ns at λ=332 nm) is found to be in good correspondence with the NapH (PhenH) fluorescence lifetime. Thus, in all cases ArH is the main or exclusive product. (In the case of 248 nm irradiation of ArI/PMMA, this conclusion has also been confirmed by Gas Chromatorgaphy/Mass Spectrometric

examination). Indeed, hydrogen atom abstraction is the exclusive mode of reaction for methylnapthyl radicals with PMMA (in solution) [29].

Upon irradiation of NapI/PMMA with dopant concentrations >1% wt. at high fluences, the probe spectra exhibit, in addition, a broad band around 360 nm and two peaks at 430 nm and 450 nm (Fig.3.1b). As shown before and confirmed by direct comparison with spectra recorded from PMMA doped with the authentic compounds, the band at 360 nm is ascribed to 1,1-binaphthalene (Nap_2) and the double peak structure to perylene (this represents the fusion of two naphthalene systems)[28]. For the PhenI dopant, $Phen_2$ formation cannot be ascertained, because $Phen_2$ fluorescence is not well differentiated from that of PhenH.

3.3 F_{LASER}-DEPENDENCE OF PRODUCT FORMATION

For the quantitative characterization of the ArH product, the probe fluorescence intensity (at λ = 332 nm –NapH- or λ=370 nm –PhenH-) is plotted as a function of the "pump" laser fluence (Fig.3.2). For the examined dopant concentrations (≤2 wt %) and film thickness (10-20 μm), the films are approximately optically thin (absorbance ≈0.3-0.4) at the probing wavelength. Thus, at low "pump" fluences, the fluorescence intensity is directly proportional to the amount of the aromatic product in the substrate (i.e., minimal self-absorption effects).

However, at higher fluences, the induced modified film morphology results in enhanced scattering of the probe beam, so that the fluorescence intensity may not represent accurately the product amount in the substrate. Comparative examination with systems doped with photostable compounds (CdSe quantum dots) indicates the discrepancy to be 10-15%. The differences observed between the systems are significantly larger than this, so that this deviation is of no particular consequence.

Most importantly at the three examined excimer wavelengths, the F_{ALSER}-dependence of the ArH product is found to be qualitatively similar (Fig.3. 2). At low fluences, the product intensity scales linearly with the "pump" F_{LASER} (slope in log-log plots generally 1.0±0.2, as determined from 5 - 6 measurements on each system), consistent with a one-photon dissociation of the dopants.

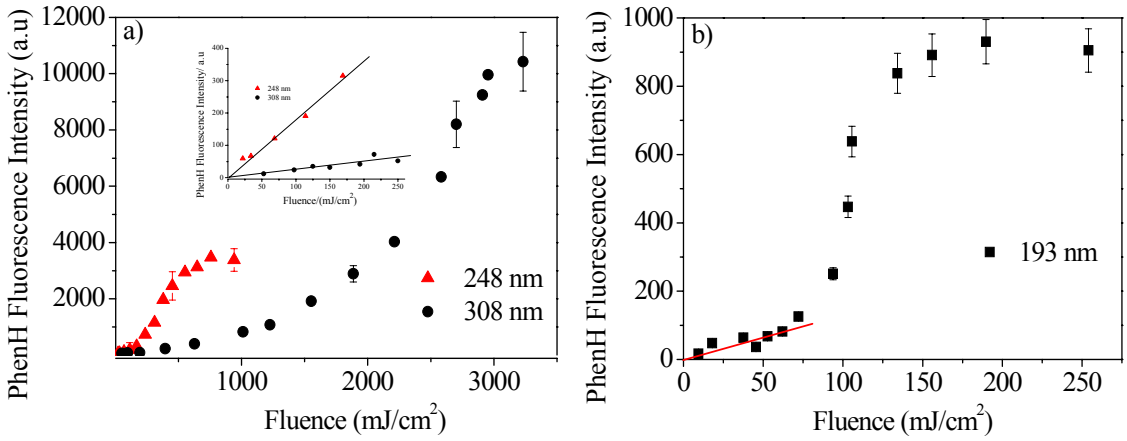

Figure 3.2: *F_{LASER}-dependence of the PhenH product in the irradiation of PhenI/PMMA (0.5% wt) at (a) 308 nm, 248 nm. The inset illustrates the linear dependence observed for PhenH formation in the irradiation at very low laser fluence. (b) The corresponding F_{LASER}-dependence at 193 nm. The error bars represent 2σ, as determined from at least 5 different measurements. In all cases, the fluorescence is recorded following irradiation with a single "pump" pulse.*

Calibration/comparison with fluorescence measurements on ArH-doped PMMA [31] shows that at these fluences, less than 10% of the photoexcited dopant reacts to ArH. However, at higher fluences, the ArH amount grows sharply with increasing F_{LASER}. The onset fluence for this deviation is observed to scale roughly inversely with the effective absorption coefficient α_{eff} of the systems (Table 1).

Product intensity reaches a plateau at fluences close to the ablation thresholds of the systems. Examination of the plasma emission induced by the pump pulse, as well as transmission measurements of the pump laser beam, show that shielding (i.e., absorption of the pump beam by the plume) [31] becomes important at fluences somewhat higher than the corresponding ablation thresholds. Thus, the levelling-off of the ArH product must be ascribed to the etching process. Importantly, for a given polymer/dopant, the signal at the plateau (i.e., the quantity of ArH product remaining upon ablation) at weakly absorbed wavelengths is quite higher than that at strongly absorbed ones (even for optically thin films).

Table1: *Linear absorption coefficients, effective absorption coefficients, the corresponding swelling and ablation thresholds at 3 excimer wavelengths for different doped PMMA systems*

SYSTEM (%w.t)	WAVELENGTH (nm)	α_{small} (cm^{-1})[1]	α_{eff} (cm^{-1})	SWELLING ONSET[2] (mJ/cm^2)	ABLATION THRESHOLD[2] (mJ/cm^2)
0.5% PhenI/PMMA	193	≈6000 (≈2500)	≈6000	-	100
	248	2000 (1860)	2750-3000	200	700
	308	70 (40)	600	1200	3500
0.4% NapI/PMMA	193	≈5000 (≈1000)	≈5000	-	170
	248	210 (60)	1000-1300	1100	700
	308	60 (20)	300-500	1700	3500
1.2% NapI/PMMA	193	≈5500 (≈3000)	≈5500	-	130
	248	350(190)	2000-2500	500	900
	308	100 (65)	700	1200	2500

[1] *Absorption coefficients determined from measurements of films cast on suprasil substrates. The numbers within the brackets indicate the absorptivity due to the dopant, as determined from literature values. The absorption coefficients of the doped PMMA differed somewhat depending on the degree of polymer purification (e.g., at 248 nm, it is measured to be ≈ 80 – 200 cm^{-1}. Literature values show an even higher scatter (50 cm^{-1} up to ≈ 500 cm^{-1})). At 193 nm, our measurements agree with the value reported by Srinivasan [15] (vs. the 2000 cm^{-1} reported by others).*

[2] *Swelling onset and ablation thresholds by profilometric examination of the indicated samples following irradiation with one laser pulse. (at 193 nm, it was difficult to characterize the swelling and thus no fluence values are reported).*

It is clear that notwithstanding chemical characteristics of the employed dopants and polymers, the quantitative features of the F_{LASER}-dependence of the ArH product are mainly determined by the absorptivity of the dopant/polymer substrate. To illustrate further this feature, we have examined the F_{LASER}-dependence for 248 nm irradiation of PMMA doped with different dopant (PhenI) concentrations, i.e., different substrate absorptivities (Fig.3.3). Qualitatively, same dependence is observed for dopant concentrations as low as possible to permit reliable signal detection (~0.1% wt PhenI)).

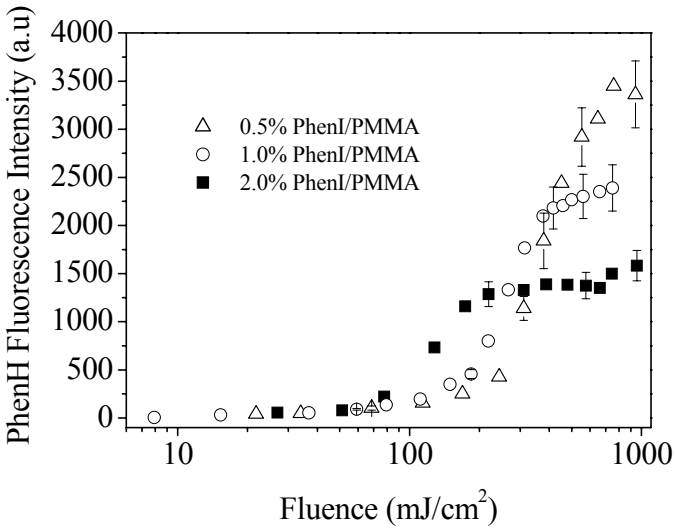

Figure 3.3: *F_{LASER}-dependence of PhenH product formed in the 248 nm irradiation of PMMA doped with 0.5%, 1% and 2% wt PhenI.*

For a given dopant/polymer system, the onset of enhanced ArH formation decreases with increasing dopant concentration, i.e. increasing absorptivity. In parallel, the amount of product remaining in the substrate following ablation is much reduced, despite the considerably higher number of photolabile chromophores present. Clearly, this result has direct and important implications for the laser processing of molecular substrates.

Concerning the biaryl species, for irradiation at the weakly absorbed 248 nm and 308 nm, these products are first detected for NapI concentrations 0.8~1.2% wt at fluences close to the onset of polymer swelling (Table 1). With increasing pump laser fluence, their yields grow until reaching a limiting value at the ablation threshold (Fig.3.4).

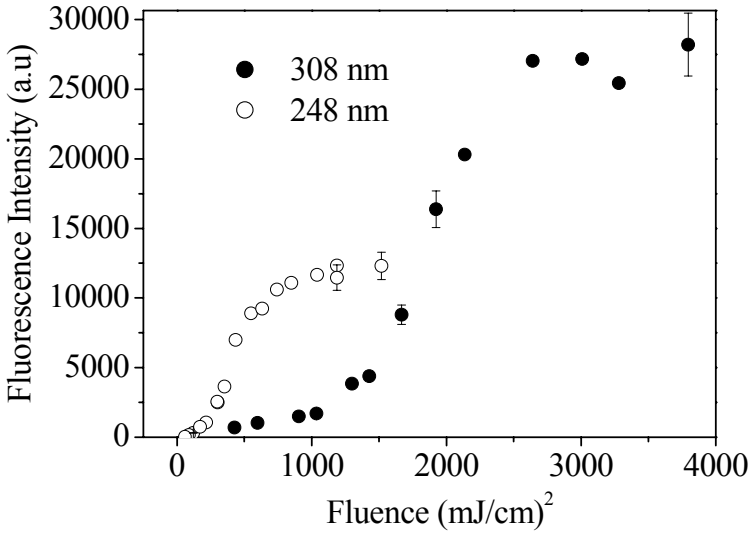

Figure 3.4: *Intensities of Nap_2 as a function of F_{LASER} in the irradiation of 1.2%wt NapI/PMMA at 248 nm and 308 nm. The error bars indicate the likely error in the estimation of the Nap_2 via the deconvolution procedure.*

The emission intensity of 1,1-binaphthalene (as well as of perylene – not shown) – measured at ≈380 nm, at which the overlap by NapH emission is small- reaches higher values for irradiation at 308 nm than at 248 nm, whereas hardly any bi-aryl species emission is detected upon 193 nm irradiation of the same dopant concentration.

3.4 DISCUSSION

In the section 3.3 is demonstrated that the dopant-deriving product patterns in the irradiation of iodoaromatics-doped PMMA at the three excimer laser wavelengths 308 nm, 248 nm and 193 nm follow well-defined trends:

(1) The F_{LASER}-dependence of ArH formation is qualitatively the same for all systems, with the quantitative differences correlated with the substrate absorptivity at the irradiation wavelength.

(2) For higher NapI concentrations (0.8-1.2% wt), biaryl species (Nap_2 and perylene) are also detected, with the extent of their formation decreasing from 308 nm to 193 nm (evidently, in correspondence with increasing dopant/polymer absorptivity).

For accounting for these observations, we establish first the reaction(s) responsible for the formation of ArH and biaryl products. Given the 2.6 eV energy of C-I bond [9 (a), 26, 27], thermal decomposition of ArI can be discounted (less than 10^{-3} of ArI is estimated to decompose thermally even if temperatures as high as 2000 K are attained in the non-ejected layers). At the three examined wavelengths, ArI absorb moderately or strongly [28], dissociating into Ar and I radicals with a quantum yield of ≈1 upon excitation [27]. Due to the very fast photodissociation of ArI (≈1 ps) [27], product formation via direct reactions of excited states can be ruled out. Therefore, the aryl products are formed exclusively by reactions of aryl (Ar) radicals formed by the ArI photodissociation. Based on the known chemistry of aryl radicals, the ArH product is formed by hydrogen-atom abstraction from the polymer and the biaryl species by diffusion-limited reaction(s) ($Nap + Nap \rightarrow Nap_2$).

In view of this conclusion, two factors have to be taken into account for modeling quantitatively product formation at the three wavelengths:

(a) differences in the absorption step, thus resulting in different number and spatial distribution of the aryl radicals ([Ar])

(b) changes in the subsequent reactivity of the photogenerated aryl radicals as a result of the different temperature and/or viscosity evolution in the irradiated substrates.

3.4.1 Absorption process

Concerning (a), absorption by ArI at low fluences is a one-photon process, as shown by the linear F_{LASER}-dependence of the ArH emission (inset in Fig.3.2). However, even at higher fluences, ArI dissociation must proceed via one-photon excitation. Indeed, assuming an absorption cross-section for the secondary step equal to that for C_6H_6 and related compounds [28], fluences in excess of 5 J/cm^2 are required for a two-photon process to compete with the fast dissociation of ArI (the 1-photon nature of ArI fragmentation at these fluences cannot be ascertained by transmission measurements of the 'pump' pulse, because of "competing" absorption by intermediates/polymer species, likely multiphoton processes, etc.)

However, besides absorption by ArI, what matters for the quantitative modeling/description is the effective absorption of the polymer/dopant system. This differs much at different wavelengths and even at a single wavelength with increasing F_{LASER}. Indeed, at the weakly absorbed wavelengths (where ablation is effected at high fluences), transmission measurements of the pump beam show multiphoton processes to become significant at fluences well below the ablation thresholds. This agrees well with previous observations on related systems [19], [33-34]. Evidently, the aryl radicals formed by ArX photolysis and/or species of the polymer decomposition absorb additional photons.

3.4.2 Excitation processes

Reasonably, upon pulsed laser irradiation, the dynamic optical properties may deviate widely from the small-signal values, resulting in a significant change of the laser propagation depth. Indeed, in the case of tissues, significant changes have been noted as a result of a change in the absorption spectrum with increasing temperature. However, in the present case the change in the absorptivity can be related to changes in the excitation step, as also seen in related systems by time-resolved absorption and luminescence spectroscopy have been used to probe the dynamics of electronic excitation and de-excitation processes. Depending on the specific properties of the electronically excited states, saturation or multiphoton processes may dominate. In the former case, a larger portion of the incident light penetrates deeper into the material. As a result, thermal and chemical modifications are induced much deeper in the bulk of the substrate.

In other cases, multiphoton processes may dominate, limiting light propagation into the substrate. The multiphoton processes may entail the absorption of successive photons exciting the molecules or chromophores to higher electronic states, (i.e. $A+h\nu \rightarrow A^* \rightarrow A^{**} \rightarrow \ldots$)

On the other hand, for irradiation at 193 nm, there is no clear evidence for a change (either multiphoton or saturation [35]) in transmission measurements at fluences *below the threshold*. Clearly, the increase in ArH formation that is observed below the

threshold is not due to absorption saturation effects (of the "pump" laser beam); instead, it represents an increase in the product amount formed per unit volume.

3.4.3 ArH Formation modelling/Temperature estimation

In view of the previous discussion, the observed dependence of ArH formation must reflect the dynamics of product formation. ArH formation can be described by a pseudo-unimolecular hydrogen atom abstraction by the Ar radicals (i.e., $d[ArH]/dt = A\exp(-E_{act}/RT(z,t))[Ar]$, where [Ar] the concentration of aryl radicals). Such reactions for small aromatic compounds are characterized by an activation energy E_{act} in the 40-60 kJ/mol range and a pre-exponential factor A of 10^5-10^7 s^{-1} [36]. For modeling the ArH formation, the temperature evolution in the substrate following irradiation is estimated by [37, 38]:

$$T(z,t) = T_0 + \frac{\alpha_{eff} F_{LASER}}{2C_P} \times \exp(a_{eff}^2 D_{th} t)$$

$$\times [\exp(-\alpha_{eff} z) erfc(a_{eff}\sqrt{D_{th} t} - \frac{z}{2\sqrt{D_{th} t}}) + \exp(a_{eff} z) erfc(a_{eff}\sqrt{D_{th} t} + \frac{z}{2\sqrt{D_{th} t}})] \quad (3.1)$$

where z the depth from the film surface (erfc: complementary error function), $T_0 = 300K$, ρ=1.19x10^3 kgr·m^{-3}, C_p=2x10^3 J·kgr^{-1}·K^{-1} (25-250°C) growing to ≈3x10^3 J·kgr^{-1}·K^{-1} at higher temperatures and D_{th}=4x10^{-8} m^2s^{-1} [4]. The effective absorption coefficients α_{eff} are fixed to average values determined by transmission measurements at selected "pump" laser fluences below the thresholds (Table 1) (whereas, the spatial distribution of Ar radicals is estimated via the absorption values for ArI). For the simulation, the substrate is divided in slabs and product formation is integrated over time. The formula neglects energy removal by desorption of volatile species (sub-ablative regime) or by material ejection (ablation), as well as heat losses due to polymer decomposition. Nevertheless, it is a relatively good description of the temperature evolution below the ablation threshold over the μs-ms time scale that product formation

takes place (product formation in the irradiation of ArI/PMMA is completed in ~600 μs at 193 nm and at ~5 ms at 248 nm as will demonstrate in the next section).

Despite any uncertainties in the effective absorption coefficients and in the reaction rate constants, the simulation reproduces nearly quantitatively the F_{LASER}-dependence of the ArH product formation at the three wavelengths (for E_{act}≈55 kJ/mol) (Fig.3.5a). At low laser fluences, only a small percentage of the photoproduced Ar radicals react to ArH (the non-reacted radicals likely recombine eventually with the corresponding geminate halogen radical).

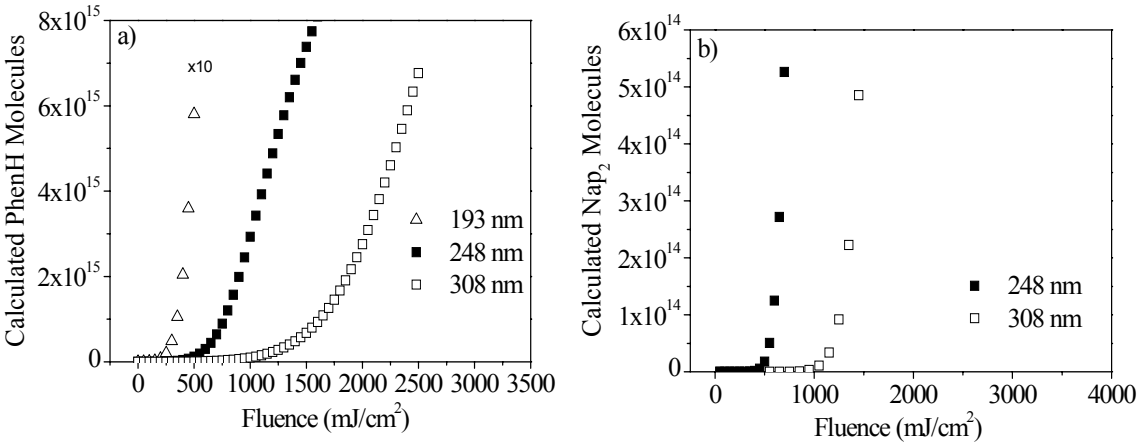

Figure 3.5: *a) PhenH product estimated to form as a function of laser fluence in the irradiation of 0.5 % wt PhenI/PMMA at 308 nm, 248 nm and 193 nm (Film thickness =20 μm). The details of the simulation are described in the text. b) Estimated F_{LASER}-dependence of Nap_2 formation for irradiation of 1.2% NapI/PMMA at 308 nm and 248 nm (Film thickness=20 μm).*

With increasing laser fluence, the reaction efficiency increases sharply and in parallel a higher percentage of the radicals in the sublayers react as a result of heat diffusion. Therefore, the reaction should be limited by the heat relaxation time $\tau_{th} \approx 1/(a_{eff}^2 D_{th})$ ($\approx 10^{-3} - 10^{-2}$ s for the weakly absorbing and $\approx 10^{-5} - 10^{-4}$ s for the strongly absorbing systems). Accordingly, ArH formation should become important (i.e., reaction of fraction r of the photoproduced radicals) at $F_{LASER} \approx \frac{\rho C_P}{a_{eff}}[\frac{(E_{act}/R)}{\ln(\frac{A}{a_{eff}^2 D_{th}}\ln(1/r))} - T_0]$. The estimated fluences (for r ≥ 0.13) are found

to be in good accord with the experimental F_{LASER} values for the onset of enhanced ArH formation. Accordingly, the effective "reaction depth" can be approximated:

$$A\exp(-E_{act}/RT(z,t))*\tau_{th}\sim 1 \Rightarrow L_{rxn}=\sqrt{\frac{1}{a_{eff}^2}\ln[\frac{(a_{eff}F_{LASER}/\rho C_P)[\ln A-\ln(\alpha_{eff}^2 D_{th})]}{(E_{act}/R)}]}\approx 7\text{-}10\ \mu m$$

for weakly absorbing systems and ≈ 1 μm for the strongly absorbing ones. Therefore, for the same absorbed energy $\alpha_{eff}\cdot F_{LASER}$, the ArH yield decreases with increasing α_{eff} (assuming all other factors being the same), as experimentally demonstrated by the comparison of ArH formation in the irradiation of different dopant concentrations (Fig.3.3).

Close to the ablation threshold, Eq.(3.1) fails. At these fluences, energy removal by material ejection and the sharp increase of the polymer c_p (due to the decomposition into smaller fragments) limit the attained temperatures, thereby resulting in the observed leveling-off of product formation in the remaining substrate (Fig.3. 2 and 3.3). The observation of a plateau is in accordance with the "blow-off" model: $l_{ejected} = 1/\alpha_{eff}\ \ln(F_{LASER}/F_{thr})$, for $F_{LASER} \geq F_{thr}$, where $l_{ejected}$ represents the etching depth. According to this, the remaining substrate is subject to F_{thr}, with the additional radicals/products formed with increasing F_{LASER} been removed by the etching process. (Of course, the formula does not provide any insight for the dependence below the threshold and may fail quantitatively due to the neglect of heat diffusion)[40].

In all, the modelling directly demonstrates that at the three excimer wavelengths, high enough temperatures are attained well below the threshold, consistent with a thermal mechanism. The estimated maximum surface temperatures at fluences close to the thresholds are: T≈900 K at 308 nm and 248 nm (which correspond well to previous assessments [19, 45]) and T≈700 K at 193 nm. Quantitative differences at the three excimer wavelengths are satisfactorily accounted by the different extent of heat diffusion. In particular, the contribution of a photochemical mechanism must be small enough. Otherwise, since multiphoton excitation/dissociation for ArI is unlikely, the ArH yield would scale nearly linearly at fluences below the ablation threshold, at sharp variance with the observed F_{LASER}-dependence (Fig.3.2 and Fig.3.3). However, though the correspondence between the simulation and experimental curves is very good at 308 nm and 248 nm, it is much less satisfactory for 193 nm (e.g., onset of enhanced ArH

formation is observed at lower fluences than calculated). It has often been noted [4] that thermal models have difficulties in the quantitative description of the 193 nm ablation of polymers, including PMMA. For instance, the ablation threshold is lower than expected by photothermal decomposition, the deviation being ascribed either to the operation of photochemical processes or even to the influence of stresses. However, on the basis of the previous discussion, these explanations cannot account for the deviation in ArH formation at 193 nm (the comparison of the simulated curve in Fig.3.5a with Fig.3.2 shows that the deviation indicates higher temperatures than estimated by Eq. (3.1))

One possible explanation for this deviation may be that heat released by exothermic reactions of polymer species/fragments produced upon irradiation at 193 nm contributes to the heating of the substrate. In recent Molecular Dynamics simulations, Garrison et al [41] have suggested that this may be a significant aspect in the laser irradiation of photolabile/reactive systems (such a contribution was considered [42] to be part of a "photochemical" mechanism, but this seems to be largely semantics. The important point is that high temperature elevations are induced in any case). On the other hand, the relatively good simulation of ArH formation at the 308 nm and 248 nm attained with the experimentally determined α_{eff} suggests that at these wavelengths, this contribution is not substantial (or, at least, it is compensated by the endothermic contribution of bond scission/decomposition processes). Though this seems to be an "attractive" explanation, the accuracy of modelling is not sufficient for the definite demonstration of this possibility (e.g., somewhat uncertain kinetic parameters as well as difficulty in establishing accurately the absorption coefficient at 193 nm-due to the high absorptivity).

Further information is obtained from the examination of the biaryl species formation. As demonstrated previously by a number of spectroscopic examinations, at the employed NapI concentrations (≤ 1.2% wt), dopant aggregation is insignificant [11]. Thus, Nap_2 and perylene must form exclusively via diffusion-limited reaction(s):

$$Nap + Nap \rightarrow Nap_2 \text{ or perylene}$$

At the employed concentrations, the average distance between dopant molecules is ≈4 nm. Assuming Fickian-type diffusion, [42] the Nap diffusion length scales as $(6D_{sp}t)^{1/2}$,

with $D_{sp} = k_B T/(6\pi\eta R_{Nap})$ (where k_B is the Boltzmann constant, η the medium viscosity and R_{Nap} the naphthalene radius). For Nap_2 formation on ms time scale (experimentally confirmed by the kinetic study) and assuming for this interval an average temperature of ~ 600 K (as indicated by the ArH simulation), η for irradiation at 308 nm and 248 nm close to the corresponding ablation thresholds is estimated to be $\approx 10^1$-10^3 Pa s, comparable to the viscosity reported for polymer **melts** [42] (on the other hand, the minimal detection of Nap_2 for 0.4% wt NapI indicates an upper bound of 10^1Pa·s for the η value).

We have modeled the Nap_2 formation in detail by a 2nd-order reaction, with a Smoluchowski-type rate constant $K = \frac{8k_B T}{300\eta}$ (η: Pa·s). At temperatures above the glass transition, the temperature dependence of polymer viscosity η is usually approximated by:

$$\eta = \eta_0 \exp\left(\frac{-C_1(T - T_{ref})}{C_2 + (T - T_{ref})}\right) \tag{3.2}$$

A number of somewhat different constants have been reported for this equation [42-44]. Corrected for the different molecular weight employed here vs. that in the reported studies, the parameters adopted for the simulation are: $T_{ref} \approx 210$ °C, $\eta_0 \approx 3.68 \times 10^4$ Pa s, $C_1 \approx 19.5$, $C_2 \approx 241$ °C. T is estimated via Eq.(3.1). (In the simulation, the influence of the competing H-abstraction reaction for ArH formation is not taken into account).

The simulation reproduces, at least semi-quantitatively, the observed F_{LASER}-dependence of Nap_2 formation (Fig.3.5b). With increasing F_{LASER}, the Nap concentration increases and in addition, viscosity decreases further, so that a much higher percentage of radicals react to Nap_2. In considering next Nap_2 formation at the 3 UV wavelengths, two factors have to be taken into account: First, since the formation rate of biaryls scales as $[Nap]^2$ (i.e. on the number of photolyzed NapI molecules per unit volume), their yield decreases with increasing polymer absorptivity. This factor accounts partly for the reduced bi-aryl species formation at 193 nm (based on the relative absorption coefficient of NapI vs. effective absorption coefficient, the concentration of dissociated NapI at 193 nm is estimated be ≈3 times lower than at 248 nm, at the corresponding ablation thresholds). Second, the melt depth (approximately,

$\eta \leq 10^6$ Pa·s) scales as [46] $h_{melt} \approx \frac{1}{\alpha_{eff}} \ln \frac{\alpha_{eff} \; F_{LASER}}{\rho C_p (T_m - T_0)}$, for $F_{LASER} > \frac{(T_m - T_o)\rho C_p}{\alpha}$ (T_m=melting temperature; T_o= ambient temperature) (in fact, it also depends on heat diffusion and any material and energy desorption/removal). The nearly inverse dependence of h_{melt} on α_{eff} and the longer melt condition promote Nap_2 formation for the lower $\alpha_{eff.}$ This may account for the somewhat higher Nap_2 at 308 nm than at 248 nm, even though the NapI absorption coefficient at 308 nm is smaller (i.e., lower Nap concentration produced). In all, the thermal model consistently accounts for the extent of Nap_2 formation at 248 nm and 308 nm, and for the failure to detect Nap_2 formation at 193 nm. Evidently, as compared to morphological or even the more elaborate interferometirc method [46-47], Nap_2 formation provides a highly sensitive probe of the polymer viscosity changes upon laser irradiation.

Despite the semi-qualitative agreement, likely limitations of using Eq.(3.2) to model the viscosity of PMMA upon laser irradiation must be noted. In particular, the parameters in Eq.(3.2) derive from viscosity measurements at much lower temperatures than those attained upon laser irradiation. Furthermore, Eq.(3.2) neglects the fact that upon laser irradiation, polymer viscosity is, in parallel, affected by the polymer thermal decomposition, formation of gaseous bubbles, etc within the substrate. This question is addressed through the examination of the kinetics of Nap_2 formation.

3.5 KINETICS OF PRODUCT FORMATION

Considering first the ArH product, at low fluences (40 mJ/cm^2 at 193 nm, 100-150 mJ/cm^2 at 248 nm), its yield scales linearly with F_{LASER}, consistent with a one-photon photolysis of ArI [11(a)]. At these fluences, its formation follows "pseudo-first-order" kinetics: plots of $\ln[(I_{t=\infty} - I_t)/I_{t=\infty}]$ vs. time t, where I_t represents the ArH emission intensity at t, are linear, with comparable rate constants at the two wavelengths ($\approx$ 6000 s^{-1}). In contrast, at higher fluences, the rate and the time scale of "quenching" of ArH formation differ considerably at the two wavelengths. As presented in the Fig.3.6

ArH product formation in the irradiation of ArI/PMMA is completed in ~600 μs at 193 nm and at ~5 ms at 248 nm.

The time of ArH formation corresponds well to the heat diffusion time $\tau_{th} \approx 1/(a_{eff}^2 D_{th}) \approx 5x10^{-3} s$ at 248 nm and ≈5x10^{-4} s at 193 nm (where α_{eff} the effective absorption coefficients of ArI/PMMA (Table 1), and D_{th}=4x10^{-8} m^{2}s^{-1} [47] the thermal diffusivity of PMMA), indicating that ArH formation is heat-diffusion limited. In support of this, ArH formation is quenched at shorter times with increasing dopant concentration (0.5, 1 and 2 wt %), i.e., increasing absorptivity and thus reduced τ_{th}.

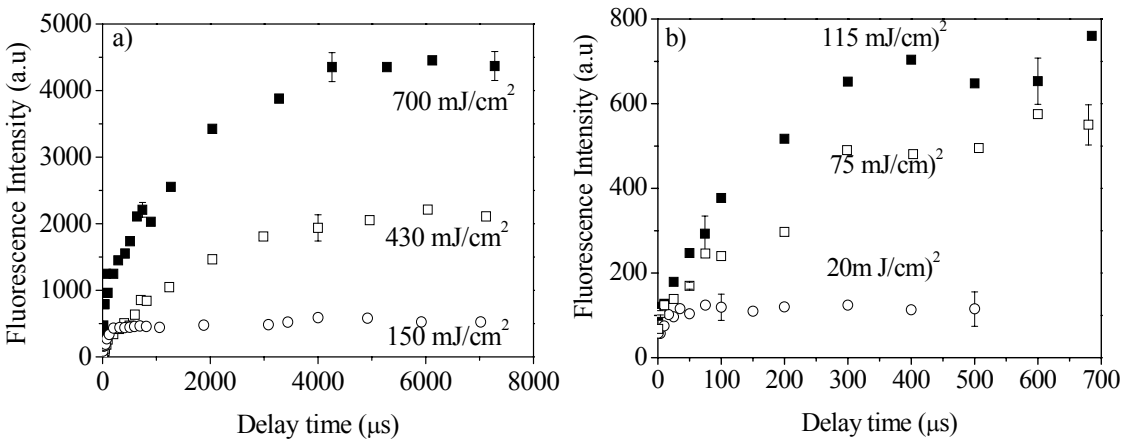

Figure 3.6: *PhenH product intensity for PhenI/PMMA films (0.5 wt%) recorded as a function of the pump-probe delay time for irradiation at (a) 248 nm (b) 193 nm. The error bars represent 2σ, as determined from 5 different measurements.*

In view of the above indication, the kinetics of ArH formation is simulated in further detail within the photothermal model [48, 6, 37, 38, 39]. Since ArH is formed via a thermally activated process, it is reasonable to consider that its rate is specified by the temperature evolution in the substrate. To this end, the substrate temperature is estimated by the Eq.(3.1).

The simulation reproduces rather well the ArH kinetics that is observed *at high fluences* at the two wavelengths (Fig.3.7). However, a discrepancy is observed in the scaling of the product with F_{LASER}, and the amount of ArH product formed at 193 nm is *underestimated* as compared with 248 nm [49].

Given the influence of scattering effects on the quantification of the LIF signals, the limitations of Eq.(3.1) and the inaccuracies in the kinetic parameters of ArH

formation, it is not worth at this moment refining further the simulation. At any rate, it is clear that ArH formation at *both* wavelengths is determined by the temperature evolution in the substrate following irradiation. Within the limitations noted above, temperatures of ≈700-900 K are estimated at the PMMA surface close to the threshold at both wavelengths (for irradiation at 248 nm, the estimated temperature agrees very well with previous assessment [39]).

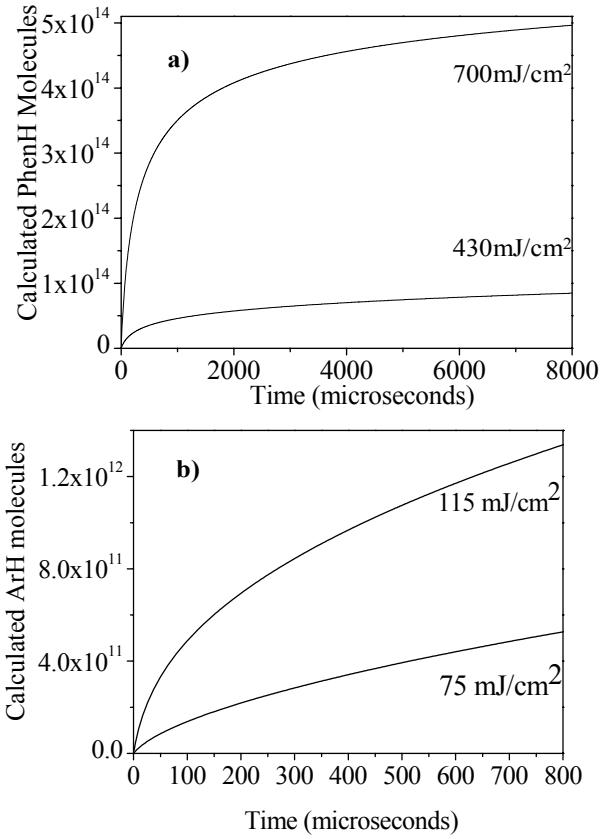

Figure 3.7: *(a) PhenH product estimated to form as a function of time in the irradiation of 0.5 % wt PhenI/PMMA upon irradiation at the indicated fluences a (a) 248 nm and (b) 193 nm. (Film thickness =20 μm). The details of the simulation are described in the text.*

Although comparable initial temperatures may be attained, the extent of the reaction is limited by the heat diffusion time. Thus, the total amount of ArH formed (at the same absorbed energy $\alpha_{eff} F_{LASER}$) is much reduced at 193 nm as compared with 248 nm.

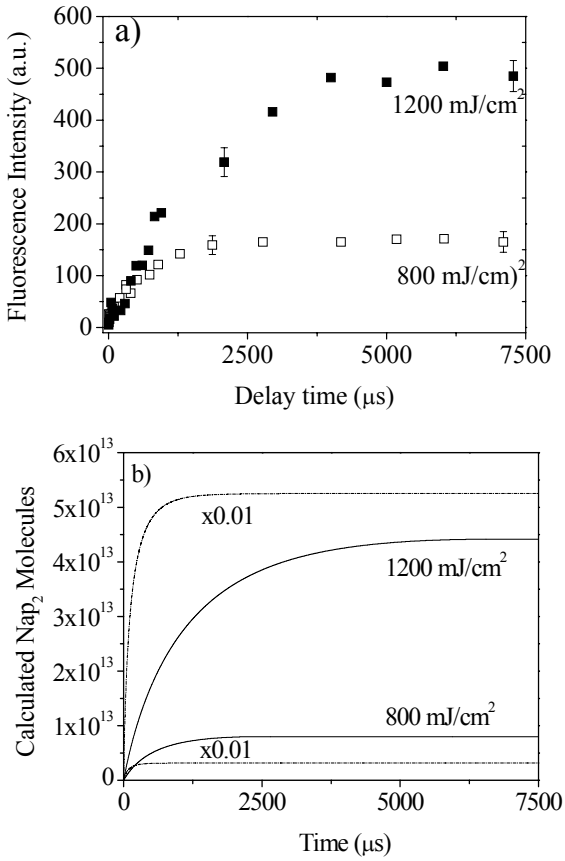

Figure 3.8: ***a)*** *Nap_2 formation kinetics in the irradiation of 1.2 wt% NapI/PMMA at 248 nm at the indicated fluences. Nap_2 intensity is probed at λ = 400 nm, at which spectral overlap by NapH and perylene is minimal. (b) The solid lines represent the simulated kinetics of Nap_2 formation.For comparison purposes, the kinetics expected on the basis of the literature viscosity is also indicated by dashed lines.*

We consider next the kinetics of Nap_2 formation in the irradiation of 1.2 wt% NapI-doped samples (Fig. 3.8a). Its formation continues up to ≈1 ms, with this time increasing somewhat with increasing fluence. As shown elsewhere [9(b)], for the examined NapI concentrations, dopant aggregation in the films is insignificant. Using the Eq.(3.1), Eq.(3.2) and Smoluchowski-type rate constant $K = \frac{8k_B T}{300\eta}$ (η: Pa·s), a satisfactory simulation (solid lines in Fig.3.8b) of Nap_2 formation kinetics is attained for C_1≈0.3x19.5. The very good correspondence establishes that at 248 nm, η decreases to values as small as 10^2–10^3 Pa·s for ≈1 ms after the laser pulse. Importantly, good modelling of the Nap_2 kinetics can be attained only by employing C_1 value in Eq.(3.2) much lower than the one determined in the conventional measurements performed at

lower temperatures (for comparison purposes, the kinetics expected on the basis of the literature viscosity is also indicated by dashed lines in Fig.3.8b). This difference can be ascribed to the fact that at the high temperatures attained upon laser irradiation at 248 nm, the extensive thermal decomposition with formation of gaseous bubbles, etc within the substrate modifies significantly the polymer melt viscosity and its temperature dependence.

On the other hand, for the strongly absorbed 193 nm, as indicated by Eq.(3.1), melting and thus Nap_2 formation is quenched on shorter time scale. As a result of this and of the reduced NapI dissociation (due to the "competing" polymer absorption), Nap_2 formation is too low for kinetic measurements.

In all, a thermal model [4, 48] consistently accounts for the observations at high fluences. We consider finally the reason for the different ArH formation kinetics observed at very low fluences (at which ArH formation scales linearly with F_{LASER}). Since at these fluences, the temperature increase is minimal, the polymer "structure" is not affected and the reaction takes place within a medium of essentially infinite viscosity. Medium viscosity generally affects much the probability of radicals to separate or recombine and thus their reaction efficiency [30,50]. Thus, aryl radical reactivity within the polymer may be described by the scheme:

$$\begin{array}{c} \text{PMMA} \\ \text{ArI} \underset{\text{Krec}}{\leftarrow} \text{Ar} + \text{I} \underset{\text{Krxn}}{\rightarrow} \text{ArH} + \text{I} \end{array}$$

The dependence of recombination probability (P) on viscosity is generally approximated by $P \propto \frac{\eta}{T^{1/2}}$ (Noyes model) [50], where the proportionality depends on the masses and of radii of the radicals. Accordingly, at low fluences, K_{rec} (specified by the probability P) dominates. Thus, the rate of ArH formation is given by $K_{rxn}/K_{rec}e^{-Krect}$. Indeed, from comparative measurements, we find the quantum yield of ArH formation in PMMA to be ≈0.1 (vs. ≈1 in solution) [11(a)], suggesting that $K_{rec} \approx 7\text{-}10 x K_{rxn}$. This high K_{rec} accounts for the fast quenching of ArH formation at these fluences. In contrast, at fluences high enough to induce melting, K_{rec} decreases much (experimentally, estimated to drop to <10%). As a result, the temperature dependence of K_{rxn} becomes the determining kinetic factor. Thus, besides the temperature, viscosity changes may

σaffect much the evolution of even simple (i.e., abstraction) reactions in the irradiation of polymers with intense UV laser pulses. This factor is probably, at least partly, responsible for the different relative extent of chain-bond scission vs. cross-linking (i.e., resulting from recombination of polymer radicals) that are often induced to polymers upon irradiation with increasing laser fluence [51].

3.6 DISCUSSION

In all, dopant reaction kinetics upon irradiation of doped PMMA at 248 nm and 193 nm at high laser fluences is well accounted by the temperature evolution following irradiation. However, quantitatively, aspects are not well described. In particular, the viscosity changes are found to differ much from extrapolations of measurements at lower temperatures. In addition, the results illustrate the importance of the interplay of temperature evolution and of the induced transient polymer melting on product formation.

Besides the mechanistic information, the results provide also insight into the factors underlying laser processing applications of polymers/biopolymers. It is usual to ascribe the importance of processing at strongly absorbed wavelengths to the good substrate morphology attained. As demonstrated here, upon ablation at strongly absorbed wavelengths, the very sharp decrease in temperature severely limits the extent of (deleterious) chemical modifications (both of thermally-activated and of diffusion-limited) in the substrate. This factor provides an important justification for the success of laser processing of even highly photolabile substrates, as e.g. encountered in medical applications and in the restoration of painted artworks. Besides laser ablation, the present results may be also relevant to polymer decomposition and dynamics under high heating rates.

3.7 REFERENCES

1. R. Srinivasan, B.Braren, Chem. Rev., **89**, 1303, (1989).

2. I.A. Boyd, Ed., Photochemical Processing of Electronic Materials; Academic Press: London, (1992).
3. Laser Ablation. Principles and Applications; Miller, J. C., Ed.; Springer Ser. Mater. Sci., Springer-Verlag: Berlin, (1994) ; Vol. 28 (1994).
4. D. Bäuerle, Laser Processing and Chemistry; Springer-Verlag: Berlin, (2000).
5. (a) T. Lippert, J.T. Dickinson, Chem. Rev., **103**, 453, (2003) (b) T. Lippert, A. Yabe, A. Wokaun, Adv. Mater., **105,** 9, (1997).
6. N .Bityurin, B.S. Luk'yanchuk, M.H. Hong, C.T. Chong, Chem. Rev. **103**, 519, (2003).
7. S. Georgiou, F. Hillenkamp, Chem. Rev., **103,** 317, (2003).
8. A. Vogel, V. Venugoppalan, Chem. Rev., **103,** 577, (2003).
9. (a) S. Georgiou, V. Zafiropulos, D. Anglos, C. Balas, V. Tornari, C. Fotakis Appl. Surf. Sci. **127-129**, 738 (1998) (b) M. Lassithiotaki, A. Athanassiou, D. Anglos, S. Georgiou, C. Fotakis, Appl. Phys. A **69**, 363, (1999).
10. G. Paltauf, P.E Dyer, Chem.Rev.,**103**, 487, (2003).
11. (a) G. Bounos, A. Athanassiou, D. Anglos, S. Georgiou, C. Fotakis, J.Phys.Chem.B, **108**, (22) 7052, (2004). (b) A. Athanassiou, M. Lassithiotaki, D. Anglos, S. Georgiou, and C. Fotakis, Appl. Surf. Sci., **154/155**, 89-94, (2000). (c) A. Athanassiou, E. Andreou, D. Fragouli, D. Anglos, S. Georgiou, C. Fotakis, J. Photochem Photobiol A: Chemistry, **145**, 229, (2001).
12. R.J. Lade, I.W. Morley, P.W. May, K.N. Rosser, M.N.R. Ashfold, Diamond Rel. Mat. **8** 1654, (1999).
13. S. Nishio, H. Sato, Electr. Eng. Jpn., **125**, 19, (1998).
14. R. Larciprete, M. Stuke, Appl. Phys. B., **42**,181, (1987).
15. R. Srinivasan, B. Braren, K. G. Casey, Pure & Appl. Chem., **62**, 1581, (1990).
16. B.R.Arnold, J.C. Scaiano Macromolecules **25**,182, (1992).
17. D.E. Hare, D.D Dlott, Appl. Phys. Lett., **64**, 715, (1994).
18. M. Tsunewaka, S. Nishio, H. Sato, Jpn. J. Appl. Phys., **34**, 218, (1995).
19. (a) H. Furutani, H. Fukumura, H. Masuhara, J. Phys. Chem., **100**, 6871 (1996), (b) T. Masubuchi, H. Furutani, H. Fukumura, H.Masuhara, J. Phys. Chem.B., **105**, 2518, (2001) (c) H. Fukumura, E. Takasshi, H. Masuhara J. Phys. Chem, **99**, 750 (1995) and references therein.
20. D. J. Krajnovich, J. Phys. Chem. A, **101**, 2033, (1997).
21. T. Lippert, R.L. Webb, S.C. Langford, J.T. Dickinson, J. Appl. Phys., **85**, 1838, (1999).
22. H. Schmidt, J. Ihlemann, B. Wolff-Rottke, K. Luther, J. Troe, J. Appl. Phys., **83**, 5458, (1998).
23. G.C Blanchet, P. Cotts, C.R Fincher, Jpn. J. Appl. Phy,s. **88**, 2975, (2000).
24. B. Hopp, M. Csete, K. Révész, J. Vinkó, Zs. Bor, Appl. Surf. Sci., **96-98**, 611, (1996).
25. F. Wagner, P. Hoffmann, Appl. Phys. A **69**, S841, (1999).
26. E. Haselbach, Y. Rohner, P. Suppan, Helv. Chim. Acta, **73**, 1644, (1990).
27. M. Dzvonik, S. Yang, R.J Bersohn, Chem. Phys., **61**, 4408, (1974).
28. J.B. Birks, Photophysics of Aromatic Molecules; John Wiley & Sons: London, p 232. (1970).

29. (a) S. Holdcroft, B. Z. Tang, , J. Chem. Soc. Chem. Comm. 280 (1991) (b) B-Z Tang, S., S. Holdcroft, J. E. Guillet, Macromolecules, **27**, 5487, (1994).
30. J.F Rabek, Mechanisms of Photophysical Processes and Photochemical Reactions in Polymers: Theory and Applications; John Wiley: Chichester, (1987).
31. Alternatively, the estimation is based on the measurement of the number of laser pulses necessary for the complete photolysis of ArI within PMMA upon irradiation at low laser fluences (50 –100 mJ/cm^2). The main error in the approach is introduced by the changes in the substrate absorptivity (due to both Ar-deriving photoproducts and PMMA decomposition products) that are induced in parallel (thus, condition of optically thin sample is not satisfied after extensive irradiation).
32. S. Lazare, V. Granier, J. Appl. Phys., **63**, 2110, (1988).
33. H. Fujiwara, H. Fukumura, H. Masuhara, J. Phys. Chem. **99,** 11844, (1995) and references therein.
34. H.Furutani, H. Fukumura, H. Masuhara, J. Phys. Chem., **100**, 6871, (1996).
35. (a) M.N Ediger, G.H Pettit, J. Appl. Phys. **71**, 3510 (1992) (b) G.W Pettit, M.N. Ediger; D.W Hahn, B.E. Brinson, R. Sauerbrey, Appl. Phys. A., **58**, 573,(1994).
36. J.C Scaiano, (Ed.), Handbook of Organic Photochemistry; CRC Press: Florida, : Vol. II. (1989); J.C. Scaiano, L.C. Stewart, J. Appl. Phys., **105**, 3609, (1983).
37. D.P Brunco, M.O. Thompson, C.E Otis, P.M Doodwin, J. Appl. Phys. **72**, 4344, (1992). (b) S.R. Cain, F.C Burns, C.E Otis, J. Appl. Phys., **71**, 4107, (1992).
38. S.V. Babu, G.C. Couto, F.D. Egitto, J. Appl. Phys., **72**, 692, (1992).
39. (a) S.Chen, I.-Y.S. Lee, W.A. Tolbert, X. Wen, D.D Dlott, J. Phys. Chem. **96**, 7178 (1992) (b) I.-Y. S. Lee, X. Wen, W.A. Tolbert, D.D Dlott, M. Doxtader, D. RArnold, J. Appl. Phys. **72**, 2440, (1992).
40. In fact, for weakly absorbing systems, a nonzero slope in the F_{LASER}-dependence, indicating deviations from this simple formula, is observed even above the threshold. However, because of the previously noted influence of scattering effects on the probing step, we refrain from assigning particular significance to the observed small slopes.
41. Y.G Yigling, B.J.Garrison, Nucl. Instr. Methods B, **203**, 188, (2003).
42. R.N. Haward and R.J.Young, The Physics of glassy polymers; Champand & Hall: London, (1997).
43. D. W. van Krevelen and P. J. Hoftyzer, Angew. Macromol. Chem., **52**, 101, (1976).
44. H. M. Laun, Pure Appl. Chem., **70**, 1547, (1998).
45. F. Beinhorn, J. Ihlemann, K. Luther, J. Troe, Appl. Phys. A., **68**, 709, (1999).
46. V. N. Tokarev, A.F.H Kaplan, J. Appl. Phys., **86**, 2836, (1999).
47. F. Weisbuch, V.N Tokarev, S. Lazare, D. Debarre, Appl. Phys. A ., **76**, 613, (2003).
48. N. Arnold, N. Bityurin, Appl. Phys., A. **68,** 615, (1999).
49. G. Bounos, A. Kolloch, T. Stergiannakos, E. Varatsikou, S. Georgiou, J. Appl. Phys., **98**, 084317 (2005)
50. R M Noyes, Prog. React. Kinet., **1**, 29, (1961).
51. N. Bityurin, S. Muraniov, A. Alexandrov, A. Mlyshev, Appl. Surf. Sci., **109/110**, 270, (1997).

Chapter 4 INFLUENCE OF POLYMER MOLECULAR WEIGHT

4.1 INTRODUCTION

In this chapter, we present the influence of polymer molecular weight (Mw) on the laser induced processes within the substrate. Mw determines the number of bonds required for monomer/oligomers formation. For a "simple" thermal process, the ablation depends strongly on formation of monomers/oligomers as presented by the bulk photothermal model. In addition, by varying the Mw all the Arrehnius decomposition parameters (per bond) remain the same. Thus, the examined systems were chemically identical, differing only in the number of bonds. On the other hand, for mechanistic aspect, Mw of a polymer is an important parameter, as it determines many of its physical characteristics such as transition temperatures, viscosity and mechanical properties. For application aspect, in several laser processing schemes on real systems such as those encountered in medical and laser conservation applications, the Mw values of the treated polymeric-like substrates may vary a lot from case to case. Thus, the understanding of the Mw influence on the processes is important for the optimization of laser processing schemes.

In the case of PMMA upon the irradiation at 248 nm it is general accepted that a thermal mechanism is taking place. However, there are still several observations that cannot be accounted in satisfactory way. D.Dlott and coworkers [1] have been reported that the processes upon the ultrafast heating of PMMA with ns pulses should differ from classical decomposition pathways. But, the nature of deviation has not been specified. In addition, Srinivasan and coworkers [2] have been presented a high cluster/monomer ratio which generally observed upon UV irradiation. He considers it incompatible with a thermal mechanism. For addressing this issue, we rely here on a methodology demonstrated previously for assessing the temperature evolution and polymer viscosity changes in the 248 nm irradiation of PMMAs with Mw ranging from 2.5 kDa to 996 kDa. Briefly, as presented in the Chapter 3, this methodology relies on monitoring the

formation of aryl products in the irradiation of polymer doped with iodonaphthalene or iodophenanthrene.

4.2 ABLATION THRESHOLDS AND MORPHOLOGICAL CHANGES

UV irradiation at 248 nm results in swelling and/or etching of PMMA films depending on the fluence. The ablation thresholds as determined by profilometry are collected in Table 2. For irradiation at weakly absorbed wavelengths, the swelling onsets and the etching thresholds increase with increasing Mw. However, with increasing doping (i.e., increasing absorption coefficient) or at strongly absorbed wavelengths, the difference in the ablation thresholds is much smaller or minimal [3]. Below the threshold, swelling is observed for both NapI- and PhenI-PMMA doped systems, but most importantly, when comparing at the corresponding ablation thresholds, swelling is much more pronounced for the higher Mw system (e.g., for the 1.2% NapI/PMMA the maximum swelling is ≈8 μm vs. ≈4 μm for the low Mw polymer). On the other hand, for PS, which is strongly absorbing at 248 nm no swelling is detected in agreement with previous reports.

Irradiation of PMMA films at 248 nm, gives rise to the growth of micro-bubbles [4] (Fig.4.1). The typical bubble diameter, estimated by at least 5 different measurements, increases expectably with laser fluence (Table 2), evidently due to the higher amount of gaseous products accumulated in the substrate by the decomposition of the polymer with increasing laser fluence [5]. Once the ablation threshold is overcome, material starts to be ejected to the plume, thus limiting any further increase of bubble size (Fig.4.2). Increasing of the optical absorption coefficient through doping (e.g. $\alpha_{1.2NapI/PMMA}$ = 360 cm^{-1}, $\alpha_{0.5PhenI/PMMA}$ = 560 cm^{-1}, $\alpha_{1.2PhenI/PMMA}$ = 910 cm^{-1}) results in a decrease of the bubble size.

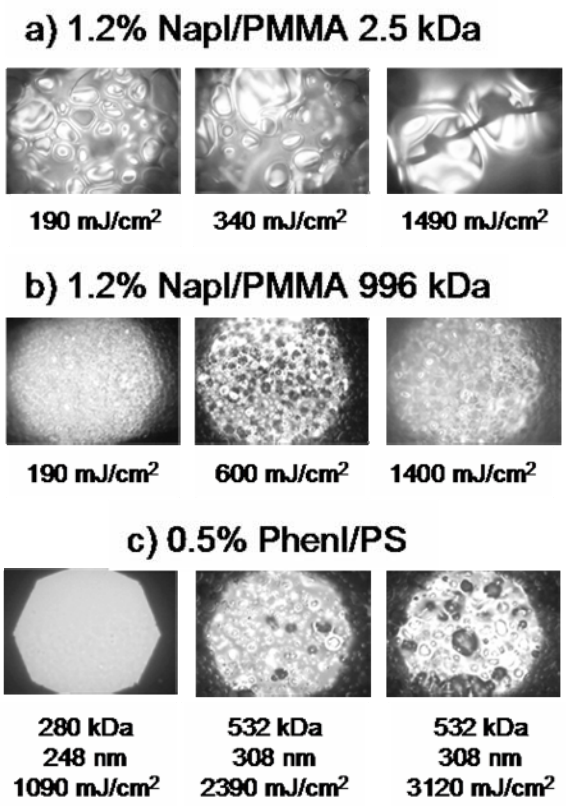

Figure 4.1: *Optical micrographs (magnification 50 x) of films areas irradiated with a single laser pulse at the indicated fluences: a) 1.2% NapI/PMMA 2.5 kDa irradiated at 248 nm, b) 1.2% NapI/PMMA 996 kDa irradiated at 248 nm, c) 0.5% PhenI/PS irradiated at 248 nm and 308 nm. The size of each picture is 70x95 μm^2.*

In the same trend, upon irradiation of highly absorbing PS at 248 nm ($\alpha_{0.5PhenI/PS}$=5380 cm^{-1}), no swelling, bubbles or other morphological modifications are visible under the optical microscope (Fig. 4.1c). Ablation at strongly absorbed wavelengths is induced without noticeable morphological modifications to the etched substrate ("clean etching"). On the other hand, irradiation of PS at 308 nm, where polymer absorption is low ($\alpha_{0.5PhenI/PS}$ = 340 cm^{-1}) induces micrometric size features in the substrate (Fig.4.1c), in close similarity with the results obtained for PMMA at 248 nm. Although decomposition pathways of PS may differ from those for PMMA, overall at comparable absorption coefficients, we find close correspondence between the two systems, as far as morphological changes are concerned.

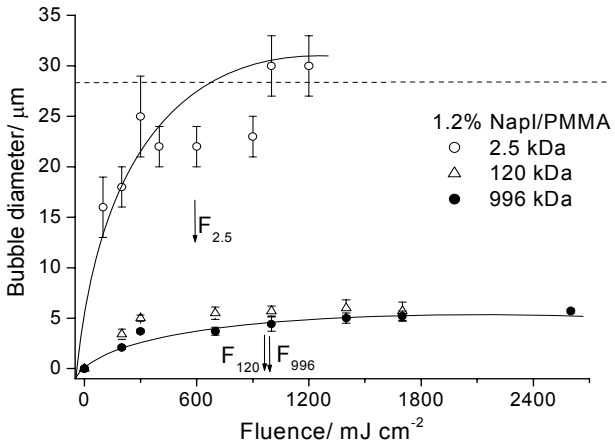

Figure 4.2: *Bubble average diameter dependence as a function of fluence for samples of 1.2% NapI/PMMA, Mw 2.5, 120 and 996 kDa irradiated at 248 nm. The horizontal dashed line is drawn at the value (28 μm) of the optical penetration depth in the 2.5 kDa substrate. Continuous lines are visual guides. The ablation threshold fluences for the different Mw systems are indicated by arrows.*

To investigate further the production of bubbles in the strongly absorbing substrates, samples of 0.5%wt PhenI/PS irradiated at 248 nm were observed with high resolution by ESEM.

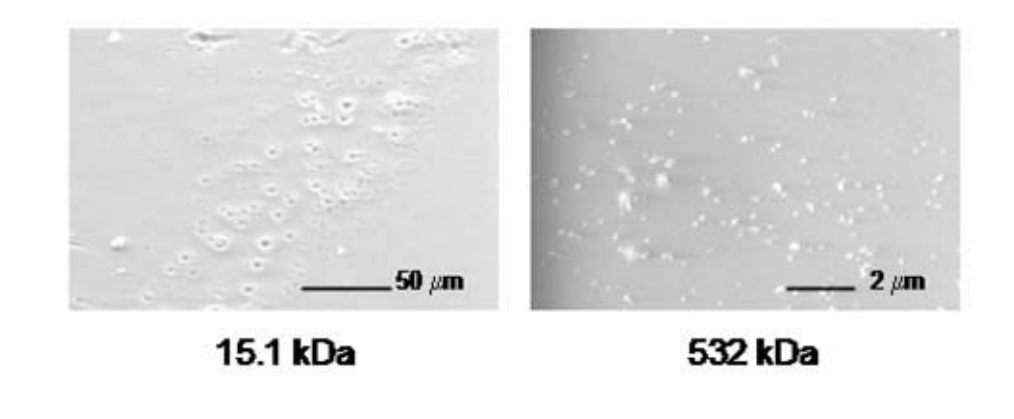

Figure 4.3: *ESEM micrographs of 0.5% PhenI/PS, irradiated with a single pulse at 248 nm. The fluence in both cases was 650 mJ/cm^2.*

As seen in Fig.4.3, no morphological changes are detected in the irradiated area of the high Mw system, except for the presence of some redeposited material. However in the low Mw system, bubbles with diameter of few μm are visible. Bubble formation and polymer surface swelling has been a common observation in ablation studies [6-8]. However the dependence of Mw has not been examined. Yet, as demonstrated here, laser induced morphological modifications, in particular the size of the bubble is

observed to depend strongly on this polymer parameter. Bubbles are on average larger in the films of low Mw, this being a general behaviour which is observed (followed) for systems with high and low linear absorption coefficient α. Generally, the maximum bubble diameter is comparable to the optical penetration depth 1/α (Table 2).

Table 2: *Swelling onset and ablation and substrate transmission transient thresholds (in mJ/cm^2), optical penetration depth as estimated from the small-signal values (1/α) at 248 nm of doped polymer films and average maximum bubble diameter after a single pulse. Errors are estimated in 10-20% for determination of thresholds and about 10% for determination of bubble size.*

System (wt)	Mw (kDa)	Swelling	Ablation	Substrate transmission transient	1/α (μm)	Maximum bubble diameter (μm)	Maximum surface swelling (μm)
1.2% NapI/PMMA	2.5	40	580	70	28	30	8
	120	100	960	[b]		6	7
	996	160	970	215		5	4
0.5% PhenI/PMMA	2.5	50	700	[b]	18	21	[a]
	120	[a]		[b]		4	[a]
	996	[a]		[b]		4	[a]
1.2% PhenI/PMMA	2.5	30	240	70	11	14	[a]
	120	[a]		[b]		5	[a]
	996	[a]		120		4	[a]
0.5% PhenI/PS	15.1	[a]	37	[a]	0.3	<0.5	[a]
	280	[a]		[a]		<0.5	[a]
	532	[a]		[a]		<0.5	[a]

[a] Not detectable.

[b] Not measured.

4.2.1 Substrate transmission

The measurements of the real-time transmission of a CW HeNe laser through the irradiated film can provide information of the time scale of the morphological changes reported above.

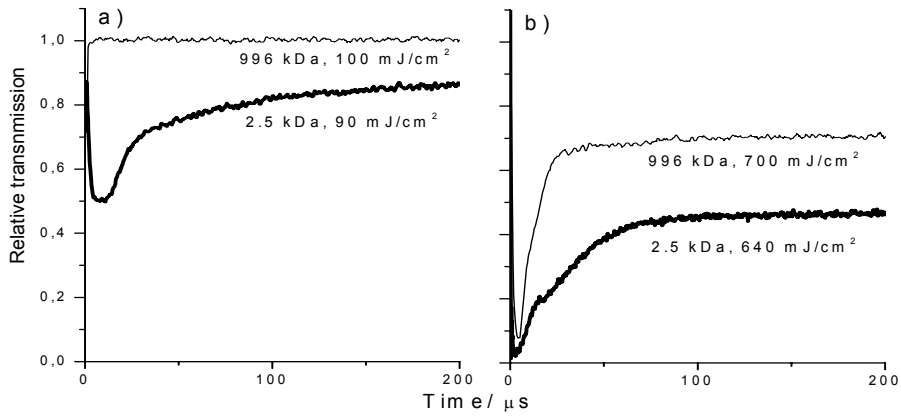

Figure 4.4: *Time resolved relative transmission of a CW HeNe laser by 1.2% PhenI PMMA films irradiated at 248 nm with polymer 2.5 kDa (thick line) and 996 kDa (thin line) at fluences: a) below ablation threshold, and b) above ablation threshold. The time origin represents the arrival of the 20 ns ablation pulse to the substrate.*

Fig.4.4 shows the transmission transients recorded by the photodiode in films of 1.2% wt PhenI/PMMA normalized to the initial transmission film value. Different transmission transients have been observed for different Mws. For 2.5 kDa films, the transmission decreases sharply by as much as 50% within few μs for a fluence below ablation threshold (90 mJ/cm^2), and by nearly 100% for a fluence above threshold (640 mJ/cm^2). After the initial sudden reduction indicative of a very fast bubble growth, the transmission recovers to a value that is lower than the initial one. In the high Mw polymer film, both the intensity and duration of the transmission transients are significantly reduced at the corresponding fluences. This is consistent with the results reported by Masuhara et al. [9,10] of a very fast expansion of the polymer surface upon irradiation, followed by a slow contraction. By using nanosecond time-resolved interferometry these authors observed expansion and contraction of the surface at fluences below the swelling onset, and eventually the recovery of the initial flat surface. On the contrary, at fluences above the swelling onset, expansion of the film was observed to start during the excitation laser pulse, followed by subsequent contraction,

but in this case the original flat surface was not recovered (i.e., swelling remained). The slow contraction corresponds roughly to the decay of the bubbles as seen in Fig.4.4. This contraction can be ascribed to the decrease of the film temperatures, so that the production of gaseous species that drives bubble growth ceases, and also to the fact that upon cooling, the viscosity and the rigidity of the polymer increases (resulting in bubble shrinkage).

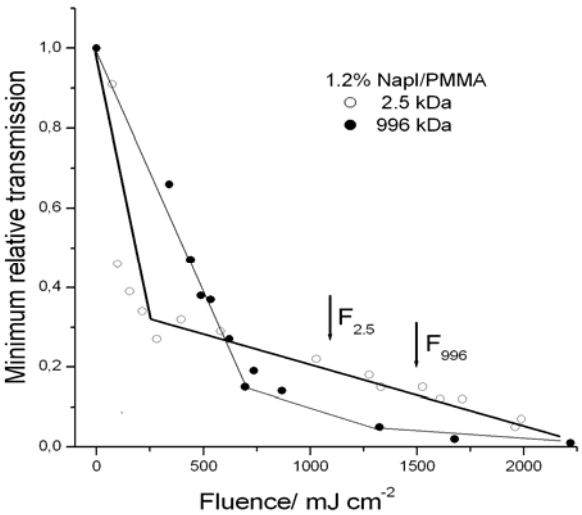

Figure 4.5: *Fluence dependence of the minimum relative transmission of irradiated films (248 nm) of 1.2% NapI/PMMA of Mw 2.5 kDa (open circles) and 996 kDa (full circles). The arrows indicate the ablation threshold of each sample. Lines are visual guides.*

Fig.4.5 depicts the fluence -dependence of the measured minimum relative transmission for 1.2% wt NapI/PMMA of 2.5 and 996 kDa. The fluence at which a significant reduction (of about 10%) of the transmission by the irradiated substrate is produced is slightly above the swelling onset of the films, and below the corresponding ablation threshold. The values of the threshold fluence for the appearance of the observed transmission transients are also listed in Table 2.

Note that the decrease is of the transmission at these fluences cannot be ascribed to scattering by material ejection, since the measurements are performed well below the ablation threshold. Thus, the transmission transients reflect the evolution of the induced morphological modifications, i.e. the time scale involved in the growth of bubbles. The production of micron-sized bubbles results in a pronounced (Mie type) scattering of the probing beam. Given their very high number especially at higher fluences, the probing beam most likely undergoes multiple scattering (changes in the refractive index of the material may also contribute partly to the probe beam decrease.

In all, the transmission measurements reveal a slower decay of the size of bubbles produced by irradiation at 248 nm in the lower Mw PMMA. Regarding highly absorbing PS-based films irradiated at 248 nm, neither the plume, nor the substrate, induce a significant attenuation of the probe beams, confirming the reduced extent of morphological modifications, as observed under the optical and ESE microscope, and the transparency of the ejected material of mainly gaseous nature [11].

4.2.2 Discussion of morphological changes

Bubble growth within viscoelastic materials, such as polymer melts, is a highly complex issue. In the case of laser irradiation, the quantitative description is further hindered by the fact that polymer properties (e.g. viscosity, etc) vary much with time, depending on the temporal evolution of the attained film temperatures and of extent of decomposition. Nevertheless, a qualitative description can account for the observations in a satisfactory way. The expansion of bubbles in a viscous liquid [30] is given:

$$R\frac{d^2R}{dt^2}+\frac{3}{2}\left(\frac{dR}{dt}\right)^2=\frac{1}{\rho}(P_g(t)-P_0)-4\frac{\eta}{R}\frac{dR}{dt}-\frac{2\sigma}{\rho R}-f(Elastic) \qquad (4.1)$$

where R denotes the bubble radius, η the viscosity, P_g the time-dependent pressure of gas accumulated within the bubbles, P_o the ambient (external) pressure, σ the surface tension and ρ the density. Thus, the rate of bubble growth increases with decreasing η and *f(Elastic)* represents the term required for the viscoelastic deformation of the polymer. It would appear that for high Mw systems, the very high η [31]

$$\log \eta = \log \eta_{cr} + 3.4 \log Mw/Mw_{cr} \qquad (4.2)$$

where η_{cr} is the viscosity at the entanglement point (~30 kDa for PMMA) could severely limit bubble growth. However, as shown above [32], much higher temperatures are attained in the high Mw and their thermal decomposition is much more extensive. As a result η is much reduced, and thus bubble formation is more efficient than expected on literature values. Both the higher rate of formation of gaseous species (oligomers, monomers), i.e. resulting in a higher P_g within the bubbles, as well as the lower σ and η and f(elastic) for the low Mw melt, contribute to produce larger and faster bubble growth for the low Mw systems. In fact, a further factor promoting bubble

formation in the low Mw, and which is not included in the simplified formula (4.1), includes the much higher diffusion of gaseous products. Because of the dependence of polymer σ and η on Mw, a correspondence between the observed bubble sizes and the glass transition temperatures may be expected. Indeed, the dependence of the size of bubbles with Mw closely follows the dependence of the mentioned polymer properties with this parameter. In the case of T_g, this dependence can be modelled by the Flory-Fox equation [33]:

$$T_g = T_{g,\infty} - \frac{K}{X_n} \tag{4.3}$$

where $T_{g,\infty}$ is the asymptotic value at high Mw, K is a constant which depends on the polymer (K= 1607 and 1635 for PMMA and PS respectively [33]) and X_n the monomer number (X_n= Mw/M_0, where M_0 is the monomer molecular weight). Values of T_g for PMMA and PS at the different Mw used in this work are listed in Table 3.

Table 3: *Glass transition temperature T_g of PMMA and PS of different molecular weights calculated according to the Flory-Fox equation.*

Polymer	**Mw (in kDa)**	**T_g (in ºC)**
PMMA	1.9	26
	2.5	47
	120	110
	996	111
PS	15.1	89
	280	99
	532	100

The corresponding values in the doped polymers could differ slightly from the ones listed due to the plastizicing effect of the dopant. However as the dopant concentration is vey low (ranges from 0.4 % wt to 1.2 % wt), its effect on T_g should be

minimal. Therefore, larger bubbles can grow in lower Mw polymer films that feature larger available free volume and lower viscosity. In addition, because of the lower opposing *f(elastic)* bubbles should decay slower in the low Mw, as indeed observed in the transmission experiments.

In view of the above conclusion, it is important to notice that the maximum polymer surface swelling (measured profilometrically) just below the corresponding ablation thresholds is much higher for the higher Mw. Considering the much higher elastic constant, the higher swelling of the high Mw PMMA clearly shows that a much higher amount of gaseous products must be accumulated/formed in the substrate for material ejection to occur.

Demonstration for a strong influence of polymer Mw on the extent and time evolution of morphological changes induced by UV laser irradiation on low absorbing polymer films has been presented. In all, both higher gaseous production and the mechanical polymer properties promote bubble formation in the low Mw PMMA. Furthermore, the observation of higher ablation thresholds as well as of higher surface swelling for the high MW PMMA can be well explained by invoking the bulk photothermal model according to which a necessary condition for ablation is the cleavage of a critical number of bonds.

4.3 ArH AND Ar_2 FORMATION

Here, we examine in detail the influence of the polymer molecular weight on UV laser ablation and the factors responsible for this dependence. To this end, we rely on a methodology described previous in the Chapter 3 for assessing the attained temperatures and the viscosity changes induced upon laser irradiation. For elucidating the responsible factors, we turn to the examination of product formation in ArI-doped PMMA on the basis of the reasoning described in the Introduction.

At low fluences, the amount of ArH formed scales linearly with F_{LASER} (slope of 1.0 ± 0.2 in log-log graphs), consistent with 1-photon photolysis of the ArI dopants. At these fluences, ArH yield is, within S/N ratio, independent of the polymer Mw. At higher fluences, the F_{LASER}-dependence of ArH amount is found to deviate from linearity (Fig.4.6). As demonstrated before [12, 13], this deviation is due to the higher attained film temperatures, resulting in higher reactivity of the aryl radicals to ArH.

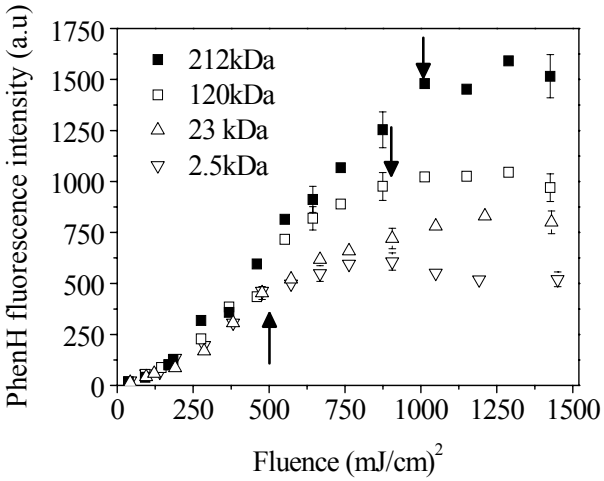

Figure 4.6: *F_{LASER}-dependence of the PhenH product formed upon a single pulse at 248 nm on virgin doped samples (0.5% wt) for the indicated PMMA Mws. The error bar represents 2σ as specified from at least 5 measurements for each system.*

Most importantly, at these fluences, the ArH intensity upon irradiation of the high Mw PMMAs is found to be somewhat higher than that in the low MW polymers. The deviation gets more pronounced with increasing Mw. The deviation in ArH formation is observed at fluences (250–500 mJ/cm^2) well below the corresponding ablation thresholds, so that this difference cannot be accounted by differences in the etching rates. For each Mw, the ArH intensity reaches a plateau at fluences close to the corresponding ablation threshold, as a result of product being removed from the substrate by the etching process. Importantly, corresponding LIF measurements on the ejected plume show that in parallel, the intensity of the ArH ejected from the low Mw PMMAs is lower than that from the high Mw ones (despite the higher amount of material removed from the former Mw). That is, ArH formation is *overall* reduced for the low Mw.

Insight into the observed difference derives from the examination of ArH formation kinetics (Fig.4.7a). At the fluences at which the linear F_{LASER}-dependence is observed, the rate of ArH formation is independent of the polymer Mw. However, at fluences >250 mJ/cm^2, the rate of ArH formation starts deviating between the various Mws. Comparing *at the corresponding ablation thresholds*, ArH formation rate increases with increasing Mw (particularly evident for times up to 1 ms). In addition, ArH formation is quenched at ≈1 ms for 2.5 kDa, whereas it continues up to ≈4 ms in

the high Mws. These differences directly demonstrate that at the corresponding ablation thresholds, higher temperatures are attained with increasing Mw.

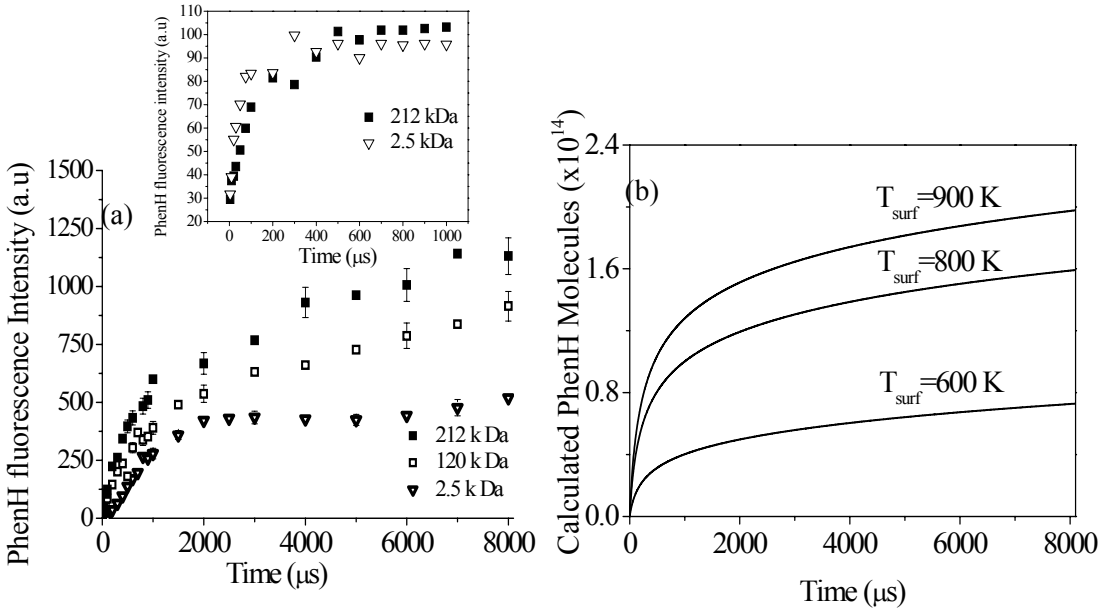

Figure 4.7: *(a) Kinetics of PhenH formation for PhenI-doped PMMA samples of the indicated molecular weights upon irradiation at the corresponding thresholds. The inset illustrates the kinetics of PhenH formation at ≈250 mJ/cm^2, showing that at low fluences, there is hardly any difference. (b) Kinetics of PhenH formation as predicted by the simulation. The maximum (surface) attained temperature for the low Mw is calculated ~600 K and ~900 K for the high Mw.*

The influence of polymer Mw on laser-induced processes is further demonstrated in the examination of the formation of the bi-aryl species in the irradiation of 1.2% wt NapI-doped samples. These include Nap_2, identifiable by the emission band at ~360 nm, and perylene identifiable by the double peak structure at ≈450 nm and ≈475 nm.

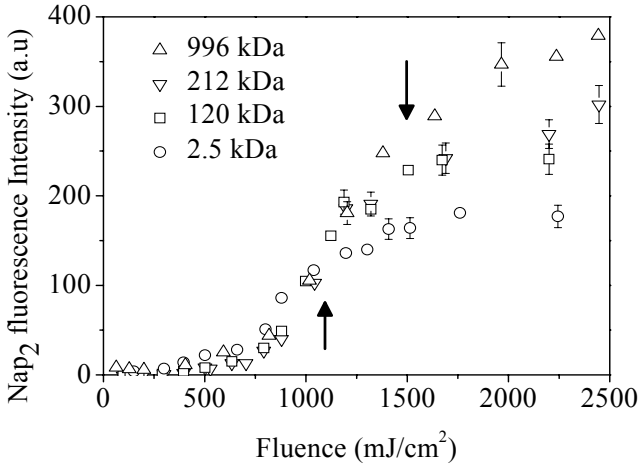

Figure 4.8: *F_{LASER}-dependence of Nap_2 formed upon a single pulse at 248 nm on virgin NapI-doped samples (1.2% wt) for different Mw PMMAs. The error bar represents 2σ as specified from 5 measurements for each system. The ablation thresholds indicated by arrows.*

For 1.2% wt NapI concentration, these species are first detected at fluences close to the swelling onset. Their yield increases with increasing F_{LASER}, reaching a plateau at the ablation threshold (Fig. 4.8). Importantly, at the same NapI concentration, Nap_2 and perylene formation is comparable or somewhat less efficient in 2.5 kDa PMMA. This is most surprising, since radical diffusion and Nap_2 formation would be expected to be more facile in the low Mw polymers.

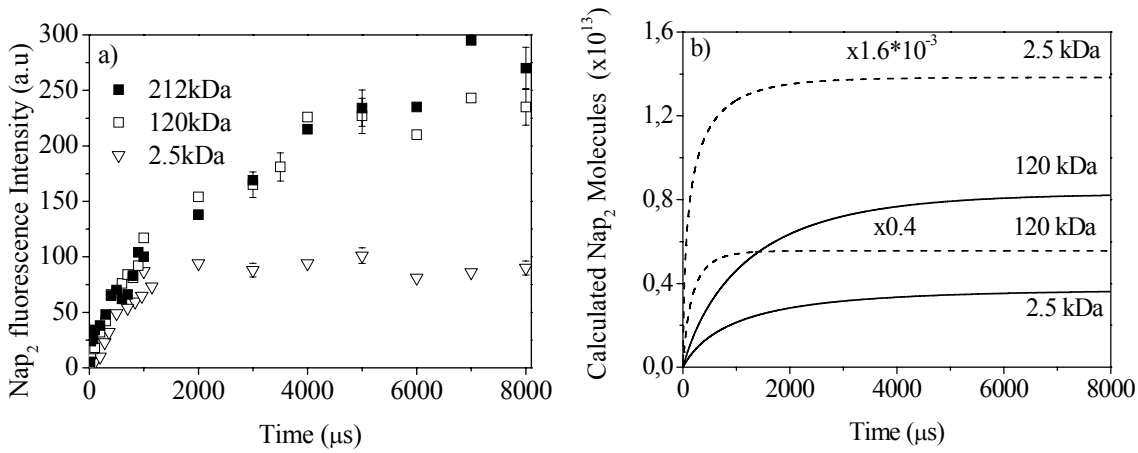

Figure 4.9: *(a) Kinetics of Nap_2 formation in the irradiation of the PMMA samples doped with 1.2% wt NapI. (b) Simulated kinetics of Nap_2 formation. The details are described in the text. The dotted lines represent the kinetics that would be expected on the basis of the literature values.*

Examination of the Nap_2 formation kinetics (Fig.4.9a) in the case of low Mws is hampered by the low Nap_2 signal. Nevertheless it is clear that Nap_2 formation is "quenched" much faster in the high Mw PMMAs. On the other hand, the initial rate of formation (in the first 500 μs in Fig.4.9a) does not appear to differ much, but as described, the data for the low Mw are subject to a large error.

4.3.1 Modelling of ArH formation; estimation of attained temperatures

The important finding of this study is that upon irradiation at 248 nm at moderate and high fluences, the extent of ArH and Nap_2 product formation in ArI-doped polymers is considerably higher for the high Mw PMMAs. At high fluences at which ablation occurs, the difference can be partly ascribed to the higher etching rates for the low Mw PMMAs. However, this explanation clearly fails at lower fluences. In this section, we consider the factors responsible for these differences and their implications for the ablation mechanisms of PMMA at 248 nm.

We estimate first the temperatures that are reached in the irradiation of the various PMMAs by modeling ArH formation kinetics. ArH is formed via a "pseudo-unimolecular" hydrogen atom abstraction from the polymer by the Ar radicals. Thus, its formation rate is simply $d[ArH]/dt = A\exp(-E_{act}/RT(z,t))[Ar](z)$, where [Ar](z) is the concentration of aryl radicals produced by the photolysis of ArI (at depth z). Hydrogen atom abstraction reactions for aromatic compounds are characterized by an activation energy E_{act} in the 40-60 kJ/mol range and a pre-exponential factor A of 10^5-10^7 s^{-1} [14-16]. The temperature evolution in the polymer following irradiation is estimated by [17]:

$$T(z,t) = T_0 + \frac{a_{eff} F_{LASER}}{2\rho c_p} \times \exp(a^2{}_{eff} D_{th} t)$$
$$\times[\exp(-a_{eff} z) erfc(a_{eff}\sqrt{D_{th} t} - \frac{z}{2\sqrt{D_{th} t}}) + \exp(a_{eff} z) erfc(a_{eff}\sqrt{D_{th} t} + \frac{z}{2\sqrt{D_{th} t}})] \quad (4.4)$$

where z the depth from the film surface, t the time after the laser pulse (erfc: complementary error function) , ρ=1.188x10^3 kgr·m^{-3} (for 120 kDa), $T_0 = 300K$. Note that in this equation there are no adjustable parameters.

Considering first absorptivity, the (small) signal value is mainly due to the dopant, since purified PMMA is nearly transparent at 248 nm. However, at higher laser fluences, non-linear absorption/multiphoton processes have been demonstrated in the 248 nm irradiation of doped PMMA [18]. We have confirmed the operation of such processes for the studied here system by transmission measurements of the "pump" beam. Most importantly, this examination shows that at fluences at which light scattering/absorption by the plume is not significant, the (effective) absorption is independent of polymer Mw. Thus, for simulating ArH kinetics, we adapt as α_{eff} an average of the values determined from transmission measurements at various fluences below the ablation thresholds.

On the other hand, because of the reduction of the number of degrees of freedom upon polymerization, c_p does decrease somewhat with increasing polymer Mw. For PMMA, we could not find literature data for the dependence on Mw, but for polystyrene [19], the difference in the $c_{p,melt}$ between 1 kDa and 490 kDa is only $0.064–7\cdot10^{-5}T$ (in $Jgr^{-1}K^{-1}$) (for T in Tg+420 K range). On the other hand, as shown by Dlott and coworkers [20], upon laser irradiation, heat capacity increases considerably (because of the extensive decomposition to smaller units/oligomers, etc). For the PMMA studied by this team (Mw~120 kDa), c_P was shown to increase from its room temperature value of $2x10^3$ $J\cdot kg^{-1}\cdot K^{-1}$ to ~$3x10^3$ $J\cdot kg^{-1}\cdot K^{-1}$ at T~600 ˚C. Thus, this increase dominates over any Mw dependence of the PMMA c_p. Finally, concerning D_{th} the polymer (melt) heat diffusivity, the limited literature data suggest weak dependence on Mw (e.g., for polystyrene, it decreases with polymer Mw by a factor of 15% [21]). Thus, we employ the same D_{th} value ($4x10^{-8}$ $m^2\cdot s^{-1}$) for all Mws in the simulations.

In view of the above, (4.4), as written, fails to account for the different temperatures attained for different Mws. The equation, as originally derived from Burns and Caine [22], neglects energy removal by desorption of volatile species (sub-ablative regime) or by material ejection (ablation), as well as heat losses due to polymer decomposition. As discussed in Chapter 3, the difference in attained temperatures must be ascribed to the different rates of material desorption and thus energy removal from the different Mw polymers (by the term "desorption" we refer to gas removal from the free polymer surface and gas diffusion into the bubbles formed within the bulk polymer – in fact, for the weakly absorbing at 248 nm PMMA, the latter contribution is the

dominant one). Both the bulk photothermal model [23] and MD simulations [24] indicate that desorption below the polymer ablation threshold is significant. Therefore, we introduce in Eq.(4.4) the term E_{rem} i.e. $\frac{a_{eff} F_{LASER} - E_{rem}}{2\rho c_p}$, for representing the energy removed by monomer/oligomer desorption (which is assumed to be fast enough, before the heat diffusion terms in Eq.(4.4) become significant). In simulating the ArH F_{LASER}-dependences and formation kinetics, all the parameters are fixed to the above indicated values and only E_{rem} is varied.

At low laser fluences, at which substrate temperature rise is minimal, ArH formation is independent of polymer Mw, as commonly observed for hydrogen-atom abstraction radical reactions within polymers [25]. At higher fluences, however, ArH formation is determined by the attained in the substrate temperatures and by the extent of heat diffusion to the sublayers. In the case of 0.5% PhenI, the thermal "influence" is estimated, in good agreement with the experiment, to become significant at ~250mJ/cm^2 (at this fluence, ~10% of the aryl radicals is indicated react to ArH). Thus, the sharper increase of the ArH yield at fluences ≥250 mJ/cm^2 in Fig.6) for the 120 kDa-996 kDa shows that higher temperatures are reached in these systems. At ≥250 mJ/cm^2, energy removal from the low Mw (2.5 kDa, 23 kDa) systems is indicated to be increasingly significant, whereas, for Mw ≥100 kDa, E_{rem} is non-negligible only at fluences above ≈500 mJ/cm^2. Therefore, though the thermal relaxation time $\tau_{th} \approx 1/(a_{eff}^2 D_{th})$ is nominally the same, heat diffusion to the sublayers is higher for the higher Mw polymers. This accounts for the longer ArH formation in these systems. Based on the modeling of kinetics (Fig.4.7b), the surface temperatures that are reached at the end of the laser pulse *at the corresponding ablation thresholds* (Table 2) are estimated to be ~600 K for the 2.5 kDa PMMA and ~800-900 K for Mw≥120 kDa.

4.3.2 Modelling of Nap_2 formation; estimation of viscosity changes

We estimate next the PMMA viscosity changes effected upon laser irradiation by considering the Nap_2 formation yields and kinetics. We have demonstrated

previously by a number of spectroscopic examinations [12] that aryl dopant aggregation is indicated only at concentrations ≥15% wt. Therefore, for the employed NapI concentrations (<2% wt), Nap_2 is formed exclusively via diffusion processes, i.e. Nap + Nap → Nap_2. At these concentrations, the average distance between dopant molecules is estimated to be ≈4 nm. Assuming Fickian-type diffusion, the distance over which Nap diffuses scales as $(6D_{sp}t)^{1/2} = [k_B Tt/(\pi\eta R_{Nap})]^{1/2}$ (where k_B is the Boltzmann constant, R_{Nap} the naphthalene radius ~ 3-4 Å). Therefore, the formation of Nap_2 up to ms times (Fig.9a) indicates that for these times, the polymer viscosity η is on average $\approx 10^1$-10^3 Pa s, comparable to the viscosity reported for polymer melts [26-27]. Consequently, the observation of Nap_2 unambiguously demonstrates melting to occur in the 248 nm irradiation for all Mw PMMAs.

For the quantitative evaluation of the viscosity changes, we model Nap_2 formation by a 2nd-order reaction, with a Smoluchowski-type rate constant $K = \frac{8k_B T}{300\eta}$ (η: Pa·s) [28]. The temperature dependence of the polymer viscosity η is approximated by the Williams-Landel-Flory (WLF) formula [25]:

$$\eta = \eta_0 \exp\left(\frac{-C_1(T - T_{ref})}{C_2 + (T - T_{ref})}\right) \tag{4.5}$$

For PMMA, the most widely used [27, 29] constants are $C_1 \approx 8.86$, $C_2 \approx 102$ °C, $T_{ref} \approx T_{glass} + 50$ [27, 29] η_0 depends on Mw as:

$$\log \eta_0 = \log \eta_{cr} + 3.4 \log \frac{Mw}{Mw_{cr}} \quad \text{for } Mw > Mw_{cr}$$

$$\log \eta_0 = \log \eta_{cr} + \log \frac{Mw}{Mw_{cr}} \quad \text{for } Mw < Mw_{cr}$$

where Mw_{cr} is the critical molar mass for entanglement coupling (~30 kDa for PMMA) and η_{cr} is the corresponding viscosity ($\eta_{cr} \approx 3 \times 10^5$ Pa s) [27]. [At temperatures exceeding the glass temperature T_{glass} by ≥200 °K, an Arrhenius-type dependence appears to be more valid [29]. However, because the parameters for this dependence are not well established in the literature, we do not use this parameterization further. Nevertheless, we examined it only to arrive at similar deviations as those noted for the

WLF formula. The temperature evolution is modeled by Eq.(4.4) and the influence of the competing H-atom abstraction reaction for ArH formation is taken into account as described in Chapter 3.

Simulations of the Nap_2 yield and kinetics on the basis of the literature parameters are in serious discrepancy with the experimental results. For instance, since Nap_2 formation in the 2.5 kDa PMMA is predicted to be nearly two orders of magnitude higher than that in the 120 kDa PMMA (dotted lines in Fig.9b), since the WLF formula suggests a much lower viscosity (and thus much higher diffusion rate of the Nap radicals) for low Mw polymers. Furthermore, Nap_2 formation is predicted to be "quenched" at much shorter times than observed experimentally.

Nap_2 formation kinetics and its F_{LASER}-dependence can be modeled in a satisfactory way only by adjusting the C_1 and η_0 parameters in Eq.(4.5). Note that Nap_2 formation kinetics is specified by the temperature dependence of η (i.e. by the exponential), whereas its yield is specified both by η_0 and by the exponential factor.

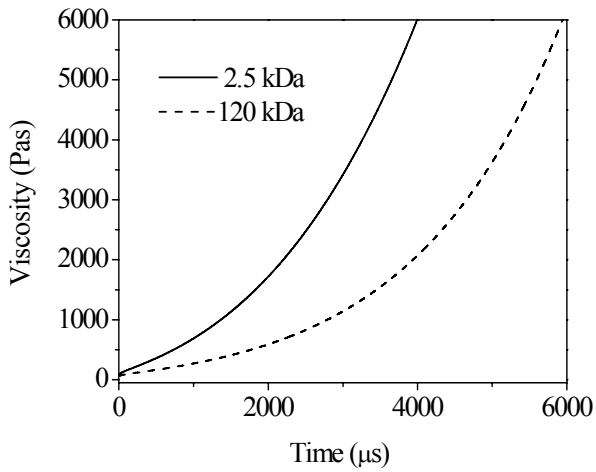

Figure 4.10: *Estimation of viscosity evolution for 2.5kDa and 120 kDa PMMA deriving from Nap_2 kinetics formation as described in the text.*

Considering first Nap_2 formation kinetics, a satisfactory simulation can be obtained by setting C_1 =0.5x8.86 for the low Mw system and C_1=0.3x8.86 for high Mw system. Simulating next the ratio of Nap_2 intensities results in $\eta_0 \approx 10^5 - 10^4$ Pas for the low Mw and the high Mw. The estimated temporal evolutions of the viscosity upon irradiation are illustrated in Fig.10. The conventional parameters for Eq.(4.5) derive from measurements at much lower temperatures than those attained upon laser

irradiation. Since laser irradiation results in polymer thermal decomposition, gaseous bubble formation, etc, it is understandable why these parameters fail to describe the polymer viscosity changes (in fact, it is even ambiguous if under these conditions, the terms "viscosity " and "radical diffusion" are valid/appropriate). The dependence of the laser-induced polymer viscosity changes on Mw can also be rationalized. Because of the higher temperatures attained in the high Mw PMMAs, the extent of decomposition and thus the decrease of η (relatively to the initial value) is higher. Indeed, optical examinations show that for the high Mws, bubbles in the substrate, although smaller in size, are much more numerous than in the low Mw systems. In addition, at the corresponding ablation thresholds, swelling is much more pronounced for the high Mw PMMAs, indicating a higher 'effective' free volume available for Nap radical diffusion.

4.4 EXAMINATION OF PMMA AT 193 nm

Based on the previous methodology, we turn next to the examination of ArH formation in the irradiation of PMMA of different Mws at 193 nm.

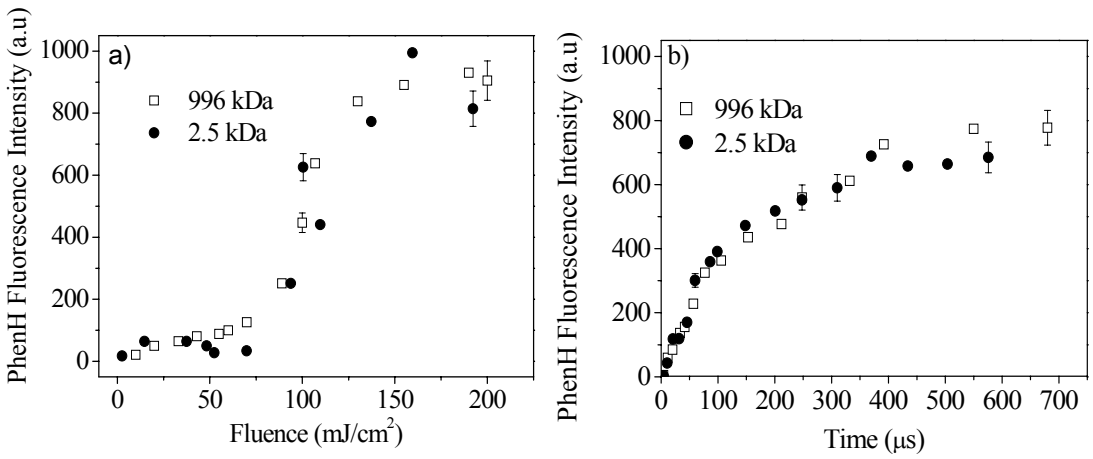

Figure 4.11: *a) F_{LASER}-dependence of PheH formed upon a single pulse at 193 nm on virgin PhenI-doped PMMA samples (0.5% wt) for two differerent Mw. The error bar represents 2σ as specified from 5 measurements for each system b) The corresponding kinetics of PhenH formation (F_{LASER}=150mJcm^{-2}).*

At this wavelength, it has been difficult to account for its ablation exclusively in the framework of a thermal model, and it has been one of the most unquestionable system for the operation of photochemical model. Srinivasan [34] has claimed that the material

ejected upon 193 nm ablation of PMMA appears exclusively in solid form. Even Baurle [35] suggests that ablation of PMMA at 193 nm must be driven by stresses, although the origin of the stresses has not been specified.

As described in Chapter 3, our methodology based on the monitoring of ArH formed upon photolysis of aryl iodides doped within the polymer suggest a substantial thermal "component". Of course, the temperature estimation hinges on values assumed for C_p and D_{th} of polymer upon ablation; so inappropriate values for these parameters may significantly affect the accuracy of estimated temperature. For more complete study, we turn to the examination of the influence of Mw. At this wavelength PMMA is a strongly absorbed system $\alpha_{0.5\%PhenI/PMMA}$=6000 cm^{-1}. Fig.4.11a illustrates the ArH formation as a function of laser fluence for 2 typical Mws. The corresponding ArH formation kinetics is illustrated in Fig.4.11b. It is immediately evident that ArH formation yield and kinetics hardly differ for different Mws. The attained temperatures are estimated via the previous method to be ~800 K indepently MW.

4.5 EXAMINATION OF POLYSTYRENE at 308 nm

Here, we extend the approach of doped polymers with simple aromatic dopant (NapI, PhenI) for examing the influence of polysterene Mw on the ablation mechanisms upon the irradiation at 308 nm. At this wavelength polysterene is a weakly absorbed system $\alpha_{0.5\%\ PhenI/PS}$=100 cm^{-1}. As illustrated in the Fig.4.12 we observed the same quantitave F_{LASER}–dependence of the product formation consistent with a thermal proposed mechanism as described in the Chapter 3. Most importantly the product formation differs quantitatively by changing the polysterene Mw. In the case of high Mw, an increased PhenH formation is observed. It means that higher temperatures are attained on the substrate of the higher Mw polysterene. This results indicates the validity of the the mechanisms independently from the polymer chemical structure and the irradiation wavelength.

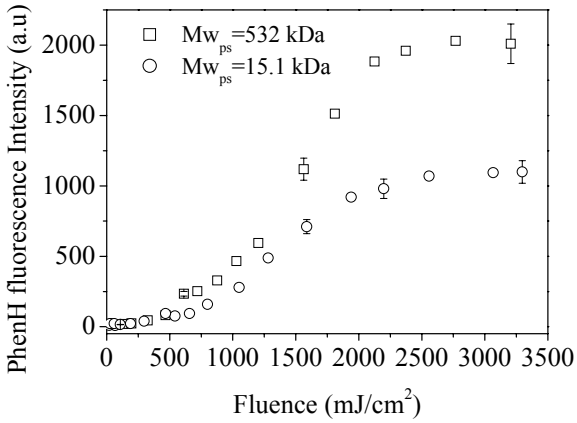

Figure 4.12: *F_{LASER}-dependence of PheH formed upon a single pulse at 308 nm on virgin PhenI-doped PS samples (0.5% wt) for different Mw PSs. The error bar represents 2σ as specified from 5 measurements for each system.*

4.6 CONCLUSIONS

The influence of PMMA Mw on laser-induced processes has been examined by probing the aryl products formed by iodo-aromatics probes dispersed in the polymer. We find that ArH yield is enhanced with increasing polymer Mw due to the higher rate and prolonged formation. The observed kinetics demonstrates that higher temperatures are attained for the higher Mw systems. In parallel, formation of Nap_2 demonstrates melting to occur for all Mws PMMA. However, the viscosity changes differ much from extrapolate ions based on conventional/literature values, with "effective" viscosity in the laser irradiation of high PMMA being comparable to that for the low Mw PMMA. The results are well accounted within the bulk photothermal model. Ejection is initiated at comparable (if not equal) degree of depolymerization of the polymers.

Besides providing a better understanding of the influence of polymer properties on laser ablation, the results may have important implications for laser-processing schemes of molecular substrates (e.g. laser medical procedures, laser restoration of artworks, etc), where the influence of the Mw has been largely neglected.

4.7 REFERENCES

1. (a) S. Chen, I.-Y.S. Lee, W. A. Tolbert, X. Wen, D.D. Dlott, J. Phys. Chem. **96**, 7178 (1992). (b) I.-Y. S. Lee, X. Wen, W.A. Tolbert, D.D. Dlott, M. Doxtader, D. R. Arnold, J. Appl. Phys. **72**, 2440, (1992) .
2. R. Srinivasan and B. Braren, Chem. Rev. **89**, 1303, (1989).
3. E. Rebollar, G. Bounos, M. Oujja, S. Georgiou, Castillejo, M. J. Phys.: Conf. Ser.(2006**)**, in press.
4. E. Rebollar, G. Bounos, M. Oujja, C. Domingo, S. Georgiou, M. Castillejo, Appl. Surf. Sci., **248,** 254, (2005).
5. E. Rebollar, M. Oujja, M. Castillejo,S. Georgiou, S. Appl. Phys. A, **79,** 1357, (2004).
6. T. Efthimiopoulos,Ch Ciagias, G. Heliotis, E. Heliodonis, Can. J. Phys., **78**, 509, (2000).
7. S. Lazare, V. Tokarev, A. Sionkowska, M. Wisniewski, Appl. Phys. A, **81**, 465, (2005).
8. R. Srinivasan, B. Braren,K.G. Casey, M. Yeh, J. Appl. Phys., **68**, 1842, (1990).
9. T. Masubuchi, F. Furutani, H. Fukumura, H. Masuhara, J. Phys. Chem. B, **105**, 2518, (2001).
10. H. Furutani, H. Fukumura, H. Masuhara, J. Phys. Chem., **100**, 6871, (1996).
11. E. Rebollar, et al, Appl. Phys. A, **84**, 171, (2006).
12. G. Bounos, A. Kolloch, T. Stergiannakos, E. Varatsikou, and S. Georgiou J. Appl. Phys. **98**, 084317 (2005) (b) G. Bounos, A. Athanassiou, D. Anglos, S. Georgiou, and C. Fotakis, J. Phys. Chem. B **108**, 7052, (2004).
13. G. Bounos, A. Athanassiou, D. Anglos, S.Georgiou, Chem. Phys. Lett., **418**, 317, (2006).
14. J. B. Birks, Photophysics of Aromatic Molecules, (John Wiley & Sons, London, 1970), pp. 232
15. J. C. Scaiano (Ed.), Handbook of Organic Photochemistry, (CRC Press, Florida, 1989), Vol.II, chapt 8
16. J. F. Rabek, Mechanisms of Photophysical Processes and Photochemical Reactions in Polymers: Theory and Applications (John Wiley, Chichester, (1987).
17. W.Schuabel, Polymer degradation (Carl Hanser Verlag Publishers, Munich, (1981).
18. H. Furutani, H.Fukumura, H. Masuhara, J. Phys. Chem., **100**, 6871, (1996).
19. a) U. Gaur, SF Lau, BB Wunderlich, B. Wunderlich, J. Phys. Chem. Reference Data **11**, 1065 (1982) (b)L. Aras, M. J. Richardson, Polymer **30**, 2246, (1989).
20. (a) S. Chen, I. -Y. S. Lee, W. A. Tolbert, X. Wen, and D. D. Dlott, J. Phys. Chem. **96**, 7178 (1992) (b) I.-Y. S. Lee, X. Wen, W. A. Tolbert, D. D. Dlott, M. Doxtader and D. R. Arnold, J. Appl. Phys. **72**, 2440 (1992).
21. J. Morikawa, J. Tan and T. Hashimoto, Polymer **36**, 4439 (1995).
22. (a) D. P. Brunco, M. O. Thompson, C. E. Otis and P. M. Doodwin, J. Appl. Phys. **72**, 4344 (1992) (b) S. R. Cain, F. C. Burns and C. E. Otis, J. Appl. Phys. **71**, 4107 (1992)

23. (a) N. Bityurin, B. S. Luk'yanchuk, M. H Hong, C.T Chong, Chem.Rev. **103**, 519 (2003) (b) N. Arnold, N. Bityurin, Appl. Phys. A **68**, 615 (1999) (c) N. Bityurin, N. Arnold, B. S. Luk'yanchuk, D. Bäuerle, Appl. Surf. Sci. **127**, 164, (1998).
24. Y.G Yigling, B.J.Garrison, J. Phys. Chem. B, **109,** 16482, (2005).
25. T. Sawaguchi, M. Seno Polymer **39**, 4249, (1998).
26. R.N. Haward and R.J Young, The Physics of glassy polymers, Champand & Hall, London, (1997).
27. J. D. Ferry, R. F.Landel and M. L. Williams, J. Appl. Phys. **26**, 359 (1955).
28. W.C Gardiner, Rate and mechanisms of chemical reactions, Physical Chemistry Monograph Series, (1969).
29. (a) D.W Van Krevelen "Properties of polymers', Elsevier, Amsterdam-Oxford-NewYork-Tokyo,(1990) (b) J. Bueche J. Appl. Phys. **26**, 738 (1955).
30. S. Beauvis, D.Reaut, R. Lazzaroni, L.D. Laude, J. Bredas, Appl.Surf. Sci, **109-108**, 218 (1999).
31. C. Wochnowski, M. A. Shams-el-Din, S.Metev, Polymer Degradation and Stability, **89**, 252 (2005).
32. N. Bityurin, B. S Luk'yanchuk, M. H Hong, C. T. Chong, Chem. Rev., **103**, 519 (2003).
33. M. A Shams-el-Din, C. Wochnowski, S. Metev, A.A..Hamza, W. Jüptner, Appl. Surf. Sci., **236**, (2004).
34. R. Srinivasan, B. Braren, and K. G. Casey, Pure & Appl. Chem., **62,** 1581, (1990).
35. D.Bauerle, Laser Processing and Chemistry, 3rd ed., Springer-Verlag, Berlin, (2000).

Chapter 5 EXAMINATION OF EJECTION PROCESS AND OF EJECTA UPON LASER ABLATION

5.1 INTRODUCTION

In this chapter, we turn to the examination of the influence of polymer Mw on the laser induced ejection process and ejecta. To this end, two main techniques have been employed; the first one is the pulsed laser deposition technique for examining the deposits deriving from irradiated polymers and the second one is the probe beam scattering (PBS) by the ejecta. The former approach is employed in order to examine the size and distribution of the particles ejected from the different Mw polymers. In the second technique (PBS), by monitoring the attenuation of the intensity of the probe beam at various distances parallel to the polymer surface, the velocity (translational) distributions of the ejected particles can be established.

5.2 CHARACTERIZATION OF DEPOSITED EJECTA

For examining the nature of the ejected material, we examine (by Scanning Electron Microscopy- SEM and Atomic Force Microscopy-AFM) the particles trapped/ deposited on a plate (substrate) placed close to and parallel to the irradiated target. Although this method does present some limitations, it has been used before successfully in ablation studies as a way of characterizing the ejected material. The main problem (limitation) of the technique is that not all ejecta stick efficiently on the receiving plate so that the obtained structures may not be fully/accurately representative of the ejecta [1]. In our case, this is not of concern because for reasons described in detail in chapter 6, our main purpose was to examine if large particles are ejected (i.e., not the stoichiometry of the ejected material). The second and most important problem is the possibility that trapped material coagulates into a film with morphology/structure quite different from that of the incident particles/material). For minimizing this problem, we have performed the experiments using the minimal number of pulses, so that the receiving plate is only sparsely coated (in all cases, the deposits consisting essentially of “islands”)-thus secondary reactions/aggregation processes on the receiving plate are

minimized [2]. Another possibility is that incident clusters, if they have high enough energy, may fragment upon collision with the substrate. In our case, since measurements are limited to fluences just above the ablation threshold, we do not expect the clusters to have that high kinetic energy; thus, fragmentation should be of major concern. Thus, the clusters observed on the trapping plates are thought to represent accurately the cluster distribution of the ejecta.

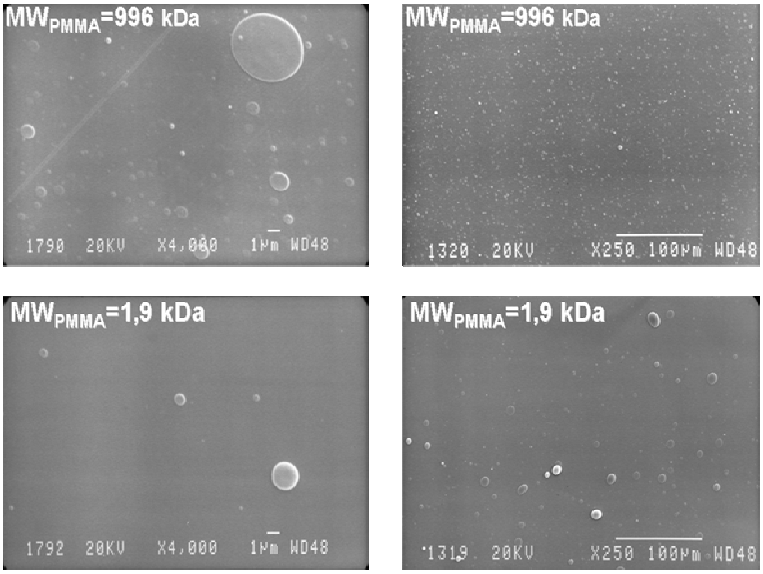

Figure 5.1: *Scanning electron microscopy images SEM (with resolution 100 μm at the left and 1μm at the right) of deposits from 1.2 wt NapI/PMMA target at 248 nm.*

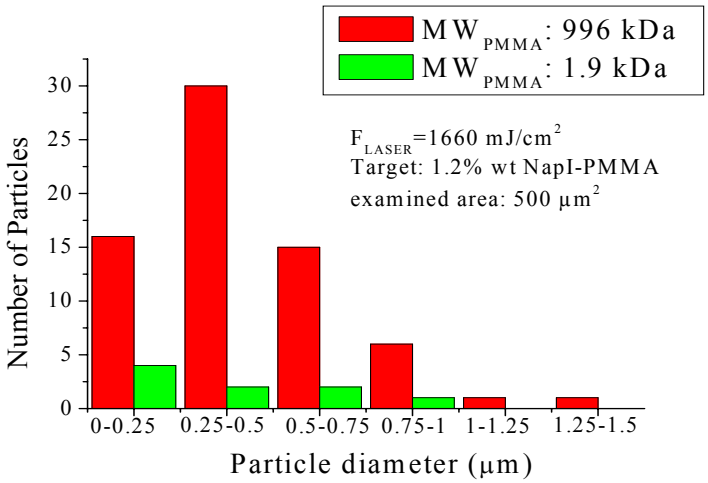

Figure 5.2: *Size distrtribution of clusters in the deposits from 1.2 % wt NapI/PMMA target at 248 nm as determined by software analysis of the SEM images Fig.5.1.*

For irradiation of doped PMMA at 248 nm, the deposit obtained from the high Mw systems (Mw>120 kDa) are very rich in small clusters. On the other hand for the low Mw (2.5kDa), hardly any clusters are deposited (under comparable number of pulses) Fig.5.1. For demonstrating this difference, Fig.5.1 presents SEM pictures of the deposits at 2 different levels of magnification. Fig.5.2 presents a comparison (evaluation) of the size distributions of the clusters in the deposits as determined by software analysis of the SEM images. However, it should be noted that for the low Mw systems here and there, droplets of μm size are detected. These droplets look like resolidified molten material and their appearance is quite different from the small, spherical clusters observed in the case of the high Mw systems. Although the average size/distribution changes somewhat with laser fluence, the above difference is observed at all ablating fluences (1-2 J/cm^2).

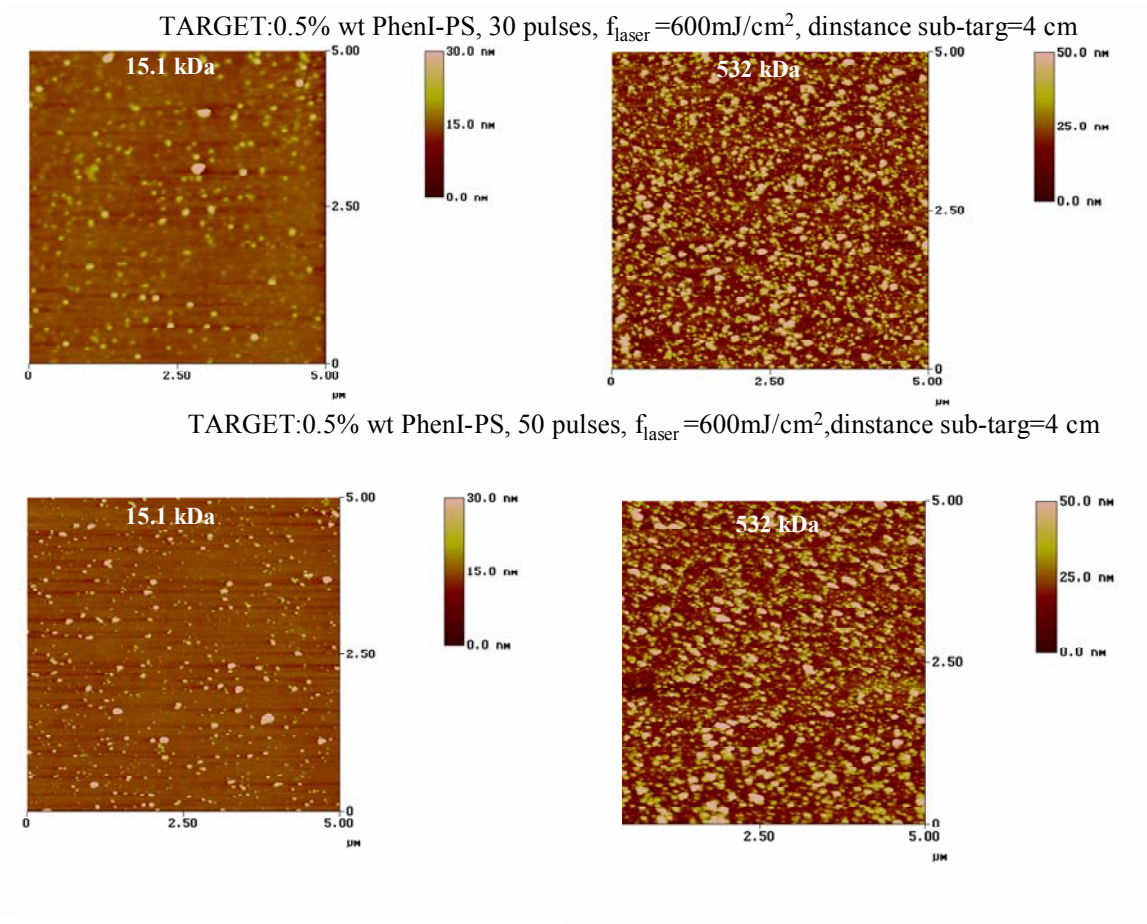

Figure 5.3: *Atomic force microscopy (AFM) images of deposits of doped polystyrene films at 248 nm. The irradiation conditions shown on the graph.*

In the case of PS at 248 nm and of PMMA at 193 nm (i.e. wavelengths strongly absorbed by the polymers), observation of structures in the deposits required irradiation for a somewhat higher number of pulses, namely 30-50 pulses. This can easily justified by the much lower etching efficiencies (and the smaller size of the clusters); thus correspondingly, material deposition is much reduced. Most importantly, even for these systems, same differences in the deposited material are observed as above: namely, the deposits obtained from the high Mw systems are much richer in clusters than the ones from the low Mw. Yet, there are some differences from the case of irradiation at weakly absorbed wavelengths. First, at least qualitatively, as compared with weakly absorbed wavelengths, even for the low Mw, the cluster distribution is rather high. The second observation is that at strongly absorbed wavelengths the size of clusters is generally is well ≤200 nm (for this reason, examined structures are best depicted in AFM images-Fig.5.3 vs. in SEM pictures), consistent with the observation of very weak scattering of the probe beam by the plume in PBS experiments. Thus, the average size of the clusters depends much on the substrate absorptivity at the irradiation wavelength. Finally and importantly, these differences/trends are observed for both PS and PMMA. Thus, though differences can be expected depending on the chemical structure of the polymer, clearly this is of secondary importance.

Observation of clusters in the ejecta is common upon laser ablation of a wide range of materials (metals, semiconductors, as well as of polymers) [1-3, 5]. However, the mechanism(s) responsible for the cluster formation remain debatable. The most usual explanation is that the clusters are formed via secondary reactions/collisions of the ejecta in the plume. In this case, the cluster growth/size should scale with the number of collisions (occurring in the plume) thus, it should scale as the square, at least of the ejected material. In the present case, since the material ejected from the high Mw polymers is much less (at weakly absorbed wavelengths) or at most comparable (at strongly absorbed ones) to that ejected from the low Mw ones (as determined by profilometric measurements described in Chapter 4), the difference in the cluster size distribution cannot be accounted by collisional/clustering effects in the plume. This is further confirmed by the fact that in PBS experiments, scattering of the probe beam is most intense when probing is performed closest to the surface. Thus, we conclude that the clusters must be ejected largely directly from the substrates. Of course, the size of

clusters may be partly modified by post desorption collisions/aggregation effects, but nevertheless not sufficient to alter the initial ejected distribution. *We conclude that generally ejection from the low Mw polymers (especially at weakly absorbed wavelengths) occurs mainly in the form of monomers or oligomers that do not stick to the glass surface, whereas ejection from the high Mw ones, takes place largely in the form of clusters.*

Cluster/droplet ejection can result from postablation liquid expulsion due to the backmomentum exerted by the primary ejected material on the remaining liquid/melt layer on the substrate. However, in the present case, the amount of material ejected from low Mw is much higher than that from the high Mw ones. Thus, though the velocity of ejecta is somewhat lower from the low Mw (Section 5.3), still the backmomentum should result in higher droplet ejection from the low Mw, at variance with observations. Cluster ejection from the high Mw polymers by post-ablation liquid expulsion can be excluded by the very fast and abrupt ejection, as demonstrated by the PBS experiments. This possibility cannot be excluded for the low Mw systems for which the few observed structures/clusters are indicated to be ejected with a slow velocity, they are of large size (i.e. clearly droplets of melt that has resolidified). Spallation is excluded, since stress confinement is negligible, e.g. $\tau_{ac}=\frac{1}{a_{eff}u_{ac}} \approx 5\text{ns} \leq \tau_{pulse}$ (u_{ac} :acoustic wave velocity). At any rate, this possibility is not consistent with all indications for thermal process demonstrated by examination in Chapter 5. The implications of the material ejection in the form of clusters for the nature of polymer thermal decomposition upon laser ablation are discussed in the next Chapter.

5.3 EJECTA TRANSLATIONAL DISTRIBUTIONS

For assessing the translational distributions of the ejecta (as well as obtaining further information on the size of the ejecta), we monitored the scattering of a probing beam (PBS) aligned parallel to the irradiated polymer substrate. Since the technique relies on scattering, it detects only particles of size comparable or larger than the probing laser light wavelength (632nm). It should be noted that upon ablation, the ejecta

range from atoms/molecules up to particles/aggregates of larger than µm size. Therefore, there is no single spectroscopic technique that can monitor this wide range of particles or their translational distributions. In our case, the photoscattering study is complemented by laser induced fluorescence monitoring/examination of the translational distributions of the ejected small fragments and of ejected ArH products, performed by the group of Dr. M.Castillejo at CSIC [4]. Here the results on the photoscattering experiments are presented.

Attenuation of the probing beam could be detected for PMMA at 308 nm and 248 nm and PS at 308 nm. For PS at 308nm, it was tried to conduct the experiments with the same dopant-concentration as used with PMMA (0.5%w.t). However at this concentration it was not possible to ablate PS upon the first pulse with the maximum laser fluence at hand. Therefore the dopant concentration was increased to 1% for further experiments. Hardly any attenuation could be detected for PS at 248nm and 193nm. Thus PBS measurements with PS were only viable at 308 nm. For PMMA, attenuation (scattering) could be detected at all three wavelengths, though the S/N ratio at 193 nm is not sufficient for reliable analysis. The above observations are easily accounted for by the results of the laser deposition/trapping of ejecta. With increasing absorption, the size of the ejected polymer fragments is as much reduced (Section 5.2) and also the amount of ejected material is reduced. Both factors contribute to reduction of the probe beam scattering at strongly absorbed wavelengths.

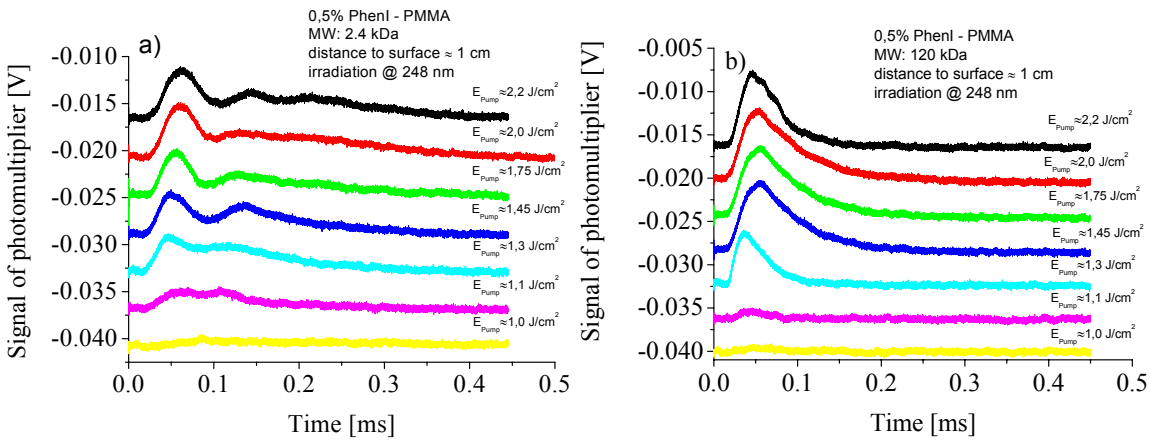

Figure 5.4: *Scattering signal (inverted) upon irradiation of the a) 2.4 kDa and b) 996 kDa 0.5% wt PhenI /PMMA with 248 nm at several fluences.*

In the cases that scattering is detectable, the onset of the signal is detected at fluences close above the corresponding ablation thresholds of the irradiated systems (as those are established by profilometric examinations). This shows that the signal detected is due to scattering of the probe beam and not simply to deflection by effusing gases. The most important finding as shown in the Fig.5.4 is that at weakly absorbed wavelengths, the low Mw systems (specifically for PMMA at Mws of 2.4kDa and 23.3kDa) are characterized by a broad, "bimodal-like" spectrum , whereas for the high Mws the spectra are quite sharp and they peak at shorter times (i.e. indicative of high velocities). For PS, it was hard to produce usable films below a molecular weight of 15.5 kDa. But for this weight a slight double structure was also detected (at 308 nm). In contrast, for the high Mw, the distribution is very sharp and in addition indicative of a very average velocity exactly as observed for PMMA at 248 nm. This difference is observed at all fluences above the ablation thresholds.

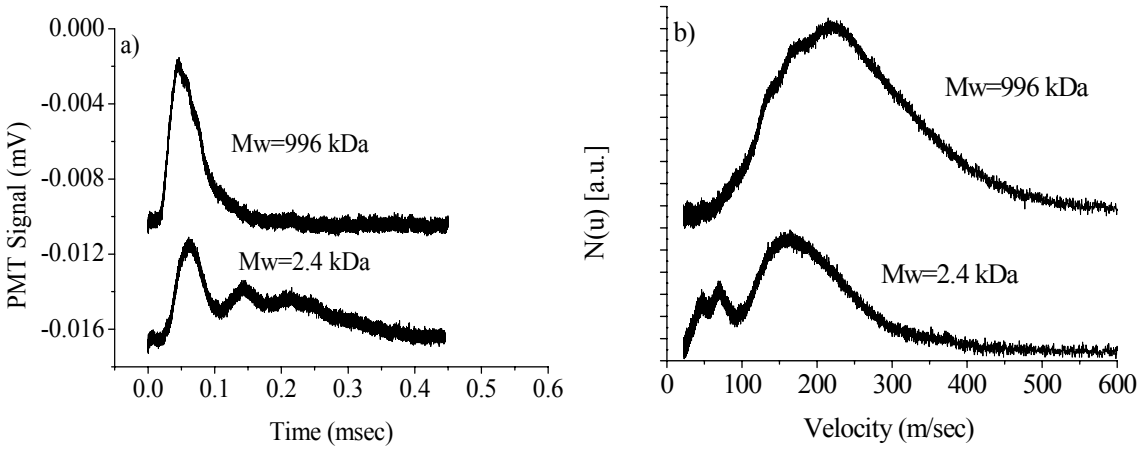

Figure 5.5: *a) Attenuation signals (inverted) for 0.5% PhenI/PMMA after irradiation at 248 nm (F_{LASER} =2,2 J/cm²).b) The corresponding velocity distributions.*

Strictly speaking, the appropriate way of presenting the data is to transform the particle flow distribution into a velocity distribution Fig.5.5. Particles with a high velocity "spend" a short time in the probed volume so that their detection is inefficient, whereas particles with a slow u result in a strong scattering signal. $I_{particle}$ over t is transformed into $N(u) = I_{particle}(t)t^2 / l$ over $u=l/t$. However for lower velocities u and therefore higher times t the noise is amplified by t^2 ($N(u) \propto t^2$). Only for spectra at high fluences and at short distances (i.e. very high S/N ratio) did the transformation

result in acceptable distribution. At any rate, fitting a Boltzmann-distribution is inapplicable as the particle mass is not known and so the fitting parameters are devoid of any meaning.

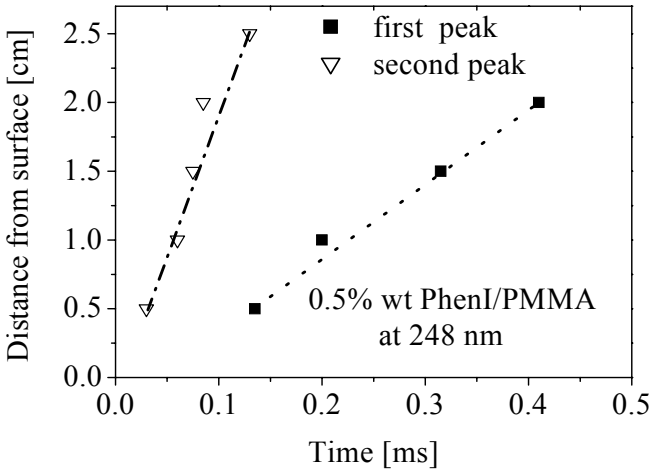

Figure 5.6: *Velocity curves for the two "peaks" observed for 2.5 kDa PMMA.*

The observed two peak-structure for the low Mw systems indicates two different species (e.g. particles of distinctly different sizes) being ejected from the surface at different speeds or one species being ejected by different mechanisms at different velocities. This seems to be supported also by Fig.5.6 of two peaks as a function of the distance of the probing beam. The data are not sufficient to distinguish between these two possibilities (this would require that angular distribution of the scattered light is examined so as to establish if the size of the 'faster' and 'slower' particles is the same or not). However, as already described in Section 5.2, the deposits obtained from low Mw systems are composed by very large droplets with a resolidified appearance. So, there seem to be two different species flying at different constant velocities: the very 'faster' component representing very small particles (size<λ), whereas the slow ones representing these very large droplets. At any rate, for the low Mw polymers, the very low average velocity suggests a thermal-type desorption/evaporation of material. In contrast, the very high and sharp velocity distribution for the high Mw polymers is indicative of an "impulsive" type mechanism; i.e. that ejection must be due to the exertion of a high pressure.

With increasing laser fluence, the distributions scale somewhat to shorter times, but the effect is not significant. This is rather surprising, because we would expect that as the amount of material ejected increases, the increased number of collisions in the plume would result in higher desorbate velocities (very much like in molecular beam expansion). On the other hand, the intensity of the signal does increase with F_{LASER}.

Integration over the full particle distribution should be proportional to the number of scattering particles. This result for different Mws PMMA doped with 0.5 % wt PhenI, is given in Fig .5.7.

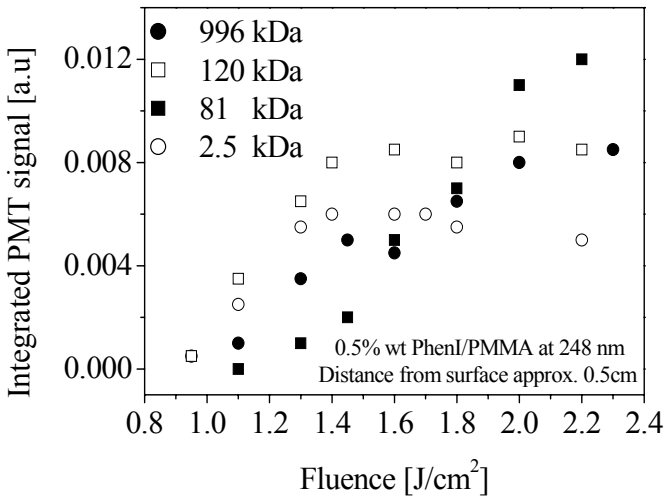

Figure 5.7: *Integrated attenuation curves for several molecular weights and pump fluences.*

The observed dependences seem to indicate that the number of the "large" scattering particles scales linearly with F_{LASER} saturating at ~ 1 J/cm^2. However, given the high variation in the data we do not give any specific importance to this indication (in addition, the proportionality between signal and scattering particles would hold only in case that the particle size does not change with F_{LASER}).

As described above, for PS at 248 nm and 193 nm, no scattering could be detected and for PMMA at 193 nm the scattering was too small for reliable analysis. For examining the influence of absorptivity, a series of experiments were performed on PMMA at 248 nm doped with PhenI at increasing concentration: 0.1% wt., 0.5% wt.,

1% wt., 1.5% wt. and 2% wt (for PMMAs of 2.5 kDa and 996 kDa), i.e. absorptivity is changed by increasing the dopant concentration.

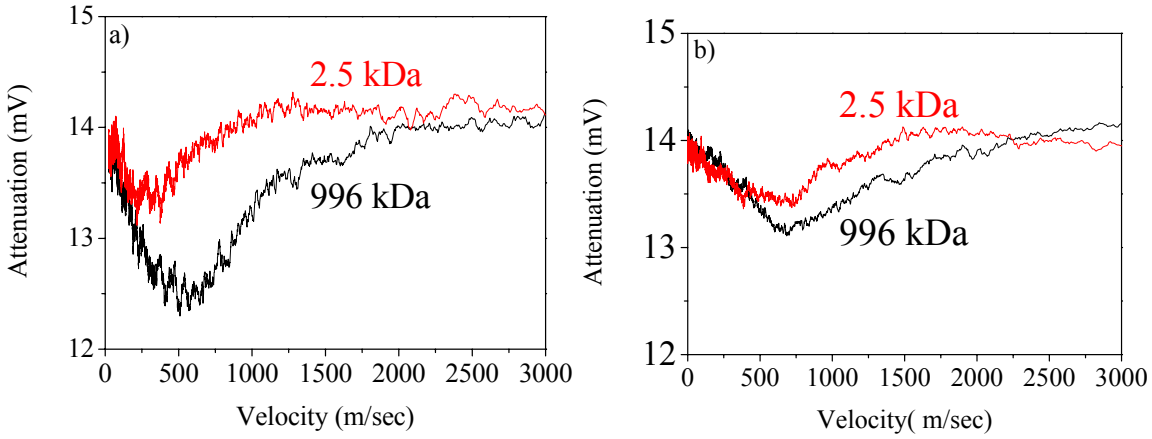

Figure 5.8: *Velocity distributions for different Mw PMMAs a) 0.5% wt PhenI/PMMA and b)2.0% wt PhenI/PMMA.*

There is clearly a correlation between the absorptivity of the sample and the intensity of scattering of the probe beam, but the dependence is not all that straightforward. Up to ~2.0% wt concentration of dopant, scattering increases with absorptivity, but beyond this concentration, scattering intensity decreases sharply (at the same pump laser fluence). The initial increase can be ascribed to the fact that for very weakly absorbing systems, increases in substrate absorptivity result in higher etching rates. On the other hand, for very high absorptivities, the etching rate (amount of material ejected) is much reduced, and also as observed in section 5.2, the size of the clusters is much smaller; both these factors result in a reduction of the scattering of the probe beam. Most importantly, these changes are paralleled by changes in the ejecta translational distributions. For dopant concentrations <2% wt, with increasing system absorptivity, the translational distributions get faster; but in all cases, for the high Mw, the distributions are sharp and of high velocity, whereas for the low Mw, the distributions are bimodal. However, above some value of absorptivity, the difference between high and low Mw polymers becomes less pronounced. Thus, it appears that for high enough substrate absorptivity, neither the temperatures in the substrate nor ejecta translational distributions differ between Mw.

5.4 PIEZOELECTRIC MEASUREMENTS

Here we present preliminary results on stress transient measurements close to ablation thresholds of the examined systems. Fig.5.9 show measured stress transients resulting from irradiation at 248 nm of 0.5%wt PhenI/PMMA for 996 kDa and 2.5 kDa PMMAs at fluences 900 mJ/cm^2 and 500 mJ/cm^2 correspondingly. At these fluences, we observed a compressive stress transient for both Mws which is inconsistent with a thermoelastic mechanism of stress generation [6-8]. The stress transient rises to its maximum in a time approximately equal to 80 ns. The oscillations on the graph are due to acoustic reflections and the electronic noise of the acoustic transducer. Most importantly the peak of the stresses resulting from the higher Mw PMMA is very pronounced than the corresponding signal from the low Mw. We believe that the generated pressure is due to the abrupt bubble growth generated from the gaseous decomposition products. Indeed, the time 80 ns for the maximum of the pressure corresponds well to the time for the maximum of bubble formation, as established by the probing experiments in Chapter 4.

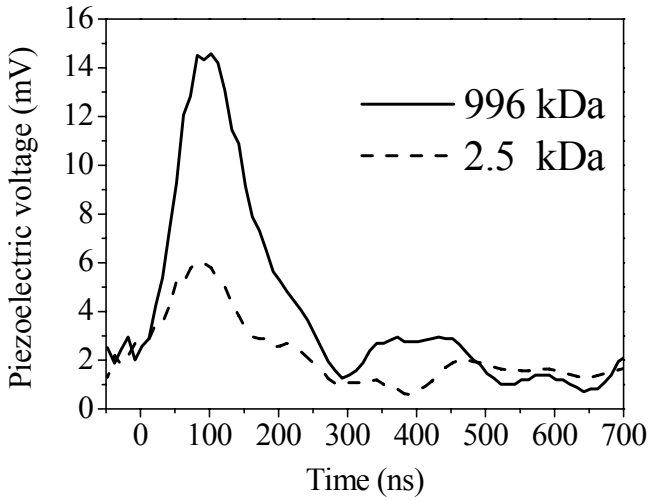

Figure 5.9: *Sample traces of stress transients as measured by stress transducer.*

The higher attained temperatures on the higher Mw systems cause a rise of pressure for these systems. In the case of the strongly absorbed wavelengths, the generated

stresses are also pronounced but there is no difference between the examined Mws of PMMA. At the moment, the high sensitivity of the acoustic system does not permit us to calibrate the piezoelectric voltage. For this reason, it is not possible to establish the absolute values of the generated pressures.

5.4 SUMMARY AND CONCLUSIONS

In this chapter the ejection upon UV laser ablation of PMMA and PS of different Mws has been examined by two techniques: namely, by laser pulsed deposition of the ejecta so as to establish their nature and second by photoscattering of probe beam for the establishing translational distributions of (of the large particles) the ejecta. The main results are:

1. For both PMMA and PS, the deposits for high Mw (≥ 120 kDa) are very rich in clusters, whereas hardly any clusters are detected for low Mw polymers. This trend is observed at all 3 excimer wavelengths examined; the only difference is that at strongly absorbed wavelengths, the size of the clusters is, on average much smaller than at weakly absorbed wavelengths. Most importantly, it is strongly indicated that the clusters are mainly ejected from the bulk (i.e. they are not formed by secondary collisions in the plume) and thus these differences reflect the difference in ejection resulting from an increase of polymer Mw.
2. The photoscattering method shows that at weakly absorbed wavelengths, the translational/kinetic energies of the high Mw are considerably higher than those from low Mw systems. At strongly absorbed wavelengths the translational energies are high and between Mws are less pronounced. The results suggest the much more “impulsive” nature of material ejection forth high Mw polymers.
3. The previous conclusions have been confirmed by preliminary piezoelectric measurements of the pressures developed in the substrate-polymers upon UV laser irradiation (at fluences below the ablation threshold).

5.5 REFERENCES

1. S.M Haskin, P.John, J.Phys. Chem.B, **103,** 4566, (1999).
2. M. Handschuh, S. Nettesheim, R. Zenobi, Appl.Surf.Sci,**137**, 125, (1999).
3. E Suske, T Scharf, Schaaf P, et al.,Appl.Phys A-Mater **79**, 1295, (2004).
4. E. Rebollar, G. Bounos, A. Kolloch, M. Oujja, S. Georgiou, M Castillejo, J. Appl. Phys. **101**, 033106, (2007).
5. R. Srinivasan, Appl.Phys.A **56**, 417, (1993).
6. A.D Zweig, V.Venugopalan, and T.F Deutch, J. Appl. Phys, **74**, 4181, (1993).
7. P.E Dyer and R Srinivasan, Appl.Phys.Lett. **48**, 445, (1985).
8. G. Paltauf, and P.E Dyer, Chem Rev. **103**, 487, (2003).

Chapter 6 MODELLING OF THE INFLUENCE OF POLYMER MOLECULAR WEIGHT

6.1 INTRODUCTION

The high estimated temperatures and the indicated melting demonstrate that a thermal mechanism dominates in the irradiation of PMMA at 248 nm, independently of Mw. Thus, we firstly try to account for the dependence of the ablation thresholds and attained temperatures, of the viscosities, etc on Mw within the framework of the bulk photothermal model, which appears to be the most appropriate for polymer ablation. This analysis shows that, though qualitatively several observations are accounted, quantitatively the theoretically predicted temperatures differ from experimental ones. Most importantly the trends differ dramatically.

The observation of a high cluster yield from the high Mw polymers immediately suggests shortcoming for the thermal model indicated thus far by the studies in Chapter 4. If low Mw are being ejected mainly in the form of monomers (so that at least two bonds with neighbouring monomers must be broken), ejection of the clusters can occur by breaking a much smaller number of bonds (only the ones around the cluster). This difference explains why a simple "thermal model" predicts that etching depth →0 with increasing Mw, whereas experimentally we find that for Mw>80 kDa the etching depth is non zero. Evidently, the energy required for material ejection turns out to be much lower than expected from the bulk photothermal model. Based on this, suggest that ablation of polymers is analogous to the explosive boiling observed in the fast superheating of liquids.

6.2 MODELLING BY THE BULK PHOTOTHERMAL MODEL

6.2.1 Qualitative description

Within a simple thermal decomposition model, upon laser irradiation, energy losses include:

1. energy "consumed" by polymer decomposition at a rate of $\Delta H_b N_0 (1-n_b) A_b \exp(-\mathrm{E}_b / k_B T)$, where ΔH_b the enthalpy per polymer "strong" bond, A_b the Arrhenius factor, E_b the activation energy for its dissociation and N_0 is the initial number density of bonds.
2. energy removal via desorption (with a rate of $\rho \Delta \mathrm{H}_{des} J$, where J represents the rate of monomer/oligomer desorption, $\Delta \mathrm{H}_{des}$ the evaporation/desorption enthalpy of these species). "Desorption" includes gas removal from the free polymer surface and gas diffusion into the bubbles formed within the bulk polymer. For the weakly absorbing at 248 nm PMMA, because of the very high number of bubbles formed within the bulk polymer, desorption into the bubble is the dominant process responsible for energy removal.

Thermogravimetric measurements show that, E_b, ΔH_b and A_b are nearly independent of Mw. Therefore, the rate of the energy "consumed" by polymer decomposition is not responsible for the observed temperature differences. On the other hand, the rate of oligomer/monomer formation should differ much with Mw. Since the polymers are chemically identical, desorption is expected to occur at the same oligomer size. However, for the high Mw systems, the rate of formation of such species is much reduced, whereas for the low Mw PMMAs, decomposition to monomers is significant at $\mathrm{F}_{\mathrm{LASER}}$ as low as 250 mJ/cm^2, thus accounting for the lower temperatures attained. Actually, the difference is expected to be larger than estimated, because Eq.(4.4) does not take into account that the low Mw PMMA examined are smaller than the "unzipping length" (≈50 kDa) of PMMA.

Though higher temperatures are attained in the high Mw, still their ablation is effected at considerably higher fluences/temperatures than for the low Mw. According to the bulk photothermal model, the ablation threshold and the etching rate are specified by the condition that a critical fraction of bonds is broken at the interface. Clearly, the model implies that a critical concentration of monomers/oligomers is reached. For high Mw, this critical concentration can be only attained at sufficiently high temperatures. The higher degree of polymer decomposition is confirmed by micro-Raman examination of the irradiated samples, as described elsewhere [1]. It is also indicated by the higher swelling of the surface attained in the high Mw vs. in the low Mw systems at

their corresponding thresholds. The swelling is ascribed to accumulation of gaseous products within the substrate. Since the optical penetration depth is the same, the depth over which gaseous products are formed is the same. Based on the previous estimation of viscosity changes, the efficiency of diffusion of the gases to the surface should be comparable. Thus, the higher swelling observed for the high Mw polymers demonstrates the much higher quantity of gaseous product formed, thus that higher decomposition is necessary for effecting material ejection.

6.2.2 Mathematical modelling

(In collaboration with Dr. N.Bityurin, Russian Academy of Science)

Here we examine first the use of bulk photothermal model for accounting for the temperatures indicated by the ArH and Ar_2 monitoring that are attained upon UV irradiation of the polymer samples. We show that although the model meets partly in accounting for the dependence on Mw, there are several features that are not fully compatible (cannot be accounted) by the model.

The high estimated temperatures and the indicated melting demonstrate that a thermal mechanism dominates in the irradiation of PMMA at 248 nm, independently of Mw. Thus, we account for the dependence of the ablation thresholds and attained temperatures, of the viscosities, etc on Mw within the framework of the bulk photothermal model, which appears to be the most appropriate for polymer ablation.

Here we present a simplified description of the influence of polymer Mw within the framework of the bulk photothermal model by limiting consideration to fluences that desorption can be neglected. Under this condition, the model reduces to the heat diffusion equation and the kinetic equation for the decomposition of polymer bonds. The heat diffusion problem is described by:

$$\frac{\partial T}{\partial t} = D_{th}\frac{\partial^2 T}{\partial z^2} + \frac{\alpha_{eff} I}{c_p \rho} \qquad (6.1)$$

with the boundary conditions $\left.\frac{\partial T}{\partial z}\right|_{z=0} = 0$, and at t=0, $T(z,0) = T_0$ (the symbols z, t, T, c_p, ρ have been defined previously). On the other hand, bond decomposition is simply

$$\frac{\partial n_b}{\partial t} = A_b(1-n_b)\exp(-E_b/T) \tag{6.2}$$

with E_b denotes the activation energy ("normalized" to R universal gas constant) and n_b the fraction of broken bonds (per unit volume). It is directly related with the initial average polymer molecular weight. If N is the average length of the polymer chain, then its value at t=0 is $n_{b,0} = 1/N$. It is convenient to introduce a new variable $b = \ln(\frac{1}{1-n_b})$, instead of n_b. b is a monotonous function of n_b with $b \approx n_b$ at n_b<<1. Then, Eq.(6.2) becomes

$$\frac{\partial b}{\partial t} = A_b \exp(-E_b/T) \tag{6.3}$$

with the initial condition that at t=0, $b_0 \equiv \ln(\frac{1}{1-n_{b,0}})$

Upon laser irradiation, the value of b at the surface is calculated by

$$b = b_0 + \int_0^\infty A_b \exp(-E_b/T_s(t))dt \tag{6.4}$$

where T_s(t) is the time dependent surface temperature. Since $\sqrt{D_{th}t_p} << \alpha_{eff}^{-1}$, heat diffusion during the pulse is negligible. Thus, the film surface temperature at the end of the pulse is: $T_{Sm} = T_0 + \frac{\alpha_{eff}^2 F_{LASER}}{c_p \rho}$.

For $t < t_p$:

$$T_S(t) = T_0 + \frac{\alpha I t}{c_p \rho} = T_{Sm} - \frac{\alpha F_{LASER}}{c_p \rho \cdot t_p}(t_p - t)$$

Whereas for $t > t_p$ T_s(t) can be approximated by

$$T_S(t) = T_{Sm}\exp[\alpha_{eff}^2 D_{th}(t-t_p)]erfc(\sqrt{\alpha_{eff}^2 D_{th}(t-t_p)}) \approx T_{Sm}[1-2\sqrt{\frac{\alpha_{eff}^2 D_{th}(t-t_p)}{\pi}}] \tag{6.5}$$

(where, as before, $erfc(z) = \frac{2}{\sqrt{\pi}}\int_z^\infty \exp(-t^2)dt$).

The fraction of broken bonds in Eq.(6.4) is the sum of the fraction of bonds broken during the laser pulse (heating) and of that after the laser pulse (cooling). Because of the

very sharp dependence of the Arrhenius exponent on temperature, bond dissociation is significant only for temperatures very close to the maximum value, T_{Sm}.

$$\int_0^{t_p} A_b \exp(-E_b / T_s(t))dt = \int_0^{t_p} A\exp(-\frac{E_b}{T_{Sm} - \frac{a_{eff}F_{LASER}}{c_p\rho \cdot t_p}(t_p - t)})dt \approx \int_0^{t_p} A\exp(-\frac{E_b}{T_{Sm}}[1 + \frac{a_{eff}F_{LASER}}{c_p\rho \cdot t_p \cdot T_{Sm}}(t_p - t)])dt \approx$$

$$\approx A\exp(-\frac{E_b}{T_{Sm}})\int_0^{\infty}\exp(-\frac{E_b a_{eff}F_{LASER}}{c_p\rho \cdot t_p \cdot T_{Sm}^2}\tau)d\tau = A_b \exp(-\frac{E_b}{T_{Sm}}) \times \frac{c_p\rho \cdot T_{Sm}^2}{E_b F_{LASER}} \times t_p \qquad (6.6)$$

Thus, the fraction broken during the laser pulse can be approximated as the product of the maximum value of the rate, $A\exp(-\frac{E}{T_{Sm}})$ and a characteristic heating time ($t_{heat} = \frac{c_p\rho \cdot T_{Sm}^2}{E_b a_{eff} F_{LASER}} \times t_p = \frac{T_{Sm}}{E_b} \times \frac{T_{Sm}}{(T_{Sm} - T_0)} \times t_p$). Similarly, the fraction of bonds broken after the end of the pulse is estimated:

$$\int_{t_p}^{\infty} A_b \exp(-E_b / T_s(t))dt \approx A_b \exp(-\frac{E_b}{T_{Sm}}) \times \frac{2T_{Sm}^2\pi}{E_b^2\alpha_{eff}^2 D_{th}} \equiv A_b \exp(-\frac{E_b}{T_{Sm}}) \times t_{cooling} \qquad (6.7)$$

Though t_{heat} and $t_{cooling}$ are proportional to the corresponding heating time t_p and cooling time $(1/\alpha_{eff}{}^2 D_{th})$, they are considerably smaller, because polymer decomposition rate is significant only during a short time period just at the end of the pulse. In all:

$$\int_0^{\infty} A_b \exp(-E_b / T_s(t))dt = A_b \exp(-E_b / T_{Sm}) \times (\frac{T_{Sm}}{E_b} \times \frac{T_{Sm}}{(T_{Sm} - T_0)} \times t_p + 2\pi\frac{T_{Sm}^2}{E_b^2} \times \frac{1}{\alpha_{eff}^2 D_{th}}) \qquad (6.8)$$

For the examined systems at 248 nm, $t_{heat} << t_{cooling}$. Thus, the integral simplifies to:

$$\int_0^{\infty} A_b \exp(-E_b / T_s(t))dt \approx A_b \exp(-E_b / T_{Sm}) \times 2\pi\frac{T_{Sm}^2}{E_b^2} \times \frac{1}{\alpha_{eff}^2 D_{th}} \qquad (6.9)$$

Thus, at low enough laser fluences at which desorption can be neglected, the fraction of broken bonds at the film surface is estimated from equations (6.4) and (6.9) to be:

$$b = b_0 + A_b \exp(-E_b / T_{Sm}) \times 2\pi\frac{T_{Sm}^2}{E_b^2} \times \frac{1}{\alpha_{eff}^2 D_{th}}$$

For the 120 kDa PMMA, $n_{b,0}^{(120)} = 1/1200 \approx 0$, whereas for the 2.5 kDa, $n_{b,0}^{(2.5)} = 1/25$. Unfortunately, the values for A_b and E_b parameters vary widely in the literature (e.g. E_b values ranging from 230 kJ/mol to 130 kJ/mol have been reported [2-6]). Assuming the parameters adopted in a recent modelling of PMMA ablation [5], $A_b \approx 3x10^{17} s^{-1}$ and $E_b \approx 130 kJ/mol$, we get that at ≈300 mJ/cm^2 the fraction of broken bonds $n^{(2.5)} \approx 0.1$, whereas $n^{(120)} \approx 0.05$. The percentage fraction of broken bonds resulting in monomer, evidently, will be higher for the low Mw polymer. In fact, the fraction of desorbing material may be approximately estimated by the number density of oligomers with the number of monomer units less than L: $N_{<L} = N_0 \cdot \overline{n}_b \cdot \left[1-(1-\overline{n}_b)^{L-1}\right]$ with $\overline{n}_b = \frac{1}{N} + n_b$, where N_0 is the number density of monomer units within the polymer, N is the initial average number of monomer units in one polymer chain, n_b is the fraction of broken bonds. Assuming that only monomers desorb, the relative ratio of desorption from the low vs. the high Mw at ≈300 mJ/cm^2 is estimated to be a factor of 4. *Thus, the model predicts the observed dependence on Mw, although quantitatively the difference appears to be less extensive than indicated experimentally.* The predicted thermal decomposition temperatures for several Mw of PMMA are presented in the Table 4. The discrepancy could in principle be ascribed to limitations of the theoretical model, e.g. the model should take into account possible unzipping process and not only random chain scission as it is in present.

Table 4: *Theoretical temperatures as predicted by bulk photothermal model and experimental temperatures at the corresponding ablation thresholds at 248 nm and 193 nm.*

Mw_{PMMA} (kDa)	**T_{theor}(K)**	**T_{exp}(K) for PMMA at 248 nm**	**T_{exp}(K) for PMMA at 193 nm**
2.5	800	600	800
22	850	750	800
80	1000	800	800
120	1250	850	830
212	1850	900	830
996	2000	900-950	830

6.3 A NEW MODEL OF ABLATION OF POLYMERS BY EXTENDING THE CONCEPT OF EXPLOSIVE BOILING

6.3.1 The factors suggesting the need of such a model

In all, the high attained temperatures and melting demonstrate that a thermal mechanism operates for all Mw polymers. However, as shown above, the correspondence between theoretical model and estimated results is not fully satisfactory, especially at strongly absorbing wavelengths. Most importantly, the ejection dynamics and the nature of the ejecta differ substantially between high and low Mws (i.e.a much higher number of clusters ejected). These differences cannot be account by the photothermal model which relies on the assumption of "complete" degradation of the polymer to desorbing monomers/oligomers. Thus, the question is how to account for these features while at the same time retaining the basic "features" of the thermal model.

A clue for addressing the above question comes from the realization that ejection from the high Mw systems exhibits features similar to the ones associated with explosive boiling in simple liquids. This suggests the possibility that the various discrepancies may be accounted by considering the applicability of explosive boiling to polymer melts. As described in the introduction, explosive boiling occurs when the system is heated to temperatures well above its boiling point [9]. This happens when the rate of heating of the substrate is sufficiently fast that the rate of bubble nucleation/formation (necessary for the transformation from liquid to gas/boiling) cannot compete with it (i.e. is much slower).

Liquids heated above the temperature corresponding to the equilibrium external pressure are thermodynamically metastable, since their chemical potential μ_L is higher than that of the vapor μ_V [10, 12]. However, the transformation (boiling) requires bubble formation, which is limited by the work necessary for the formation of a new interface within the liquid (i.e., the surface tension σ)[12].The free energy for bubble formation is:

$$\Delta G = 4\pi R^2\sigma - \frac{4}{3}\pi R^3 (P_V - P_L) + \frac{4}{3}\pi R^3 \frac{P_V}{k_B T}(\mu_V - \mu_L) \qquad (6.10)$$

where R is the bubble radius, σ the surface tension, k_B the Boltzmann's constant, T the saturation temperature of liquid and P_V, P_L are respectively the pressure inside the bubble and the ambient pressure of the liquid. In the above equation, the first term represents the energy necessary for the liquid-vapor interface formation, the second the work directed against the pressure forces and the third the "driving force" of bubble formation. For small R, the surface term dominates and so ΔG>0; only for sufficiently large R, ΔG<0 as necessary to lead to bubble growth. The radius for this change is specified by the condition of "mechanical" equilibrium of the bubble $\left(P_V - P_L = \frac{2\sigma}{R}\right)$ and of "thermodynamic" equilibrium $\left(\mu_L(P_L) = \mu_V(P_{sat})\right)$ [where P_{sat} is the saturation pressure of the liquid phase]. This radius is donated as the "critical" radius and in this case $\Delta G_{cr} = \frac{16\pi\sigma^3}{3k_B T(P_V - P_L)^2}$. Thus, the rate at which homogeneous bubbles of critical size are generated (J_{cr}) is given by:

$$J_{cr} = J_0 \exp\left(-\Delta G_{cr}/k_B T\right) = J_0 \exp\left(-\frac{16\pi\sigma^3}{3k_B T(P_V - P_L)^2}\right) \qquad (6.11)$$

where σ is the surface tension and P_V, P_L are respectively the pressure inside the bubble and the ambient pressure of the liquid and $J_0 = N_L\left(\frac{3\sigma}{\pi m}\right)^{1/2}$ where N_L is the number of liquid molecules per unit volume and m is the molar mass. Because in Eq. (6.11) both σ and (P_V - P_L) factors depend sensitively on temperature, critical bubble formation depends crucially on the maximum attained value and temporal evolution of the film temperature.

However, the surface film temperature drops rapidly after the end of the laser pulse as a result of evaporative cooling [10]. For low overheating, the reduction in the free energy upon phase change is insufficient to compensate for the surface tension limitation and thus bubble growth eventually halts (~100 ns). In that case, the system can be heated to higher and higher temperatures until the rate of bubble formation, becomes competitive, i.e. J·V·t>1 (where J the rate of bubble formation at T, V is the heated volume and t the time that the volume retains temperatures T). However, with increasing fluences/temperatures, due to the sharp decrease of σ and the increase of $(P_V\text{-}P_L)^2$ factors, J increases sharply. At a sufficient degree of superheating, the number

of interconnected bubbles and high pressure exerted by them result in the violent (supersonic beam-like) material ejection. Because J increases sharply exponentially, the onset for material ejection exhibits a "threshold-like" behavior. The maximum temperature to which a system can be superheated is the so-called spinodal limit, at ~0.8T_c where T_c is the critical temperature [10, 12]. At this limit, the nature of liquid-gas transformation changes qualitatively from that at lower temperatures, long wavelength fluctuations become dominant and the system spontaneously decays into a mixture of superheated liquid droplets and of gas. This limit, spinodal limit, is specified by the criteria $\left(\frac{\partial P}{\partial V}\right)_T = 0$ and $\left(\frac{\partial S}{\partial T}\right)_P = 0$ (stability criteria) and occurs at ~ 0.8T_c, where T_c is the critical point of the compound.

For simple compounds, the spinodal limit is a well-defined physical parameter/characteristic [11]. Even for mixtures of simple compounds, the spinodal limit is a well-defined parameter, although the description of explosive boiling and phase explosion is mathematically quite more complex than that for neat compounds [10].

The extension, however, of the concept to polymers presents important theoretical and experimental difficulties. The fundamental problem is that thermal decomposition occurs at temperatures well lower than "boiling" can be effected. Thus, we cannot define experimentally a boiling point or even a critical point of the system. Qualitatively, we can deduce that critical point changes by employing the Van der Waals equation: $(P + \frac{a}{V^2})(V - \beta) = RT$ where α represents the attractive force between molecules (which roughly increases with increasing number of interacting units) and β the excluded volume. Now, for the critical point:

$$\left(\frac{dP}{du}\right)_{T_{CR}} = \left(\frac{d^2P}{dV^2}\right)_{T_{CR}} = 0 \Rightarrow P_{CR} = \frac{a}{27\beta^2}; T_{CR} = \frac{8a}{27R\beta} \tag{6.12}$$

Thus, with increasing a, (with increasing "strength"of intermolecular interactions, i.e. cohesive energy) T_{CR} increases and the temperature required for vaporization is much higher. Thus,

1) there is not a reference (P, V) point in comparison to which we can claim that the system is overheated and

2) even worse, as we heat up the system, its composition continuously changes (due to the thermal decomposition) so that the temperature at which explosive boiling or phase explosion occurs becomes also a function of the heating rate.

6.3.2 Semiquantitative modelling of explosive boiling of polymers

Yet, experimentally, there are specific features that can be considered to be representative of explosive boiling: (a) bubble formation within the melt should occur (b) ejection of the melt occurs in the form of a mixture of gas and droplets (c) relatively high pressures (due to bubble formation). It is clear that the features we have observed generally accord to this idea.

Theoretical work on explosive boiling of polymers has been limited to few studies by Skripov [7]. He has suggested that the process can be considered as explosive boiling of a temporally-varying composition mixture consisting of 'involatile', higher Mw polymeric species and of the superheated oligomers/monomers formed through the thermal decomposition. In analogy to the explosive boiling of mixtures of simple compounds, explosive boiling of this system should be specified by the mole fraction of the monomer/oligomer component vs. the invo1atile, high Mw polymeric component.

For establishing the temperatures needed for polymers to undergo explosive boiling we assume that as for simple compounds, explosive boiling occurs at temperatures ~ 0.8 T_c, where T_c is the critical temperature. For establishing T_c for polymers as a function of their "size", we rely on a generic/simple extension of the van-der-Waals equation to polymer description. From the general principles of statistical mechanics, the equation for pressure may be written as follows:

$$p=2K/3+U/3 \tag{6.13}$$

where K is the specific (per unit volume) kinetic energy of molecules and U is the potential energy of the system (per unit volume). Let us consider a polymeric liquid as a system of n monomers. Polymerization reduces the degrees of freedom of a bound monomer with respect to the free one. Then the specific kinetic energy of the polymer can be written:

$$K = (1 - \varepsilon)\, 3nk_BT/2 \tag{6.14}$$

where $\varepsilon = 1 - N_e/n$, $(1-\varepsilon)<1$, N_e: the number of chains. (6.15)

Polymerization in addition changes the potential energy U between the monomers. However, this is rather complicated and polymer specific. There are several different equations of states for polymers proposed in the literature and future work should take these into account. However, in this initial work where the purpose is a qualitative description, we assume this to remain the same between monomers. In that case, for a liquid of free monomers, at the critical point $T_\kappa° = 8a/(27bR)$, $p_\kappa° = a/(27b^2)$ and $n_\kappa° = 1/(3b)$. Then for systems of the same polymer Eq.(6.13) may be transformed to the dimensionless form:

$$\pi = \frac{8\nu\tau}{3-\nu} - 3\nu^2 - \frac{8}{3}\varepsilon\nu\tau \tag{6.16}$$

where $\tau = T/T_\kappa°$, $\pi = p/p_\kappa°$, and $\nu = n/n°$. Using the condition for a spinodal $(dn/dv)_\tau = 0$, we determine the coordinates τ, π and ν of the spinodal of a polymeric melt:

$$4\tau = \frac{\nu(3-\nu)^2}{1-\varepsilon(1-\nu/3)^2} \tag{6.17}$$

$$\frac{\pi}{\nu^2} = 3 - \frac{2\nu}{1-\varepsilon(1-\nu/3)^2} \tag{6.18}$$

Here, the reduced density ν ranges from 0 to 3. Using the condition for critical point, we find for the melt density at the critical point ν_k :

$$1 = \nu_\kappa + \varepsilon(1 - \nu_\kappa/3)^3 \tag{6.19}$$

Solution of the system of Eq.(6.16)-Eq.(6.18) gives the spinodal surface for a polymeric liquid. With decreasing N_e (and, consequently, increasing ε), the critical temperature of a polymeric liquid increases and the critical pressure, on the contrary, decreases. In the limiting case of an infinitely long chain ($\varepsilon = 1$), we have $\tau_k = 3.375$, $\pi_k = 0$. Thus for high Mw, the temperature at the critical point (if it could be attained) is 3.4 times higher than that for the monomer, whereas the pressure is nearly zero. Since the spinodal is 0.8 T_c, the spinodal of a large Mw polymer is located, except in the vicinity of the critical point, in the region of negative pressures (i.e. tensile pressure must be applied in order to induce "boiling").

The above specifies the likely temperature for explosive boiling of a polymeric system as a function of its degree of polymerization. However, as described above,

upon heating a polymer, thermal decomposition occurs in parallel. Thus, the "point" of explosive boiling will depend on the polymer/oligomer composition. Thus, the next problem is to estimate the polymer/oligomer/monomer ratio of decomposition and its dependence on heating rate.

In the course of heating, the degree of depolymerization increases as a result of the thermal decomposition. There are several models in the literature concerning how the polymer chain distribution changes upon thermal decomposition. The models differ according to bond dissociations occurring randomly in the chain bonds or preferentially at the chain ends, to the extent of 'unzipping' etc. In attaining a good quantitative description of the laser ablation of polymers, these processes must be taken into account. However, for demonstrating the applicability of the model, we restrict ourselves here to the simplest possible situation, namely to the random chain bond scission.

In that case, the rate of bond dissociations is simply proportional to the number of chain bonds:

$$-\frac{dm}{dt} = mB\exp\left(-\frac{E}{k_B T}\right) \tag{6.20}$$

where E is the activation energy of a bond break and B is the kinetic coefficient. The number of bonds in a unit volume is $m=n-(1+i)N_0$, where i is the number of cuts, N_0 the specific number of chain molecules. Thus, for linear heating at a heating rate $\dot{T}$ and with the initial value i=0,

$$m = B\int_{T_1(t=0)}^{T(t=\tau)} \exp\left(\frac{-E}{k_B(T_0+\dot{T}t)}\right)dt \Rightarrow \frac{i+1}{N_e} = 1-\left(1-\frac{N_0}{n}\exp\left[\left(-\frac{BE}{k_B\dot{T}}\int_{w(0)}^{w(t)}\exp\left(-\frac{1}{x}\right)dx\right)\right]\right) \equiv \alpha \tag{6.19}$$

where $W(t) = k_B\dot{T}(t)/E$. Eq.(6.19) predicts nonlinear $\varepsilon(T)$ dependence at a given heating rate. An estimation of the degree of depolymerization for a linearly heated polymer with typically parameters is presented in Fig.6.1.

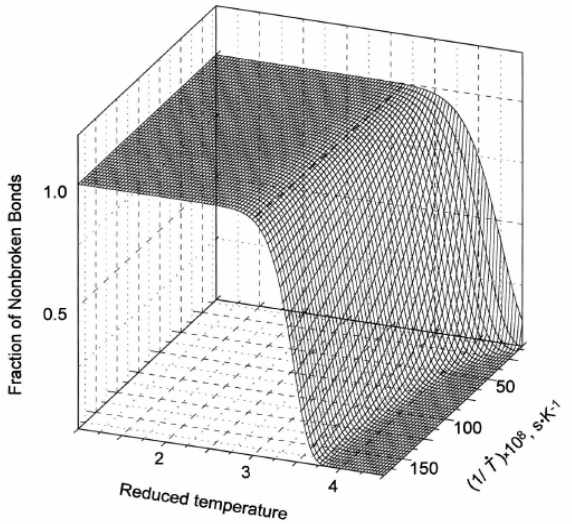

Figure 6.1: *Parameter ε versus reduced temperature and reciprocal heating rate for E= 200 kJmol^{-1}, B=4 x 1 0^{11}s^{-1}, T_0 = 300 K. The dashed line shows the track of intersection of this surface and the polymer spinodal at π=0.*

Of course the modelling of the polymer structure and decomposition is overly simplistic, but it does give a basis for discussion of how to describe explosive boiling in the superheating of polymers. Based on the previous analysis, the temperature and the moment of boiling-up of a polymeric liquid are determined by the point of intersection of the trajectory of the heating *T(t)* with the spinodal of liquid for the current value of ε*(t)*. In Fig.6.1 we plot approximately the reduced temperature at which explosive can occur for a polymer as a function of the heating rate. Simply the graph shows that for low heating rates, there is extensive decomposition to monomers, whereas for high heating rates, the decomposition is not sufficient to compete, thus higher temperatures attained, but also higher pressures.

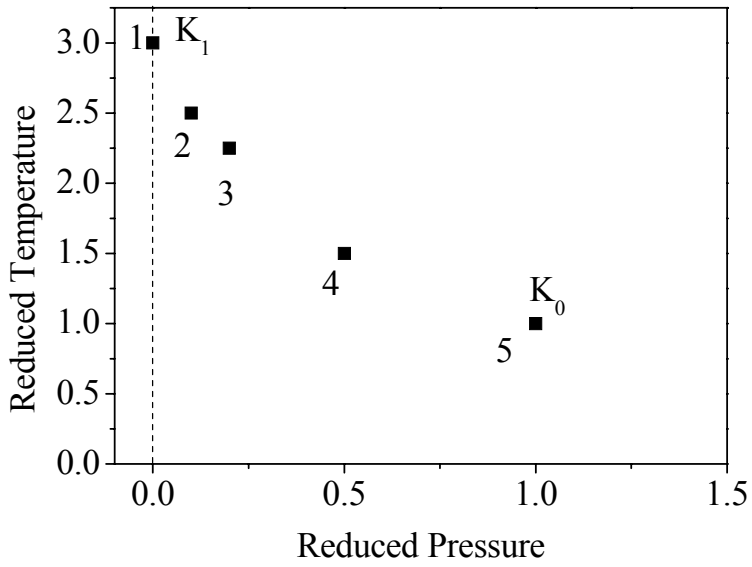

Figure 6.2: *Critical point for explosive boiling for a polymer+monomer system. Point 1 corresponds to the number of molecules (chains) vs. total number of monomers being 10^{-3}(i.e., chain length= 10^{3}), point 2 to chain length 100, point 3 to 1, point 4 to dimmer and point 5 to a system composed exclusively of monomers. The heating rate was T= 10^{7} K s^{-1}. The remaining data are identical to those in Fig 6.1.*

Fig.6.2 shows in the π-τ plane the boiling-up temperatures for a decomposed polymer and for its solutions in a monomer obtained by solving the system of Eq.(6.17)-Eq.(6.19).

6.3.3 Application to the UV ablation of polymers

Based on the above considerations, we can now provide a consistent picture for the differences observed with increasing Mw upon laser irradiation. We consider first the differences for polymers of different Mws at a single wavelength/absorption coefficient, so this corresponds to the same heating rate. For a relatively low αbsorptivity (α=1000 cm^{-1}), the heating rate is relatively slow (i.e. ~ $1.5x10^{7}$ $Ksec^{-1}$). For low Mw polymers, N/N_{chain}, where N the monomers formed per chain, is very high at T>400-500K (Fig.6.2), i.e. the major percentage of bond has broken into monomers and thus material ejection occurs largely in the form of monomer. The efficient energy removal via decomposition to monomers and their subsequent desorption limits the

"excursion" of the system into 'metastability'. Thus, the process exhibits largely the characteristics of a simple thermal process (e.g. in the desorbate translational distributions and the nature of the ejecta).

With increasing Mw, however, monomer formation and consequently energy removal rate is estimated to drop. Thus at the same fluence higher temperatures are attained for the high Mw systems. Yet, the composition of the melt is still so high in high Mw oligomers that explosive boiling does not occur (point 2 in Fig.6.2). Ablation requires even further overheating of the system. However, with increasing temperature, the rate of monomer formation (even from the high Mw systems) becomes significant and at the same time, any gases produced by the thermal decomposition are now strongly superheated. As a result of the higher overheating of the monomer/oligomer component (i.e. higher vapor/bubble pressure) a stronger acceleration of the ejecta is effected and a larger percentage of the material is ejected in the form of clusters/droplets.

Alternatively, explosive boiling may be described in terms of bubble nucleation theory. The formation/ growth decay of the bubbles in the substrate has been confirmed via the time resolved attenuation of the CW HeNe probe beam, at least in the case of weakly absorbing wavelengths.

These ideas are further illustrated by the extent of polymer swelling observed below the ablation threshold. Since the optical penetration depth (and thus the depth of gaseous product formation/accumulation) is the same/independent of polymer Mw, the formation of larger bubbles in the lower Mw polymers can be ascribed to the larger free volume and lower viscosity. In contrast, for the high Mw polymers, despite the higher matrix stiffness, the maximum swelling attained is higher, demonstrating that a much higher P_G and decomposition degree is required for effecting material ejection (note that the rate of consumption of energy by the bond dissociation is the same for both systems).

We consider next the influence of the absorption coefficient and in particular way at strongly absorbing wavelengths, there is minimal if any difference between the different molecular weights. Assuming, if the critical energy for inducing ablation (explosive boiling) is the same (i.e. independent of wavelength) then the ablation thresholds scale as E_{cr}/α – that is at strongly absorbed wavelengths, the difference in the ablation thresholds of the different Mw would be smaller, but still finite (well -defined). As

shown previously, for irradiation of PMMA at 193 nm and PS at 248 nm, the ablation thresholds for different Mw are, within S/N, nearly identical. The kinetics of ArH formation is all nearly identical, thus establishing that temperatures are comparable. This sharply contrasts the pronounced difference /dependence observed upon irradiation at weakly absorbing wavelengths. Note also that the ejecta have exactly the same velocity distribution for different Mws. On the other hand, in similarity to what observed at weakly absorbed wavelengths, the ejecta from the high Mw are rich in clusters but not from the low Mw. It is likely that in this case, since the material being ejected is a quite low amount (superficial layer of material that as soon as some gas is produced, ejection occurs without requiring the built-up of high pressure).

The second feature is that for high α, the rate of superheating is extremely high: for instance for PMMA (0.4% wt NapI) at 248 nm, the effective absorption coefficient, α_{eff} ~500cm^{-1} , but 3000-5000 cm^{-1} at 193 nm. Since the rate of heating is $\frac{dT}{dt} = \frac{\alpha I}{\rho C_p}$ (*I*: intensity of laser), for the same intensity, the rate of overheating is correspondingly 6-10 times higher. With increasing heating rate (e.g. at 193nm for PMMA), explosive boiling becomes more dominant. Thus, even for low Mw systems, the rate of bond decomposition cannot compete with the heating rate, so the systems /polymers can be heated to higher temperatures. Therefore, even for low Mw systems the amount of material ejected in form of clusters is higher and deviations from the higher Mw are reduced (as compared to irradiation at weakly absorbed wavelengths). For explosive boiling to occur, bubbles must grow up to same critical size r_c. With increasing absorptivity α, the rate J of bubble formation per unit volume ($J= t^{-1}V^{-1}$) increases. Since the bubble size cannot exceed/grow beyond the superheated layer, it scales as $1/\alpha$, which explains why bubbles are too small to detect for irradiation at strongly absorbed wavelengths. (Note also: the temperature gradient is much more pronounced for high α). In addition, the average cluster size is correspondingly reduced; which accounts for the very small clusters in the ablation of PS at 248 nm and for PMMA at 193 nm.

There is an additional factor that may be involved which does directly relate to explosive boiling but rather with viscoelastic response of polymers. The faster heating rate suggests that viscoelastic response dominates (so that fragmentation becomes more

brittle-like). This may explain why at 193nm efficient decomposition (photomechanical like) is observed, whereas the condition of stress-confinement is far from fulfilled.

In view of the above, explosive boiling can explain in a consistent way most, if not all features, of ablation:

1) That material is ejected in the form of liquid droplets and gas. The relative amount will depend on degree of superheating of gaseous species vs. degree (rate) of thermal decomposition. It should be noted that even for simple compounds, Molecular Dynamics [9] predict that at threshold, most compound is ejected mainly in the form of droplets rather than monomer. This suggestion may account for one of the major claims of Srinivasan [13] that in ablation of polymers, the monomer/gaseous product is only a minor percentage of the ejecta
2) Because the material is ejected mainly in the form of droplets, the energy required for material ejection is much lower than estimated by a simple photothermal model. This explains how ejection of material, especially from high Mw polymers, occurs at temperatures much lower than those estimated by the bulk photothermal model (which assumes that every bond between monomers is broken).
3) the nature of the ejecta, e.g. amount of aggregates vs. monomers was already noted by Srinivasan [13] in the erliest (80's) studies of UV laser ablation of polymers that differ considerably between 248 nm, 193 nm, vs. $C0_2$ laser irradiation (rather significant differences were also observed between 248 nm and 193 nm). The main observation was that ablation at 193 nm was characterized by a high degree of monomers/clusters and he proclaimed this to be a signature of photochemical mechanism. What we have shown here is at 3 different UV laser wavelengths, the relative contribution of clusters vs. monomers differs for the otherwise optically and chemically identically polymers. Thus, immediately our results show that his argument about the relative contribution of clusters vs. monomers is not unique to wavelength, but also to the Mw initially employed. Consequently, the whole argumentation in the field of UV laser ablation that the ejection of different species distributions provides a unique approach for distinguishing between

thermal/chemical/photochemical mechanisms of UV ablation appears to be failing.

4) Other authors like Dlott [14], who have on the basis of their results suggested that a photothermal mechanism may be operative, had difficulty in explaining why at ablation threshold, only a very small percentage (~10%) of PMMA is gasified. They do not mention in the article the Mw of the polymer they employed, but most probably it is a high Mw system. Dlott and coworkers realized the limitations of their analysis and suggested that likely thermal decomposition process at high heating rate differ from those at conventional thermogravimetric studies; however, they were not able to specify the basis for this deviation. Clearly, the suggested model of explosive boiling fully accounts for observations, as well as it provides a consistent basis for accounting for the suggested differences in the thermal decomposition of polymers at the high heating rates achievable with nanosecond lasers vs. conventional thermogravimetric studies.
5) Our results indicate an important factor responsible for several discrepancies reported in studies from between different laboratories. For instance, different labs have often reported that the nature of ejecta differ significantly between them -in retrospect, as indeed confirmed by the examination of their studies, this differences are largely due to the fact that they had used different Mw polymers.

6.4 CONCLUSIONS AND IMPLICATIONS

It has shown in Chapter 4 that for both PMMA and PS, high temperatures are attained and in all cases, viscosity decreases to values indicative of polymer melts. Thus a thermal mechanism is strongly indicated. To this end, in this chapter, we present first a detailed comparison of the experimentally estimated temperatures to the ones predicted by the bulk photothermal model, which is considered to be the state-of-the-art theoretical model in this field. It is found that the experimental trends deviate significantly from the theoretically predicted ones.

We argue that overall observations are analogous/similar to the ones observed for explosive boiling in the fast superheating of liquids. Despite several theoretical

difficulties, we argue that at least, semiquantitatively, the explosive boiling of polymers can be described as that of a mixture of oligomers/ higher polymeric chains of time varying composition. It is shown that this model consistently accounts for all features observed in this study and in addition it explains the various inconsistencies that have been reported in previous ablation studies of polymers.

6.5 REFERENCES

1. E. Rebollar, G. Bounos, M. Oujja, C. Domingo, S. Georgiou, M. Castillejo, J. Phys. Chem. B, **110**, 14215, (2006).
2. R. H. Boyd, in Thermal Stability of Polymers, edited by R. T. Conley Dekker, New York, (1970).
3. L. E. Manring, Macromolecules **21**, 530, (1988).
4. D. W. Van Krevelen, J. Appl. Phys. **26**, 738, (1955).
5. H. Schmidt, J. Ihlemann, B. Wolff-Rottke, K. Luther, and J. Troe, J. Appl. Phys. **83**, 5458, (1998).
6. Z. Gao, I. Amasaki, T. Kaneko, and M. Nakada, Polym. Degrad. Stab. **81**,125, (2003).
7. P. A. Pavlov and P. V. Skripov, International Journal of Thermophysics, **20**, No. 6, (1999)
8. M. G. Kendal and P. A. P. Moran, Geometrical Probability, Griffin's Statistical Monographs and Courses, No. 5 (C. Griffin, London, 1963)
9. (a) L. V. Zhigilei, P.B. S. Kodali, B. J. Garrison, J. Phys. Chem. B **101**, 2028, (1997). (b) L.V. Zhigilei, E. Leveugle, B. J. Garrison, Y. G. Yingling, M.I. Zeifman, Chem. Rev. **103**, 321, (2003). (c) L.V. Zhigilei, B. J. Garrison, J. Appl. Phys. **88**, 1281, (2000).
10. P. Debenedetti, Metastable Liquids: Concepts and Principles; Princeton University Press: Princeton, NJ, (1996).
11. Y. P. Skripov, Metastable Liquids; John Wiley & Sons Inc.: New York, (1974).
12. C. T. Avedisian, J. Phys. Chem. Ref. Data **14**, 695, (1985).
13. R. Srinivasan and B.Braren, Chem Rev., **89**, 1303, (1989).
14. (a) S. Chen, I.-Y.S. Lee, W. A. Tolbert, X. Wen, D.D. Dlott, J. Phys. Chem. **96**, 7178 (1992). (b) I.-Y. S. Lee, X. Wen, W.A. Tolbert, D.D. Dlott, M. Doxtader, D. R. Arnold, J. Appl. Phys. **72**, 2440, (1992).

Chapter 7 FEMTOSECOND POLYMER ABLATION

7.1 INTRODUCTION

Material processing with femtosecond pulses is indicated to afford a number of unique features [1-3]. Generally, three factors have been emphasized for the special features of fs interaction. First, the heat-affected zone is minimal, therefore several of the side-effects accompanying observed for longer (nanosecond) pulses are reduced or minimized. Second, because of material ejection occurring well after the laser pulse, there is no plasma shielding. Thus, maximum coupling of the incident laser energy into the substrate is affected. Third, because of negligible loss due to heat diffusion and of the efficient operation of multiphoton/avalanche ionization process, processing is possible at much lower fluences than with nanosecond pulses. (i.e. the ablation threshold is much reduced). This enables processing of substrates that are transparent or weakly absorbing at the irradiation wavelength. Indeed, in some fields, fs irradiation has already resulted in powerful, new material processing capabilities [2, 3]. It is generally demonstrated that quality of structuring with fs pulses far surpasses that attained in ns ablation.

Thus far, the emphasis of laser based structuring with femtosecond laser pulses has been placed on the high control attained over the induced of morphological modifications. However, in the laser processing of molecular substrates (e.g. in applications such as in processing of tissues, laser restoration of artworks), the major issue concerns the extent of the chemical modifications effected to the photolabile substrates. Thus, the above advantages aside, the success of fs laser processing of molecular substrates, (e.g. polymer/biopolymer processing in microelectronics, biology, medicine and laser restoration of painted artworks) will depend critically on the nature and the extent of the induced chemical modifications. Surprisingly, despite the increasing number of publications in that direction, very little has been reported in this direction. Nonetheless, it has been noted that even analytical/spectroscopic applications of fs-laser-based techniques (e.g. 2-photon imaging of biological tissues) may be largely

limited by the induced chemical modifications. In the case of cells/tissues, the chemical modifications have been ascribed to the efficient generation of reactive oxygen species. (O_3, OH, $^1O_2$) [4].

Herein, we rely on the methodology we have described previously for examining the nature of chemical processes induced upon fs irradiation of polymers in the UV (248 nm). Briefly, the employed methodology relies on the examination of dopant deriving product formation upon irradiation of the polymer doped with photolabile iodoaromatics (iodonaphthalene or iodophenanthrene). The iodoaromatic dopants are characterized by well-specified reaction patterns, thereby enabling detailed elucidation of the laser-induced chemical processes. We demonstrate here that the modifications induced to the dopant upon irradiation at 248 nm with 500 fs pulses differ qualitatively from the corresponding ones in the ns irradiation. A tentative mechanism is advanced to account for the different chemistry observed upon fs irradiation.

7.2 ETCHING RATES AND MORPHOLOGICAL CHARACTERISTICS

Typically etching rates upon irradiation of NapI and PhenI-doped systems with 248 nm, 500 fs pulses are shown in Fig.7.1. As compared with ns laser pulses, the determination of the etching rates in the present case is subject to a large error because:

1. the etching rates per pulse is very small so that a multipulse protocol was used (in which case, the determined depth represents an average over several ~ 10 ps, but this may vary a lot from pulse to pulse and
2. because as described below, fs irradiation resulting various surface structures/irregularities, so that there is considerable uncertainity in determining the “average” etching value.

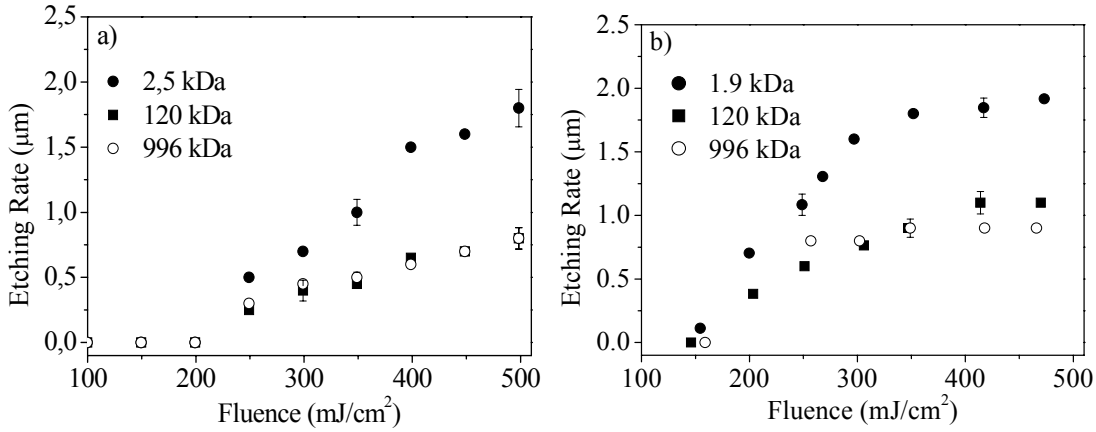

Figure7.1: *Etching rate curves for the systems: a) 0.5%PhenI PMMA and b) 1.2%wt NapI PMMA upon the irradiation with 500 fs at 248 nm. The molecular weights of PMMA are illustrated on the graphs. The error bars represent 2σ, as determined from 5 different measurements.*

Nevertheless, the determined etching curves are comparable to ones reported previously for other polymeric systems. The ablation thresholds for the 500 fs pulses are much lower (5-10 times) than the corresponding ones in the ns irradiation and similar differences are observed concerning the etching depth. We will ascribe these differences to the fact that in the irradiation with fs pulses efficient multiphoton process occurs, resulting in the high reduction of the 'effective' optical penetration depth.

PS (MW 532 kDa), F=1.2J/cm²

1 pulse **10 pulses**

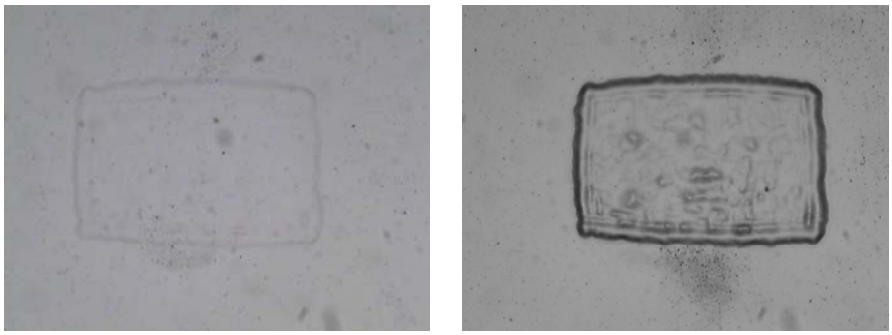

Figure 7.2: *Wavy- like structure formation on PS upon irradiation with one and ten 500 fs pulses at 248 nm.*

The morphology of the irradiated areas is found to depend on laser fluence and on the number of the pulses (Fig.7.2). At low laser fluences (but still above the threshold), the irradiated area (spot) with one pulse is of excellent optical quality, sharply contrasting the morphology obtained at 248 nm with nanosecond laser pulse. This result is also consistent with the expectation that due to multiphoton absorption, a

high energy is absorbed in a thin layer thus resulting in 'efficient' etching. However, at fluences ~5 times the ablation threshold (i.e. F_{LASER}=1-2 Jcm^{-2}), the irradiated area is highly structured. Similarly, structures are observed at lower fluences upon irradiation with successive laser pulses. The appearance of the structures is different for PMMA and PS, in case of PMMA being spike-like, whereas for the later polymer, wavy-like. No specific dependence on polymer Mw is found.

Surface structure formation has been a common observation in the femtosecond irradiation/ablation of a wide range of materials. A number of different mechanisms have been advanced to account for their formation, but there is a little evidence for these suggestions. Several authors [5, 6] suggest that a scattered wave on or near the surface interferes with the direct wave thereby generating periodic regions of low and high intensity. The spacing of the patterns can be described by $\Lambda = \frac{\lambda}{n \pm \sin(\theta)}$ where the negative and positive signs correspond to forward and backward scattering respectively, Λ is the spacing of the LIPS (Laser Induced Periodic Structure), λ is the wavelength of the excitation laser in vacuum, and ''n'' is the refractive index of the material. To explain the observed period of the ripples, the authors introduce the idea that a thin surface layer of the material has a refractive index that ranges between that of bulk polymer and 1 ~the index of the air. The size of the structures we have observed is quite different from the size of periodicities suggested by this formula and thus this mechanism does not seem to be operative in the studied systems.

Structure formation has also been noted in the irradiation of polymers with Ti:Sap laser. In that case, there are clear indications for polymer melting. On the other hand, as described below, for PMMA and doped PMMA at 248 nm, 500 fs there is no evidence for melting; so it is likely that the mechanism of structure formation in our case differs from that in the corresponding Ti:Sap irradiation. Indeed, the spacing in the structure/ripples is quite different in the two cases. Further studies are required in order to establish the origin (mechanism) for the structures observed upon 500 fs UV irradiation (e.g. comparative studies of the structures formed in the irradiation of different polymers). In addition, it is most important to establish the time scale of the formation of these structures, e.g. by time resolved examination of the scattering of the probe beam incident on the substrate (polymer).

7.3 EXAMINATION OF CHEMICAL EFFECTS IN ArI DOPED POLYMERS

Here, we focus on the main objective of this chapter, namely on examining the chemical effects upon UV sub-picosecond laser ablation. The purpose was to see if studies on ArI-doped polymers provide further insight into the recent femtosecond processing of biomolecules and tissues and also provide the basis for further studies on UV fs ablation. There are a number of important and well defined differences between the fs and the ns case. As described in chapter 3, in the nanosecond UV irradiation, for NapI concentration of > 1.2% wt, efficient Nap_2 formation is observed at fluences well below the ablation thresholds (at ≥200 mJ/cm^2) even upon the first pulse. In the case of irradiation with UV subpicosecond pulses at low fluences (50 mJ/cm^2), by-product formation (most likely, Nap_2 as well as products of the polymer (photo)decomposition) occurs as demonstrated by the broadening of the LIF probe spectra with successive laser pulses (Fig.7.3a). However and most importantly, for irradiation at higher fluences, no broadening is observed (Fig.7.3b). Even after extensive irradiation, the probe spectra indicate exclusively ArH formation. Note that not only Nap_2 formation but even products of polymer decomposition.

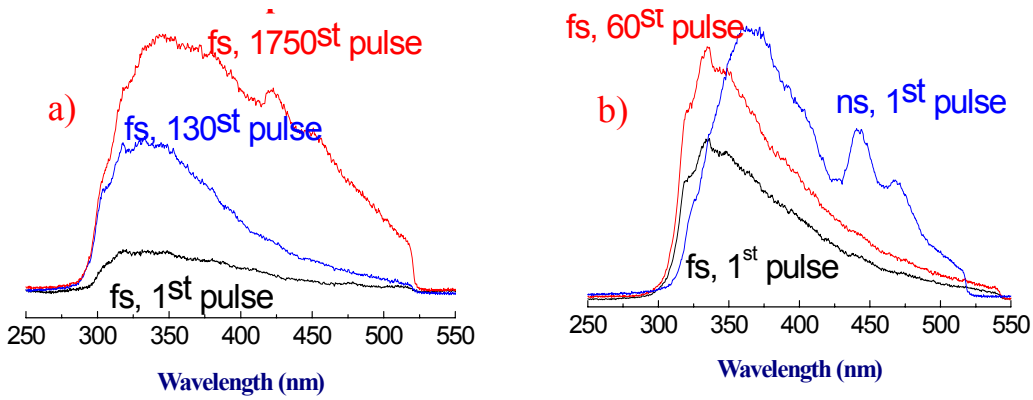

Figure 7.3: *LIF spectra of 4.0 % wt NapI/PMMA upon the irradiation with 500 fs at 248 nm. The excitation is performed by 248 nm pulse (30ns). The number of pulses is illustrated on the graphs a) F_{LASER}=10mJ/cm^2 and b) F_{LASER}=300mJ/cm^2.For comparison purpose we present the corresponding ns spectrum.*

In parallel, the quantitative dependence of ArH formation on successive laser pulses differ markebly between ns and fs irradiation. Fig.7.4a depicts its yield as a function of the incident fs laser fluence; for comparison purposes, the corresponding

dependence determined in the irradiation with ns pulses (λ=248 nm, $\tau_{pulse}\cong$ 30 ns) is also included (Fig.7.4b).

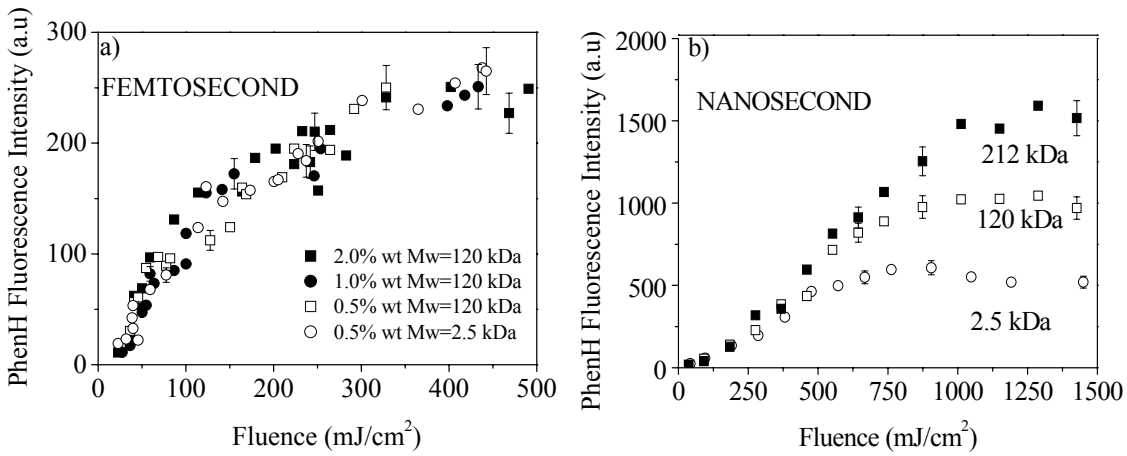

Figure 7.4: *a) F_{LASER}-dependence of the PhenH product in the irradiation (λ=248 nm, τ_{pulse}=500 fs) of PhenI/PMMA. The dopant concentration and the polymer molecular weight of each irradiated system are illustrated on the graph. In all cases, the fluorescence is recorded following irradiation with a single "pump" pulse. b) For comparison purposes the corresponding nanosecond F_{LASER}-dependence for the same system is presented. The excitation is performed by 248 nm pulse with pulse duration 30ns. The error bars represent 2σ, as determined from at least 5 different measurements.*

For ns irradiation, the ArH yield is found to scale linearly with laser fluence at very low fluences (as expected for one photon photolysis), but at fluences above to the swelling onset it increases supralinearly). As we demonstrated in chapter 4, this sharp increase is due to the higher temperatures and higher heat diffusion to the sublayers, thereby resulting in a higher efficiency of the (thermally activated) reaction of aryl radicals for hydrogen atom abstraction. In the ns case, the onset fluence for this increase of the product formation efficiency depends strongly on the (effective) absorption coefficient. As shown in Fig.7.4a in contrast, in the femtosecond laser irradiation, the F_{LASER}-dependence of ArH yield differs markedly from the ns one. ArH yield increases with increasing fs laser fluence reaching a plateau at the ablation threshold. We cannot distinguish any changes in the slope of ArH formation yield at low laser fluences, such as seen in Fig.7.4b. This could imply that ArH formation in the fs case is not determined by temperature changes (as the case is in the ns irradiation). However, measurements of the transmitted 248 nm beam show that multiphoton processes become important at fluences as low as 5-10 mJ/cm^2. Thus, likely, the shape of the F_{LASER}-dependence of ArH formation yield is determined by changes in the effective optical penetration depth

(as a result of increasing efficiency of multiphoton excitation with increasing F_{LASER}). Most importantly (in particular for applications), the maximum ArH product formed is nearly ~10 times lower than what in the irradiation with ns pulses (at 248 nm). A further noticeable difference is that in fs case, ArH formation is nearly independent of the concentration of the dopant (i.e. of the linear absorption coefficient of the system) despite a change of a factor of 4.

The mechanisms that may plausibly be responsible for these observations will be discussed below. Yet, independently of the mechanisms, these results clearly demonstrate that in the subpicosend UV laser ablation, chemical modifications/effects are highly selective and limited. Thus besides the other advantages (i.e. excellent morphology, limited heat "load" to the substrate etc) that have been noted before, it appears that an additional factor for the success of the fs laser processing of biopolymers and tissues relates to this high chemical selectivity.

7.4 TIME RESOLVED OPTICAL MONITORING OF EJECTION PROCESS

For understanding the factors responsible for why behavior differs so dramatically from that observed upon ns irradiation, preliminary experiments relying on optical techniques were performed for monitoring the structural changes that take place within the bulk upon irradiation as well as for monitoring the ejection process with 500 fs laser pulses.

Considering first optical imaging of the plume ejection a clear deformation above the irradiated area is first ensured at ~ 1 ns. The observed deformation at ~1 ns is certainly partly due to refractive index change of the air just above the irradiated area. However, within the resolution of the images, it consists of an elevation of the substrate of less than few μm. Material ejecta are, however, with confidence detected at 2-3 ns afterwards. At 38 ns after the laser pulse, a shock wave at ~50-100 μm in the air above the surface is detected and at 25 μm from the surface, a dark region ascrible to scattering by particles is also clearly delineated. In between, change in the images (i.e. in the refractive index) is probably due to gases that eject before the particles. Because of the technical difficulties (accuracy of the interferometer for long spacing), the

ejection process could be followed only for times up to ~80 ns (thus, not enough images could be collected for establishing the velocity.

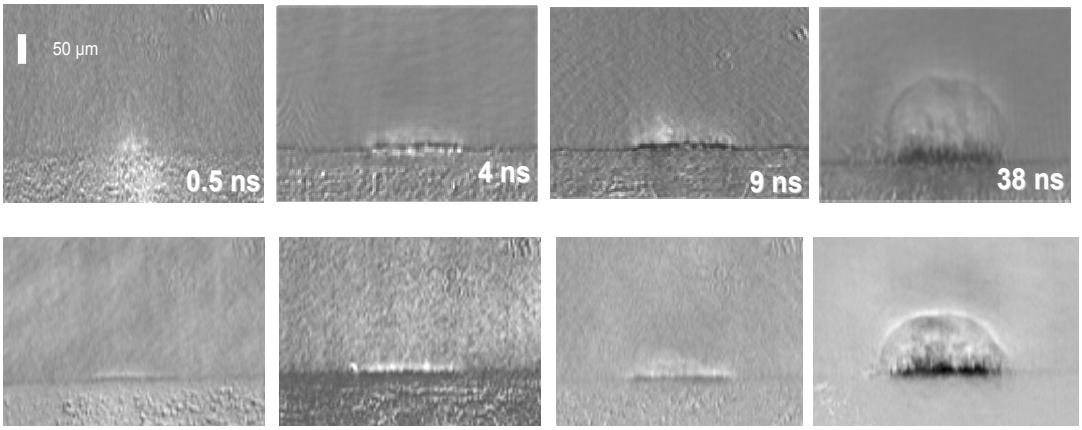

Figure 7.5: *Shawdographic examination of the material ejection process for the system 0.5%wt PhenI PMMA upon the irradiation with one pulse at 248 nm with pulse duration 500 fs.* Mw_{PMMA}*=996 kDa for above and* Mw_{PMMA} *=2.5 kDa for below series. The photos are obtained by a 496 nm (probe) pulse with the same pulse duration.*

These experiments were performed for two Mw PMMAs (2.5 kDa and 996 kDa). The evolution of processes is largely the same, except that velocity of ejecta is somewhat higher for low Mw. These finding do not appear to be spectacularly different from the case of nanosecond ablation/ejection dynamics. Certainly, the evidence indicates that whereas in ns ablation, ejection starts at ~5-10 ns, in the femtosecond, most or the majority of material is already ejected on these times.

More promising results have been obtained by the use of temporally resolved techniques for monitoring refractive index/absorption changes within the substrate upon irradiation with 500 fs laser pulses. In these experiments, it is absolutely crucial for the correct evaluation of the results that (1) both the surface of polymer and most importantly, the sides of the polymer sample (through which the probe beam propagates) are of excellent optical quality, (2) the relative geometry of the substrate in relationship with the pump/probe beams (i.e. their incident angles) remains exactly the same. However, as the sample has to be moved in order to get each time fresh area and the surface of the thick polymer samples (as thick to satisfy criterion (1) -prepared by evaporation from bulk solutions-) is rather anomalous, a significant error was introduced. Thus, in Fiq.7.6, the exact position of the polymer surface cannot be accurately specified and thus the maximum of transmission drop (i.e. it likely coincides

with the 0) cannot be accurately established. An additional difficulty is introduced by the fact that, as shown below, change are limited to a very small depth close to the polymer surface.

Despite these limitations, clearly transmission of the sample at the probe wavelength (496 nm) drops substantially for the first 2-5 ps within a depth of 2-4 μm. This is much lower than that expected from the linear absorption coefficient or even the effective absorption coefficients determined for the same systems in the corresponding UV nanosecond (248 nm) irradiation. Because of the experimental difficulties described above, it has been difficult to follow in detail the subsequent time evolution of the changes within the bulk. Further changes in the distribution pattern of this darkening are again noted at ≥ 2 ns.

Though the above results are very limited and call for a more thorough, detailed and reliable examination, they still provide a plausible scenario of the processes in the UV ablation of polymers.

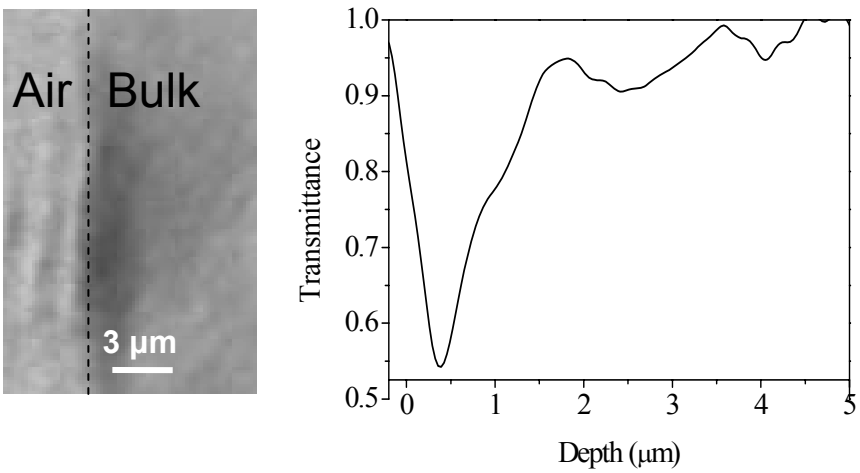

Figure 7.6: *a)Ultrafast photografic examination in the bulk of neat PMMA upon the irradiation with one 248 nm pulse with pulse duration 500 fs. The photo is obtained by one 496 nm (probe) pulse. The delay between pump and probe pulse is 2 ps. b) The corresponding reduction of transmittance within the substrate deriving from the picture analysis.*

The very pronounced transmission decrease observed within the substrate at ~2-5 ps could be due to the absorption of the probe beam by excited electronic states of PMMA or even by products formed by the polymer or dopant decomposition. At present, these possibilities cannot be excluded. Time resolved (spectrally-resolved)

absorption studies (by white light continuum) can provide the means for addressing this question. However, it appears more likely that the absorption is due mainly to free electrons generated by photoinization processes by UV laser pulse.

7.5 PLAUSIBLE EXPLANATION/MECHANISMS

The much lower ArH product formation for fs irradiation can be easily explained by a highly reduced 'effective' optical penetration depth. For the studied systems, indeed, the absorption of the pump fs beam is found to increase at fluences > 10 mJ/cm^2 In the early study Stuke [7] and co-workers indicated that at least a 2-photon process 'dominates' in the 248 nm irradiation of neat PMMA with 500 fs pulses. This conclusion was reached by fitting the etching depth dependencies. Since the sensitivity of such fittings is limited (e.g. dependence on which step is the rate-limiting one), it is highly that the process is of much higher order than suggested. In particular, the near insensitivity (independence) from the "linear" absorption coefficient of the systems strongly indicates that avalanche ionization process dominate, resulting in a weak plasma that absorbs strongly. We advance the following tentative explanation for the above observations.

As shown by typical transmission measurements, multiphoton excitation of the studied systems becomes significant at fluences as low as 5 mJ/cm^2. Absorption of two or more 248 photons excites PMMA well above the ionization potential. Thus, there is a good probability for the production of 'free' electrons. Such free electrons can participate in avalanche ionization processes thus resulting in a much higher energy density deposition per unit volume (actually, the electrons in condensed phase are either bound to a particular molecule or 'quasi-free' when they posses sufficient kinetic energy to move without being captured. For simplicity, we use the terms 'free' electrons' and 'ionization').

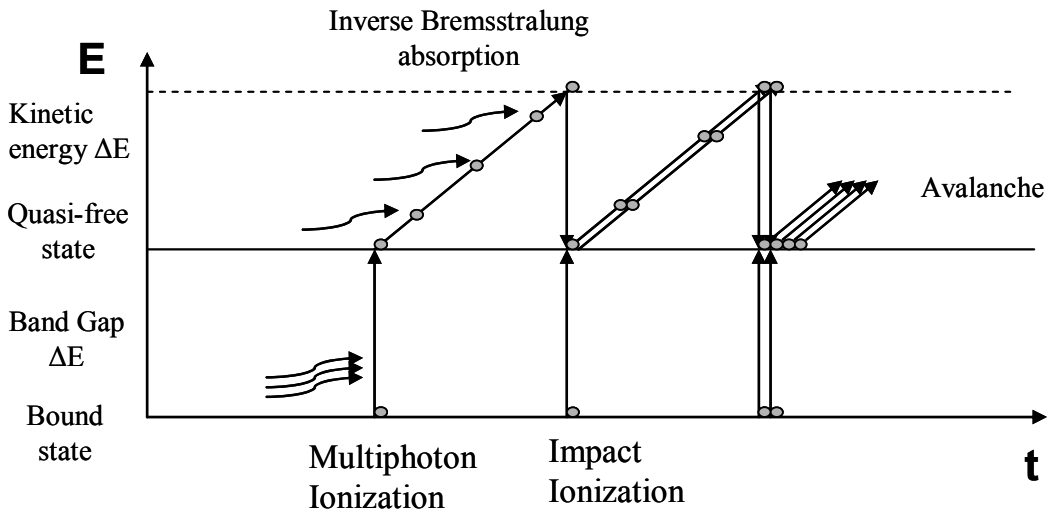

Figure 7.7: *Interplay of multiphoton and avalanche ionization in the process of plasma formation. Avalanche ionization consists of a series of multiple inverse Bremsstrahlung absorption events followed by impact ionization.*

Free electrons form via an interplay between multiphoton and avalanche ionization processes, as depicted schematically in Fig.7.7. The multiphoton ionization rate is proportional to I^k, where I is the laser irradiance and k the number of photons required for ionization. Once a free electron is produced in the medium, it can absorb photons via a nonresonant process called "inverse Bremsstrahlung absorption" (IBA) in the course of collisions with other charged particles (ions) (so as to conserve energy and momentum during optical absorption). Absorption of the photon increases the kinetic energy of the free electron. After k IBA events, the kinetic energy of the electron exceeds the band gap energy, E, and the electron can produce another free electron via impact ionization. After impact ionization, two free electrons with low kinetic energies are available which can again gain energy through IBA. The recurring sequences of IBA events and subsequent impact ionization lead to a rapid growth in the number of free electrons if the irradiance is sufficient to overcome the losses of free electrons through diffusion out of the focal volume and recombination. Moreover, the rate of energy gain through inverse Bremsstrahlung must be more rapid than energy losses through collisions with heavy particles. The process involving both IBA and impact ionization is called "avalanche" or "cascade" ionization. Cascade ionization depends on the number density of free electrons in the focal volume. Thus, it becomes significant only after a large number density of free electrons has been provided by multiphoton ionization.

Several authors [8, 10] have used rate equations based on the Drude model to describe the temporal evolution of the volumetric density of free electrons, ρ, and to calculate breakdown thresholds for various laser parameters. The generic form of such a rate equation is:

$$\frac{d\rho}{dt} = \eta_{mp} + \eta_{casc}\rho - g\rho - \eta_{rec}\rho^2 \qquad (7.1)$$

The first two terms on the right-hand side of the equation represent the production of free electrons through multiphoton and cascade ionization, respectively. The last two terms describe electron losses through diffusion out of the focal volume and recombination, respectively. The cascade ionization rate and the diffusion loss rate are proportional to the density of free electrons, while the recombination rate is proportional to ρ^2, as it involves an interaction between two charged particles (an electron-hole pair). Instead of trying to solve this the Eq.(7.1), we consider individually the contribution of impact ionozation and of multiphoton ionization to plausible plasma formation.

Estimation of plasma density in PMMA (λ=248nm, t_p=500fs)

(In collaboration with N.Bityurin)

Estimation of the role of impact ionization: For femtosecond pulses when electron–phonon energy exchange can be neglected during the laser pulse, number density of free electron at the end of the pulse can be estimated as [9]:

$$n_e < n_e^{multi} \cdot \exp(\frac{F_{LASER}}{F_{aval}})$$

where n_e^{multi} represents the free electron number density provided by multiphoton ionization, F_{aval} is 'characteristic' avalanche fluence. This fluence is: $F_{aval} \geq \frac{h\nu}{\sigma_e}$ here $h\nu$ is the photon energy. For KrF laser $h\nu = 5eV = 8\cdot 10^{-19} J$, σ_e is the effective free electron absorption cross-section from the Drude formula:

$$\sigma_e = \frac{4\pi e^2}{cn_0 m_e(\omega^2 + \nu_{e-p}^2)}\frac{\nu_{e-p}}{\omega} = 1.2\times 10^{-18} cm^2$$

here n_0 is refractive index, e and m_e are charge and mass of electron , c is light velocity, $\omega = 7.6\cdot 10^{15} s^{-1}$ for $\lambda = 248nm$, ν_{e-p} is the electron-phonon transport (momentum)

scattering rate. For $\nu_{e\text{-}p}$, there is some discussion in literature about its value, but generally $\nu_{e-p} = 10^{14} - 10^{15} s^{-1}$. Thus, the estimated value for F_{aval} is $F_{aval} \approx 670 mJ/cm^2$.

In fact, it is often suggested that if $F_{LASER} < \frac{F_{aval}}{5}$ then impact ionization is negligible. At any rate, at fluences <670 mJ/cm^2 *impact ionization is estimated not to be significant* and we will further neglect it.

We consider next **estimation of plasma density within the model of multiple photon ionization by the *femtosecond* pulse.** We will suppose that ionisation needs absorption of three photons of 248 nm, because absorption of a single photon of 125 nm is not enough for ionisation. Thus, we consider consecutive single-photon transitions from the ground state. In the following n_0 is the number density of the ground state, n_1 is the number density of first excited state, n_2 is the number density of second excited state, and n_e is the number density of free electrons. Pulse duration (500 fs) is larger than the phase relaxation time but smaller than population relaxation time. It means that we can use simple kinetic equations for population of excited states neglecting relaxation of these populations. These are them:

$$\frac{dn_1}{dt} = \sigma_{01} n_0 \frac{I}{h\nu} - \sigma_{12} n_1 \frac{I}{h\nu} \tag{7.2}$$

$$\frac{dn_2}{dt} = \sigma_{12} n_1 \frac{I}{h\nu} - \sigma_{23} n_2 \frac{I}{h\nu} \tag{7.3}$$

$$\frac{dn_e}{dt} = \sigma_{23} n_2 \frac{I}{h\nu} \tag{7.4}$$

When writing the set Eq.(7.2)-Eq.(7.4), we neglect the induced emission from level 1 to ground state and from level 2 to level 1. Solution of set Eq.(7.2)-Eq.(7.4) yields the number density of plasma electrons, n_e at the end of the laser pulse:

$$n_e = \sigma_{01} n_0 \frac{F_{LASER}}{h\nu} - n_1 - n_2 = \sigma_{01} n_0 \frac{F_{LASER}}{h\nu} \cdot [1 - \frac{f_1(F_{LASER}/h\nu)}{\sigma_{12} \cdot (F_{LASER}/h\nu)} - \frac{f_2(F_{LASER}/h\nu)}{\sigma_{23} \cdot (F_{LASER}/h\nu)}] \tag{7.5}$$

where $f_1 = 1 - \exp(-\sigma_{12} \frac{F_{LASER}}{h\nu})$ and $f_2 = 1 - \frac{\sigma_{23}}{\sigma_{23} - \sigma_{12}} \exp(-\sigma_{12} \frac{F_{LASER}}{h\nu}) + \frac{\sigma_{12}}{\sigma_{23} - \sigma_{12}} \exp(-\sigma_{23} \frac{F_{LASER}}{h\nu})$

Functions f_1 and f_2 are smaller than unity. If $\sigma_{12} \frac{F_{LASER}}{h\nu} >> 1$ the term with population n_1 (the second term in squared brackets) can be neglected, i.e. the transition from the

first to the second level is 'saturated'. The same is also valid for the transition from the second level to free electron state if $\sigma_{23}\frac{F_{LASER}}{h\nu} >> 1$. If both intermediate transitions are saturated then the number density of free electrons given by:

$$n_e \approx \sigma_{01} n_0 \frac{F_{LASER}}{h\nu} \tag{7.6}$$

Then, for F_{LASER}~50 mJ/cm^2-100 mJ/cm^2 and assuming $\sigma_{01} n_0 = 150 cm^{-1}$ (taken from nanosecond experiments), Eq.(7.6) yields the estimation $n_e \approx 10^{19} cm^{-3}$. Unfortunately, the above result depends on the values assumed for σ_{12} and σ_{13}. To give an estimate of the dependence of the results on these parameter, let us consider for simplicity that $\sigma_{12} = \sigma_{23} \equiv \sigma$, in which case, Eq.(7.5) can be written as:

$$n_e = \sigma_{01} n_0 \frac{F_{LASER}}{h\nu} \cdot \eta$$

where $\eta = 1 - \frac{2}{\sigma \cdot (F_{LASER}/h\nu)}[1 - \exp(-\sigma \cdot (F_{LASER}/h\nu)] + \exp(-\sigma \cdot (F_{LASER}/h\nu)$

For $F_{LASER} = 50 mJ/cm^2$, the estimated n_e for various values of the absorption cross section σ is presented in Table 5.

Table 5: *Dependence of estimated free electrons density on the absorption cross-section*

$\sigma = 10^{-16} cm^2$	η=0.682 $n_e = 7 \cdot 10^{18} cm^{-3}$
$\sigma = 10^{-17} cm^2$	η=5x10^{-2} $n_e = 5 \cdot 10^{17} cm^{-3}$
$\sigma = 10^{-18} cm^2$	η=6x10^{-4} $n_e = 6 \cdot 10^{15} cm^{-3}$
$\sigma = 10^{-19} cm^2$	η=6.5x10^{-6} $n_e = 6.5 \cdot 10^{13} cm^{-3}$

In conclusion: At F_{LASER}~50 mJ/cm^2, where onset for the selectivity of chemical processes is observed, multiphoton excitation results in 'electron cloud' with density ~10^{13} e/cm^3 at minimum, and as high as 10^{17} e/cm^3.

The argument of multiphoton processes reducing the effective penetration depth can account for the reduced ArH formation upon fs irradiation as compared with ns ablation. However, it is clearly insufficient to account for the highly selective chemical

modifications observed upon fs irradiation. It would be tempting to argue that Nap_2 formation upon fs irradiation does not occur because of absence of melting (so that radical diffusion is highly restricted). However, this argument is incomplete, because in view of the indicated multiphoton processes, we can estimate that at fluences at least close to this ablation threshold, the absorbed energy should be sufficient to result melting. It could be suggested than in fs ablation, material ejection occurs very fast, thereby resulting in very fast energy removal. Indeed, the preliminary experiments in the section 7.4 indicate that material ejection is already initiated at 1-2 ns. Diffusion for this time scale is insignificant. However, this evident suggestion cannot account (at least fully) for the observed selectivity in ArH formation because highly ArH formation is observed at fluences well below the ablation threshold.

There is another possibility, namely that product formation is determined by the formation of weak plasma suggested before. The presence of these electrons may result in new reaction pathways in particular, electrons are known to attach organic-substituted halides and result in their fragmentation:

$$ArI + e^- \rightarrow ArI^- \rightarrow Ar^- + I^-$$

The aryl radical produced as above may be highly (vibrationally) excited and react exclusively by fast hydrogen-atom abstraction. Of course, as indicated thus far, the evolution of process under femtosecond irradiation conditions, appear to be quite complex and it is highly likely that chemical process in the presence of a weak plasma deviate much from conventional concepts. Preliminary experiments for verifying this via white light absorption measurements of the kinetics of the electrons and ions formation/decay generated upon irradiation are underway.

The dissipation of the absorbed energy in bulk material and the corresponding material removal take place mostly after pulse duration, which also remain poorly understood and has many different views. Among the views, one main mechanism has been extensively discussed called Coulomb explosion. According with this mechanism, excited electrons escape from the bulk materials and form a strong electric field that pulls out the ions within the impact area

7.6 CONCLUSIONS

The chemical modifications induced to ArI dopants within PMMA have been examined for irradiation at 248 nm with subpicosecond laser pulses and are compared with the corresponding ones for ns irradiation. To this end, ArH formation has been examined as a function of laser fluence, and is found to differ quantitatively and qualitatively from the ns dependence. Most importantly no spectral broadening indicative of decomposition is observed with successive laser pulses at high fluences. In addition, ArH product form is also quantitatively much reduced from that in ns ablation.

The efficient operation of multiphoton process suggests highly reduced optical penetration depth and thus a highly reduced depth of product formation and accumulation. This should enable the successful processing of a wide range of artworks, even in the near absence of "protecting" varnish layer.

In addition, our results suggest that in the biological applications reported thus far, a major factor involved and been responsible for their success (i.e. subcellular treatment with retainment of the biological /cellular functionality) must relate to the indicated herein highly restricted and selective chemistry.

7.7 REFERENCES

1. K. König, I. Riemann, W. Fritsche, Opt Lett., **26**, 819, (2001).
2. Baudach S, Krüger J, Kautek W "Femtosecond Laser Processing of Soft Materials" Rev Laser Eng **29**, 705, (2001).
3. Bäuerle D "Laser processing and chemistry", 3rd edn. Springer, Berlin Heidelberg New York (2000).
4. T. Tirlapur, K. König , Exp.Res.Cell, **36**,167,(2003).
5. a) J.E Sipe et.al, Phys.Rev. B., 27,1141, (1983) b) J.F Young et.al, ibid *27*, 115,(1983), c)J.F Young, J.S Preton,H.M van Driel, and J.E Sipe, ibid, **30**, 2001, (1984).
6. M.Bolle and S. Lazarre, J.Appl.Phys., **73**, 3516, (1993) .
7. S. Preuss, M. Spath, Y. Zhang M Stuke, App.l Phys. Lett., **62,** 3049, (1993).
8. P.K Kennedy, IEEE J. Quantum Electron.,**QE-31**, 2241, (1995).

9. M.H Niemz, Appl. Phys.Lett., **66,** 1181, (1995).

10. B.C Stuart, et.al., Phys.Rev. B., **53,** 1749, (1996).

11. A. Vogel, J. Noack, G. Hüttmann, G. Paltauf, Proc SPIE **4633,** 23, (2002)

12. S. Sowa, W. Watanade, T. Tamaki, J.Nishii, K. Itoh, Opt. Exp. **14**, 291, (2006).

APPENDIX: FORTRAN program for ArH and Ar_2 calculation

```
      PROGRAM CALC
      DOUBLE precision R(200),R2(200)
      DOUBLE precision abs,Re,Rt,n,a,a1,a2,a3,a4,a5
      DOUBLE precision a6,ra7,a8,a9,rnomol,abs2,Rpr
      DOUBLE precision,rat,rda,rke,rn,rpr1,rb,rn1,rat1,R4
      open(30,file="KINNAP2.dat")
      open(20,file="FDNAP2.dat")
      open(10,file="FDARH.dat")
      read(*,*)abs,abs2
      do f=100,3000,100
      Rt=0.
C     the next section calculates the # Ar radicals produced per
C     layer of sample (thickness 20 µm,step 0.1 µm)
      do i=1,200,1
      R(i)=exp(-abs*1.d-5*float(i-1))-exp(-abs*1.d-5*float(i))
      R(i)=R(i)*f*0.125*1.d16*(abs2/abs)
      ra7=R(i)
      rnomol=1.14*1.d14
C     rnmol represents the # of ArI molecules per layer; thus the
C     maximum Ar radicals that may be formed
      IF (ra7.GE.rnomol) THEN
      R(i)=2.28d16/200
      ENDIF
      Rt=R(i)+Rt
      R2(i)=0.0
      enddo
      rat1=0.0
      rpr1=0.0
      do i=1,10000,1
      do j=1,200,1
C     The next lines calculate the temperatures at time and depth z
      a1=(abs*f)/(1000*2*1.19*2.5)
      a2=exp(abs*abs*float(i)*4.d-10)
      a4=exp(-abs*float(j)*1.d-5)*erfc(abs*SQRT(4.d-10*float(i))
     &-(float(j)*1.d-5)/(2.*SQRT(4.d-10*float(i))))
      a5=exp(abs*float(j)*1.d-5)*erfc(abs*SQRT(4.d-10*float(i))
     &+(float(j)*1.d-5)/(2.*SQRT(4.d-10*float(i))))
      a=300+a1*a2*(a4+a5)
      a3=1.d6*exp(-4.5d4/(8.3145*a))
      IF(a3.LT.0.01)THEN
      R2(j)=0.0
      ELSE
      Rpr=R(j)
      R(j)=R(j)*(1.-a3*1.d-6)
      R2(j)=Rpr-R(j)
      ENDIF
      rat1=rat1+R2(j)
      IF(a.GT.433.)THEN
      rb=5.202-(0.3*8.86*(a-433.)/(101.6+a-433.))
      rn=10**rb
      IF(a.GT.533.)THEN
      rn=2.799*10**(-3.3)*exp(1.3*7818.138/a)
```

```
          ENDIF
C         rn Williams Landel Flory viscosity equation
          rn=3.68d4*exp(-19.49*((a-273)-210)/(240.8+(a-273)-210))
C         rke Smoluchowski equation of the rate
          rke=8*8.8314*a/(3*6.022*rn)
          rda=1.d-20*rke*R(j)*R(j)
          R(j)=R(j)-rda
          rat=rda/2
          rpr1=rpr1+rat
          ELSE
          rda=0.
          R(j)=R(j)
          rat=0.0
          rpr1=rpr1+rat
          ENDIF
          enddo
          write(30,*)i,rpr1
          enddo
          write(20,*)f,rpr1
          write(10,*)f,rat1
          enddo
          close(30)
          close(20)
          close(10)
          end
```

CURRICULUM VITAE

GIANNIS BOUNOS

Date of Birth: July 19th 1976

EDUCATION

Dec.2003-	PhD work, IESL-FORTH and Dept of Physics, University of Crete
Sep.2000-Apr.2003	M. Sc., Graduate Program of Microelectronics and Optoelectronics, Dept of Physics, University of Crete. Title of Thesis: 'Kinetics of product formation in the UV ablation of doped polymers'
Jun.-Jul. 2000	Summer School of Advanced Physics, ranked 5/48, University of Crete
Sep.1995-Sep.2000	B.A in Physics, Dept of Physics, University of Crete (6.71/10)
Feb -Mar. 2005	Short Term Scientific Mission to Institute of Physical Chemistry "Rocasolano", CSIC, Madrid, Spain Host's Name: Dr. Marta Castillejo

PUBLICATIONS

1. **G. Bounos**, A. Athanassiou, D.Anglos, S.Georgiou, C. Fotakis **"**Product formation in the laser ablation of doped PMMA at 248 nm: Implications for Chemical Effects in UV Ablation" **,** *Journal of Physical Chemistry B* ***108****, 7052-7060 (2004)*

2. **G. Bounos**, A Kolloch, T. Stergiannakos, E. Varatsikou, S. Georgiou "Assessment of the attained temperatures and of melting in the nanosecond irradiation of doped polymethylmethylacrylate at 308, 248, and 193 nm via the examination of dopant reactivity" *Journal of Applied Physics* ***98****, 084317 (2005)(selected for Virtual J. Nanotechnology, Nov. (2005) issue)*

3. E. Rebollar, **G. Bounos,** M. Oujja, C. Domingo, S. Georgiou, M. Castillejo "Influence of polymer Molecular Weight on the UV ablation of doped PMMA" *Applied Surface Science,* ***248****, 1-4, 254-258 (2005)*

4. **G. Bounos**, A. Athanassiou, D. Anglos, S Georgiou "Dynamics of dopant product formation in the nanosecond irradiation of doped PMMA at 248 and 193 nm: Temporal evolution of temperature and viscosity" *Chemical Physics Letters* ***418****, 313–318 (2006)*

5. **G. Bounos**, E. Rebollar, A. Selimis, N. Bityurin, M. Castillejo, S. Georgiou, "Dependence of UV laser-induced desorption and ablation processes on polymer molecular weight: Poly(methyl methacrylate) at 248 nm", *Journal of Applied Physics,* ***100****,11323, (2006)*

6. E. Rebollar, **G. Bounos,** M. Oujja, C. Domingo, S. Georgiou, M. Castillejo, "Influence of polymer molecular weight on the chemical modifications induced by UV laser ablation" *Journal of Physical Chemistry B,****110****, 14215-14220 (2006)*

7. E. Rebollar, **G. Bounos**, M Oujja, S Georgiou, M Castillejo "Effect of molecular weight on the morphological modifications induced by UV laser ablation of doped polymers" *Journal of Physical Chemistry B,* ***110****,16452-16458 (2006)*

8. E. Rebollar, **G. Bounos**, A. Kolloch, M. Oujja, S. Georgiou, M Castillejo "Analysis of plume following UV laser ablation of doped polymers: dependence on polymer molecular weight", *Journal of Applied Physics* ***101****, 033106 (2007)*

9. E. Rebollar, **G. Bounos,** M. Oujja, S. Georgiou, M. Castillejo, "Morphological and chemical modifications and plume ejection following UV laser ablation of doped polymers: Dependence on polymer molecular weight", accepted to *Applied Surface Science*

IN PREPARETION:

10. **G. Bounos**, E Rebollar, A. Selimis, A. Kolloch, N. Bityurin, M. Castillejo, S. Georgiou, "Demonstration of Explosive Boiling in the UV nanosecond laser irradiation of polymers"

11. **G. Bounos**, E Rebollar, A. Selimis, N. Bityurin, D. Papazoglou M. Castillejo, S. Georgiou, "Novel chemical processes in the UV sub-picosecond ablation of doped polymers"

12. **G. Bounos**, E Rebollar, M. Castillejo, S. Georgiou, "Dependence of UV laser induced process on polymer molecular weight: Polystyrene "

BOOK CHAPTER

G. Bounos, A. Nevin, S. Georgiou, C. Fotakis,
'Laser restoration of painted artworks:Fundamentals, Modelling and Advances' in the book Laser Ablation and its Applications, **Springer Series in Optical Sciences**, Vol. 129, 588 p, Claude Phipps (Ed.) 2007.

PROCEEDINGS

- S. Georgiou, **G. Bounos**, A. Athanassiou, D. Anglos, V. Tornari, C. Fotakis, "Chemical and structural modifications in the UV ablation of polymers", Proc. SPIE, Vol 4760, p. 274-280, High-Power Laser Ablation IV, Claude R, Ed., 2002

- E. Rebollar, M. Oujja, M. Castillejo, **G. Bounos**, S. Georgiou, "Effect of molecular weight on the physicochemical modifications induced in the UV laser ablation of doped polymers", Journal of Physics Conference Series (in press)

- C. Fotakis, V. Zorba, E. Stratakis, P. Tzanetakis, I. Zergioti, D. G Papazoglou, K. Sambani, G. Fillipidis, M. Farsari, P. Pouli, **G. Bounos**, S Georgiou. "Novel aspects of materials processing by ultrafast Lasers: From to Electric to Biological and Cultural Haritage Applications, Journal of Physics Conference Series (in press)

PARTICIPATION IN CONFERENCES

- **G. Bounos**, A. Athanassiou, D. Anglos, S. Georgiou, 19th National Conference of Solid State Physics and Material Science, Heraklion, Creece, 2002, **Oral Presentation:** "Photoproduct characterization in the UV laser ablation of doped polymers"

- **G. Bounos**, A. Athanassiou, D. Anglos, S. Georgiou, International symposium, New trends in laser cleaning, Hersonissos, Creece, Oct , 2003, **Poster Presentation:** "Dynamics of photoproduct formation in the UV laser ablation of doped polymers"

- **G. Bounos,** E. Rebollar, A. Athanassiou, D. Anglos, S. Georgiou, Int. Conf. on Laser Ablation, Hersonissos, Creece, Oct 2003, **Poster Presentation:** "Dynamics of product formation in the UV laser ablation of doped polymers with different molecular weight"

- **G. Bounos,** A. Athanassiou, D. Anglos, S. Georgiou, Int. symposium, Rank Prize Funds, Grasmere, England, July 2004, **Oral Presentation:** "Dynamics of photoproduct formation in the UV nanosecond and subpicosecond laser ablation of doped polymers"

- **G. Bounos,** et al, 21th National Conf. on Solid State Physics and Material Science, Ioannina, Creece, 2004, **Oral Presentation:** "Photoproduct characterization and Dynamics in the UV laser ablation of doped polymers. The influence of Molecular weight"

- **G. Bounos,** E. Rebollar, D.G. Papazoglou M. Castillejo, S. Georgiou European Materials Research Society, E-MRS 2006 Spring Meeting, Nice (France), May, 2006 **Oral presentation:** "Unique features in the UV femtosecond ablation of polymers"

- **G. Bounos,** et al, European Materials Resesearch Society, Nice (France), May 2006, **Poster Presentation:** "Morphological and chemical modifications and plume ejection following UV laser ablation of doped polymers: Dependence on polymer molecular weight"

- **G. Bounos,** et al, Int. Workshop on Laser Interface Interactions and Laser Cleaning 4-7 July 2006 Konstanz, Germany **Oral presentation:** "Dependence of UV laser ablation of polymers on molecular weight"